2019

Development and Application of the Variational Two-Electron Reduced Density Matrix Complete Active Space Self-Consistent Field Method to Address the Electron Correlation Problem in Quantum Chemistry

Elvis Maradzike

FLORIDA STATE UNIVERSITY

COLLEGE OF ARTS AND SCIENCES

DEVELOPMENT AND APPLICATION OF THE VARIATIONAL TWO-ELECTRON REDUCED DENSITY MATRIX COMPLETE ACTIVE SPACE SELF-CONSISTENT FIELD METHOD TO ADDRESS THE ELECTRON CORRELATION PROBLEM IN QUANTUM CHEMISTRY

By

ELVIS MARADZIKE

A Dissertation submitted to the
Department of Chemistry and Biochemistry
in partial fulfillment of the
requirements for the degree of
Doctor of Philosophy

2019

Elvis Maradzike defended this dissertation on July 8, 2019.
The members of the supervisory committee were:

A. Eugene DePrince, III

Professor Directing Dissertation

Richard Bertram

University Representative

Oliver Steinbock

Committee Member

Wei Yang

Committee Member

The Graduate School has verified and approved the above-named committee members, and certifies that the dissertation has been approved in accordance with university requirements.

ACKNOWLEDGMENTS

I would like to thank my advisor, A. Eugene DePrince, III, without whose guidance the work presented in this dissertation would not have been possible. I am grateful for how thoughtful he was in making my own PhD experience rewarding. I appreciate the example he has set as a mentor and as a professor.

I would also like to thank the rest of my dissertation committee members, Dr. O. Steinbock, Dr. W. Yang, and Dr. R. Bertram. I am grateful for their feedback and encouragement over the last few years.

I would also like to acknowledge former and current members of the DePrince Research Lab; former members for being especially supportive when I was finding my way around the lab just after joining the research group, and to current members for being such good company both as colleagues and as friends.

I have had several mentors over the years. I would like to specially acknowledge Rebecca Zeigler Mano, whose work at Education USA in Harare made it possible for me to come to the United States for the first time to further my studies, Professor J. R. Friedman at Amherst College for providing me my first research project and a place in his lab, and Professors K. Jagganathan and L. Hunter for their support over the years.

Last but not least, I would like to thank my friends, here in Tallahassee and beyond, and my family, particularly my mother, Cathrine, and brother, Allen, for their support and encouragement over the past few years.

TABLE OF CONTENTS

LIST OF TABLES

LIST OF FIGURES

ABSTRACT

The goal of this dissertation is to describe a series of developments and applications of the variational two-electron reduced density matrix (v2RDM-) complete active space self-consistent field (CASSCF) method to the electron correlation problem in electronic structure theory. The v2RDM-CASSCF method is a complete active space (CAS) method based on optimizing the two-electron reduced density matrix (2RDM). Since the 2RDM is a more compact object than the N-electron wavefunction, it is possible to formulate a CAS approach that scales polynomially, rather than exponentially, with respect to the size of the active space. For this reason, computer implementations of v2RDM-driven CASSCF are capable of treating active spaces much larger than the limit of current implementations of wavefunction-/configuration interaction (CI-) driven wavefunction CASSCF. The work described in this dissertation addresses three deficiencies of v2RDM-CASSCF: the lack of an analytic energy derivative code, the lack of an efficient code with which to compute excited states, and the lack of a method with which to correct the v2RDM-CASSCF energy for dynamical correlation. We develop analytic first derivatives of the v2RDM-CASSCF energy, and we show, in fact, that the expressions for the analytic first derivative of the energy are identical to those for CI-based CASSCF. For the excited state problem, we improve an approach by which excited states and excited state properties can be computed from the ground state 2RDM. Lastly, we develop a model for dynamical correlation for v2RDM-CASSCF references. With this model, energies computed at the v2RDM-CASSCF level of theory can be corrected to account for the effects of dynamical correlation.

CHAPTER 1

DISSERTATION OUTLINE

Chapters 2, 3, 4 and 6 cover the background necessary for a close reading of this dissertation. Chapter 2 covers some mathematical background and commonly used notation in electronic structure theory; Chapter 3 provides some context for and illustrates the electron correlation problem. Chapter 4 briefly describes the variational two-electron reduced density matrix (v2RDM)-complete active space self-consistent field (CASSCF) approach to electronic structure theory while Chapter 6 outlines some approaches for excited states. Chapter 9 contains some final remarks.

In Chapter 5, we show that the first derivative of the energy computed at the v2RDM-CASSCF level of theory is stationary with respect to all variables in the optimization of the two-electron reduced density matrix (2RDM), and that orbital response contributions to the gradient are identical to those in CI-based CASSCF. We apply the v2RDM-CASSCF method and the formulation of analytic gradients to the geometry optimization of molecules with both modest and large active spaces. We assess the impact of the N-representability constraints enforced on the variable 2RDM on final optimized geometries.

We describe, in Chapter 6, an excited state approach based on applying the extended random phase approximation (ERPA) within the context of Rowe's equation of motion (EOM). When one assumes a reference from CASSCF, the resulting generalized eigenvalue problem can be written in terms of the elements of 1- and 2RDMs computed at the CASSCF level of theory. Solving this eigenvalue problem gives information concerning excited states and excited state properties. We use RDMs obtained from v2RDM-CASSCF calculations to compute excitation energies and associated oscillator strengths for near K-edge excited states of compounds containing second row elements. We assess the quality of excited states by comparison with results from experiment and from time-dependent coupled cluster calculations. We also assess the effect, and ultimately, importance, of using reference RDMs from

CASSCF calculations, with which correlation effects are accounted for, rather than RDMs from restricted Hartree-Fock calculations, with which correlation effects are not accounted for, or from density functional theory (DFT), with which correlation effects are not explicity accounted for by multiconfigurational approaches. We also assess the effect on excited state properties of N-representability conditions used to compute the 1- and 2-RDMs at the v2RDM-CASSCF level of theory.

In Chapter 7, we develop a method by which the v2RDM-CASSCF energy can be improved to account for the effects of dynamical correlation that are not accounted for at the CASSCF level of theory. The method is based on an adiabatic connection (AC) model by Pernal and coworkers. Pernal and coworkers have shown that it is possible for formulate a correction for dynamical correlation effects to an energy computed at the CASSCF level of theory, if the active space is well-selected to take care of nondynamical correlation effects. We use this method to compute corrected energies for a set of small molecules using geometries near and far from equilibrium. We also compute relative/reaction energies for several reactions.

CHAPTER 2

INTRODUCTION AND MATHEMATICAL BACKGROUND

2.1 Introduction

The accurate determination of molecular electronic structure and properties is the goal of quantum chemistry. The motion of the molecule's constituent particles is governed by quantum mechanics in the form of partial differential equations involving the wavefunction. The solution of these equations gets more challenging as the number of particles increases. Therefore, one of the defining features of quantum chemistry is the development of methods that allow for approximate solutions to the many-particle problem. Since the vast majority of molecules are chemical compounds of the light elements, one of the key simplifications that is made is the *non*-relativistic approximation which yields the Schrödinger equation. A further approximation is the Born-Oppenheimer approximation that decouples the nuclear and electronic degrees of freedom to give the electronic Schródinger equation. The Born-Oppenheimer approximation is justified by the fact that the changes in electronic structure that define chemistry occur at much shorter timescales than the change in nuclear coordinates. Even though the electronic Schrödinger equation is much simpler than its molecular analog, its solution remains a challenge, particularly for larger systems that are often of interest to the wider chemistry community.

The exact solution of the *non*-relativistic electronic Schrödinger equation within the orbital approximation by full configuration interaction (CI) leads to complexity that scales very steeply with respect to the number of electrons and orbitals. This explains the popularity of less computationally expensive *single*-configuration approaches such as the Hartree-Fock (HF) method and Kohn-Sham (KS-) density functional theory (DFT). These approaches provide accurate descriptions of electronic structure in some cases. However, because they

are not formulated in a way in which electron-electron motion is $fully$ correlated, these methods cannot guarantee an accurate description of the electronic structure for general molecular systems. This is particularly true for molecules for which different electronic configurations are near-degenerate, and for which the wavefunction is best described by multiple electronic configurations. In this dissertation, we describe a series of developments by which we compute molecular properties while taking advantage of the computational efficiency afforded by the variational two-electron reduced density matrix (v2RDM)- complete active space self-consistent field (CASSCF) method, which can treat systems whose wavefunctions are multiconfigurational, and which avoids the factorial scaling associated with full CI, or CI-based CASSCF. We discuss in this dissertation three developments: the first implementation of analytic gradients for the v2RDM-CASSCF method; an improved method for computing excited states using RDMs computed at the v2RDM-CASSCF level of theory, since the v2RDM-CASSCF method by itself cannot be used to compute excited states; and the development of a model for dynamical correlation for the v2RDM-CASSCF, which brings energies computed at the v2RDM-CASSCF level of theory in better quantiative agreement with those computed from full CI.

In this chapter, we will cover the mathematical background and conceptual ideas that are needed in order to understand both single-configuration as well as multiconfiguration-based descriptions of electronic structure. We will round off the chapter with a brief history of the development of RDM-based methods in quantum chemistry.

2.1.1 Many-electron wavefunctions

The many-electron wavefunction can be represented in a basis of electronic configurations, each of which is antisymmetric with respect to particle exchange. Here we derive a representation of such electronic configurations in terms of spin orbitals. Although our goal is to develop a respresentation for the wavefunction of a fully interacting system, we ignore that for the moment and consider a simpler system having a Hamiltonian, $\hat{H}_0$, that involves

the coordinates of just one particle

$$\hat{H}_0 = \sum_{i=1}^{N} \hat{h}(x_i). \tag{2.1}$$

Each term in the sum in 2.1 involves the kinetic energy operator $-\frac{1}{2}\nabla_i^2$, but it can also include a potential energy U such that

$$\hat{h}(x_i) = -\frac{1}{2}\nabla_i^2(x_i) + U. \tag{2.2}$$

If we take the eigenfuctions of $\hat{h}$ to be a set of spin orbitals $\{\phi_\nu\}$, then we can define, for each single electron, an eigenvalue problem

$$\hat{h}(x_i)\phi_\nu(x_i) = \epsilon_\nu \phi_\nu(x_i), \tag{2.3}$$

where ν is a label for a spin orbital. The spin orbitals from 2.3 form an orthonormal

$$\int dx\, \phi_\nu^*(x)\phi_{\nu'}(x) = \delta_{\nu,\nu'} \tag{2.4}$$

and complete

$$\sum_\nu \phi_\nu^*(x)\phi_\nu(x') = \delta(x - x') \tag{2.5}$$

set, with $\int dx$ denoting integration over all spatial ($\mathbf{r}$) and spin (σ) coordinates:

$$\int dx \equiv \sum_\sigma \int d^3r, \tag{2.6}$$

and

$$\delta(x - x') = \delta(\mathbf{r} - \mathbf{r}')\delta_{\sigma,\sigma'}. \tag{2.7}$$

An antisymmetric N-electron configuration which is an eigenstate of the non-interacting Hamiltonian $\hat{H}_0$ can be constructed from these spin orbitals:

$$\Phi(x_1, ..., x_N) = \frac{1}{\sqrt{(}N!)} \sum_{P \in S_N} sgn(P) \cdot P\phi_{\nu_1}(x_1)\phi_{\nu_2}(x_2)...\phi_{\nu_N}(x_N), \tag{2.8}$$

where $sgn(P)$ denotes the sign of the permutation P. An even (odd) number of two-particle permutations yields a positive (negative) sign for $sgn(P)$. The many-electron wavefunction in 2.8 can be written as a determinant (more commonly referred to as a Slater determinant)

$$\Phi = \begin{vmatrix} \phi_{\nu_1}(x_1) & \dots & \phi_{\nu_1}(x_N) \\ \vdots & & \vdots \\ \phi_{\nu_N}(x_1) & \dots & \phi_{\nu_N}(x_N) \end{vmatrix} \tag{2.9}$$

2.2 Second quantization

Working with electronic configurations written in the form of 2.9 can be quite inconvenient. In this section, we introduce the language and notation of second quantization. Second quantization provides a more succinct way of representing the information in electronic configurations by expressing both the configurations and operators in terms of a single set of creation and annihilation operators.

2.2.1 Creation and annihilation operators

In second quantization, creation and annihilation operators create and annihilate electrons in specified spin orbitals. Electronic configurations are constructed as products of creation operators acting on the *vacuum state*, which is a unique state containing no electrons.

In second quantization, the occupation number representation is used to represent electronic configurations. Here an electronic configuration with n_1 particles in spin orbital 1, n_2 particles in spin orbital 2, n_3 particles in spin orbital 3, etcetera can be written as

$$|n_1, n_2, n_3, n_4, \dots\rangle. \tag{2.10}$$

where n_i can only take the values 0 or 1. We can now define the creation operator $\hat{a}_\nu^\dagger$, with ν being a label for a spin orbital, such that, if there is already an electron in spin orbital ν, the action of the creation operator on a determinant $|n_1, n_2, n_3, \dots, n_\nu, \dots\rangle$ returns 0, and if there is no electron in spin orbital ν, then the result of acting on $|n_1, n_2, n_3, \dots, n_\nu, \dots\rangle$ is the creation of an electron in spin orbital ν. That is

$$\hat{a}_\nu^\dagger |n_1, n_2, \dots, n_\nu, \dots\rangle = \text{phase factor } |n_1, n_2, \dots, 1_\nu, \dots\rangle \tag{2.11}$$

where the phase factor equal to +1 or -1. The value of the phase factor depends on whether the total number of electrons in spin orbitals with labels less than ν is even or odd. This is because the action of two different creation operators which nonetheless act on the same orbitals should be to create different states (or 0). For example, the action of the operators $\hat{a}_1^\dagger \hat{a}_2^\dagger$

and $\hat{a}_2^\dagger \hat{a}_1^\dagger$ on the vacuum state $|0\rangle = |0_1, 0_2, 0_3, \dots\rangle$ should result in different configurations:

$$\hat{a}_1^\dagger \hat{a}_2^\dagger |0\rangle = \hat{a}_1^\dagger |0_1, 1_2, 0_3, \dots\rangle = |1_1, 1_2, 0_3, \dots\rangle \tag{2.12}$$

whereas

$$\hat{a}_2^\dagger \hat{a}_1^\dagger |0\rangle = \hat{a}_2^\dagger |1_1, 0_2, 0_3, \dots\rangle = -|1_1, 1_2, 0_3, \dots\rangle. \tag{2.13}$$

In fact, any electronic configuration can be created by acting on the vacuum state with the appropriate set of creation operators in an appropriate order

$$|1_1, 1_2, 1_3, \dots\rangle = (\hat{a}_1^\dagger)(\hat{a}_2^\dagger)(\hat{a}_3^\dagger)\cdots|0\rangle. \tag{2.14}$$

Having defined the creation operator, we can now define its complement, the annihilation operator, $\hat{a}_\nu$, by requiring that its action on a configuration in which spin orbital ν is occupied result in a configuration in which that spin orbital is unoccupied, that is,

$$\hat{a}_\nu |n_1, n_2, \dots, n_\nu, \dots\rangle = \text{phase factor } |n_1, n_2, \dots, 0_\nu, \dots\rangle, \tag{2.15}$$

where the phase factor is as defined in 2.11. The result is 0 if there is no electron in state ν. It also becomes apparent that the vacuum state is such that when it is acted upon by an annihilation operator, the result is always 0. That is,

$$\hat{a}_\nu |0\rangle = 0 \text{ for all } \nu. \tag{2.16}$$

Since $\hat{a}_\nu^\dagger |\Phi_N\rangle$ is a state with $N+1$ electrons, $\hat{a}_\nu^\dagger$ is a mapping between a Hilbert space with N electrons and another with $N+1$ electrons, we can write

$$\hat{a}_\nu^\dagger : \mathcal{H}_N \to \mathcal{H}_{N+1}. \tag{2.17}$$

Similarly, $\hat{a}_\nu$ is a mapping between a Hilbert space with N electrons and another with $N-1$ electrons, so we can write

$$\hat{a}_\nu : \mathcal{H}_N \to \mathcal{H}_{N-1}. \tag{2.18}$$

From their definitions, $\hat{a}_\nu^\dagger$ and $\hat{a}_\nu$ are mutual adjoints

$$\hat{a}_\nu^\dagger = (\hat{a}_\nu)^\dagger; \;\; \hat{a}_\nu = (\hat{a}_\nu^\dagger)^\dagger \tag{2.19}$$

It can also be shown, from the definitions in 2.11 and 2.15, that the two operators obey the following anti-commutation relations:

$$\{\hat{a}_\mu, \hat{a}_\nu\} = 0, \tag{2.20}$$

$$\{\hat{a}_\mu^\dagger, \hat{a}_\nu^\dagger\} = 0, \quad \text{and} \tag{2.21}$$

$$\{\hat{a}_\mu^\dagger, \hat{a}_\nu\} = \delta_{\mu,\nu}. \tag{2.22}$$

where the anti-commutator between two operators, say, A and B, is defined

$$\{A, B\} \equiv AB + BA. \tag{2.23}$$

2.2.2 Second-quantization representation of single-particle and two-particle operators

Here, we apply the Slater-Condon rules to derive the expressions for one- and two-electron operators in terms of creation and annihilation operators. If we consider the matrix elements of an operator $\hat{O}$ between configurations $|\Phi_a\rangle$ and $|\Phi_b\rangle$, we can show that if $\hat{O}$ is a single-particle operator, the matrix element between $|\Phi_a\rangle$ and $|\Phi_b\rangle$ is non-zero if $|\Phi_a\rangle$ and $|\Phi_b\rangle$ differ in occupation by no more than two orbitals. This means that the second-quantized version of single particle operators is a sum of terms, each of which only changes, at most, the occupation of two spin orbitals. So, a one-electron operator such as $\hat{H}_0$ can be written

$$H_0 = \sum_{i=1}^{N} \hat{h}(x_i) \rightarrow \sum_{pq} \langle p|\hat{h}|q\rangle \hat{a}_p^\dagger \hat{a}_q, \tag{2.24}$$

where

$$\langle p|\hat{h}|q\rangle = \int dx \phi_p^*(x) \hat{h}(x) \phi_q(x). \tag{2.25}$$

Similarly, the matrix element for two particle operators is a sum of terms each of which only changes, at most, the occupation of four spin-orbitals. Therefore, a two-electron operator can be written

$$\sum_{i \neq j}^{N} \hat{v}(x_i, x_j) \rightarrow \sum_{pqrs} (pq|\hat{v}|rs) \hat{a}_p^\dagger \hat{a}_r^\dagger \hat{a}_s \hat{a}_q \tag{2.26}$$

where

$$(pq|\hat{v}|rs) = \int\int dxdx' \phi_p^*(x)\phi_q(x')\hat{v}\phi_r^*(x)\phi_s(x'). \tag{2.27}$$

We can therefore write down, using second quantization, operators such as the molecular Hamiltonian

$$\hat{H}_{mol} = \sum_{pq} h_{pq}\hat{a}_p^\dagger \hat{a}_q + \frac{1}{2}\sum_{pqrs}(pq|rs)\hat{a}_p^\dagger \hat{a}_r^\dagger \hat{a}_s \hat{a}_q + h_{nuc} \tag{2.28}$$

where

$$h_{pq} = \int dx \phi_p^*(x)\big(-\frac{1}{2}\nabla^2 - \sum_{I=1}^{N_{atom}} \frac{Z_I}{r_I}\big)\phi_q(x), \tag{2.29}$$

$$(pq|rs) = \int\int dxdx' \frac{\phi_p^*(x)\phi_q(x')\phi_r^*(x)\phi_s(x')}{r}, \text{and} \tag{2.30}$$

$$h_{nuc} = \frac{1}{2}\sum_{I\neq J}\frac{Z_I Z_J}{R_{IJ}}. \tag{2.31}$$

Here, I is a label for atoms, Z_I denotes the nuclear charge associated with atom I, r_I is the nuclear-electron separation, r the separation between an electron at x and another at x', and R_{IJ} is the internuclear separation.

2.3 Density matrices

In this section, we express one- and two-electron density matrices in the notation of second quantization. This can be done by considering the evaluation of expectation values of operators with respect to a normalized reference wavefunction $|\Psi_0\rangle$. The expectation value of the one-electron operator $\langle\Psi_0|\hat{a}_p^\dagger \hat{a}_q|\Psi_0\rangle$ and that of the two-electron operator $\langle\Psi_0|\hat{a}_p^\dagger \hat{a}_r^\dagger \hat{a}_s \hat{a}_q|\Psi_0\rangle$ define the elements of the one- and two-electron density matrices. These can be written more compactly using the following notation

$${}^1D_q^p = \langle\Psi_0|\hat{a}_p^\dagger \hat{a}_q|\Psi_0\rangle, \tag{2.32}$$

and

$${}^2D_{qs}^{pr} = \langle\Psi_0|\hat{a}_p^\dagger \hat{a}_r^\dagger \hat{a}_s \hat{a}_q|\Psi_0\rangle. \tag{2.33}$$

2.3.1 The one-electron density matrix

Here, we investigate the mathematical properties of the one-electron density matrix. The density matrix defined by 2.32 satisfies

$$({}^1D_q^p)^* = {}^1D_p^q \tag{2.34}$$

The one-electron density matrix is therefore Hermitian. Its elements define a Hermitian $M \times M$ matrix, with M being the number of spin orbitals. We call this matrix the spin orbital one-electron density matrix. For real wavefunctions, the one-electron density matrix is symmetric

$${}^1D_q^p = {}^1D_p^q. \tag{2.35}$$

The one-electron density matrix is positive semidefinite, that is, its eigenvalues are non-negative. This is because its elements can be either be zero, or inner products of occupation number vectors or configurations that can be defined with $N-1$ electrons and M orbitals. Its diagonal elements can be written

$${}^1D_p^p = \langle\Psi_0|\hat{a}_p^\dagger\hat{a}_p|\Psi_0\rangle = \langle\Psi_0|\hat{N}_p|\Psi_0\rangle \tag{2.36}$$

where we have replaced $\hat{a}_p^\dagger\hat{a}_p$ with $\hat{N}_p$. Since the operator $\hat{a}_p^\dagger\hat{a}_p$ effectively counts the number of electrons, it is known as the occupation number operator and is usually denoted $\hat{N}$. This occupation number operator is idempotent, that is, $\hat{N}_p = \hat{N}_p\hat{N}_p$, we can write down the diagonal element of the one-electron density matrix by an occupation number ω_p:

$$\omega_p = \langle\Psi_0|\hat{N}_p\hat{N}_p|\Psi_0\rangle. \tag{2.37}$$

The wavefunction $|\Psi_0\rangle$ is generally a linear combination of occupation number vectors

$$|\Psi_0\rangle = \sum_{\mathbf{k}} c_{\mathbf{k}}|\mathbf{k}\rangle, \tag{2.38}$$

with $\sum_{\mathbf{k}}|c_{\mathbf{k}}|^2 = 1$ (normalization) so

$$\hat{N}_p|\Psi_0\rangle = \sum_{\mathbf{k}} k_p c_{\mathbf{k}}|\mathbf{k}\rangle \tag{2.39}$$

where k_p counts contributions from kets where ϕ_p is occupied, and is zero otherwise. The occupation numbers ω_p can now be written in the form

$$\omega_p = \sum_{\mathbf{k}} k_p |c_{\mathbf{k}}|^2. \tag{2.40}$$

The occupation numbers ω_p are real numbers between 0 and 1 inclusive

$$0 \leq \omega_p \leq 1. \tag{2.41}$$

The occupation number takes the value of 0 if all orbitals ϕ_p are unoccupied in all kets or occupation number vectors. It takes the value 1 if ϕ_p is occupied in all kets or occupation number vectors. It takes values between 0 and 1 if ϕ_p is occupied only in some of the occupation number vectors. The sum of the occupation numbers, which is also the trace of the density matrix, is equal to the number of electrons

$$Tr(^{\mathbf{1}}\mathbf{D}) = \sum_p \omega_p = \sum_p \langle \Psi_0 | \hat{N}_p | \Psi_0 \rangle = \langle \Psi_0 | \hat{N} | \Psi_0 \rangle = N \tag{2.42}$$

For a state consisting of a single occupation number vector or electronic configuration, the one-electron density matrix has a simple diagonal structure

$$^1 D_q^{p,\mathbf{k}} = \langle \mathbf{k} | \hat{a}_p^\dagger \hat{a}_p | \mathbf{k} \rangle = \delta_{pq} k_p \tag{2.43}$$

By contrast, for an electronic state containing several occupation number vectors, the density matrix is not diagonal. But, since $^{\mathbf{1}}\mathbf{D}$ is Hermitian, its off diagonal elements may be eliminated completely by diagonalization with a unitary matrix:

$$^{\mathbf{1}}\mathbf{D} = \mathbf{U} \eta \mathbf{U}^\dagger. \tag{2.44}$$

The eigenvalues of $^{\mathbf{1}}\mathbf{D}$ are real numbers $0 \leq n_p \leq 1$, and are known as *natural orbital occupation numbers*. The sum of the natural orbital occupation numbers is equal to the number of electrons. From the eigenvectors $\mathbf{U}$ of the density matrix, we obtain a new set of spin orbitals called the *natural spin orbitals* of the system.

2.3.2 The two-electron density matrix

Here we outline the important mathematical properties of the two-electron density matrix. For two-electron density matrices, it is important to note that the elements are not all independent. Due to anticommutation relations,

$$ {}^2D^{pr}_{qs} = -{}^2D^{pr}_{sq} = {}^2D^{rp}_{sq} = -{}^2D^{rp}_{qs} \tag{2.45} $$

Also, according to the Pauli principle,

$$ {}^2D^{pp}_{qs} = {}^2D^{pr}_{qq} = {}^2D^{pp}_{qq} = 0 \tag{2.46} $$

The two-electron density matrix is Hermitian, since

$$ ({}^2D^{pr}_{qs})^* = (\langle\Psi_0|\hat{a}^\dagger_p\hat{a}^\dagger_r\hat{a}_s\hat{a}_q|\Psi_0\rangle)^* = \langle\Psi_0|\hat{a}^\dagger_q\hat{a}^\dagger_s\hat{a}_r\hat{a}_p|\Psi_0\rangle = {}^2D^{qs}_{pr} = {}^2D^{pr}_{qs} \tag{2.47} $$

Further, the two-electron density matrix is positive semidefinite, since its elements are zero or equal to the inner products of occupation number vectors that can defined with $N-2$ electrons and M spin orbitals. We can use anticommutation relations to show that the diagonal elements

$$ {}^2D^{pq}_{pq} = \langle\Psi_0|\hat{a}^\dagger_p\hat{a}^\dagger_q\hat{a}_q\hat{a}_p|\Psi_0\rangle \tag{2.48} $$

can be written in terms of pair number operators

$$ {}^2D^{pq}_{pq} = \langle\Psi_0|\hat{N}_p\hat{N}_q|\Psi_0\rangle, \tag{2.49} $$

provided $p \neq q$, so that these diagonal elements $\langle\Psi_0|\hat{N}_p\hat{N}_q|\Psi_0\rangle$ represent simultaneous occupations of pairs of spin orbitals. Similar to the approach taken for the one-electron density matrix, we can define

$$ \omega_{pq} = \langle\Psi_0|\hat{N}_p\hat{N}_q|\Psi_0\rangle, \tag{2.50} $$

to represent the part of the wavefunction where spin orbitals ϕ_p and ϕ_q are simultaneously occupied. So we have:

$$ \hat{N}_p\hat{N}_q|\Psi_0\rangle = \sum_{\mathbf{k}} k_p k_q c_{\mathbf{k}}|\mathbf{k}\rangle. \tag{2.51} $$

The occupation of a given spin-orbital pair cannot exceed those of the individual spin orbitals. That is,

$$0 \leq \omega_{pq} \leq \min(\omega_p, \omega_q) \leq 1. \tag{2.52}$$

The trace of the two-electron density matrix is

$$Tr(^{\mathbf{2}}\mathbf{D}) = \sum_{p>q} \langle \Psi_0 | \hat{N}_p \hat{N}_q | \Psi_0 \rangle = \frac{1}{2} \sum_{pq} \langle \Psi_0 | \hat{N}_p \hat{N}_q | \Psi_0 \rangle - \frac{1}{2} \sum_{p} \langle . \Psi_0 | \hat{N}_p | \Psi_0 \rangle = \frac{1}{2} N(N-1) \tag{2.53}$$

Thus the sum of pair occupations ω_{pq} is equal to the number of electron pairs in the system. For a wavefunction containing a single occupation number vector, the two-electron density matrix has a simple diagonal structure with elements

$$^2 D_{rs}^{pq,\mathbf{k}} = \langle \mathbf{k} | \hat{a}_p^\dagger \hat{a}_q^\dagger \hat{a}_s \hat{a}_r | \mathbf{k} \rangle = \delta_{pr} \delta_{qs} k_p k_q. \tag{2.54}$$

For such a wavefunction, the two-electron density matrix can be constructed from elements of the one-electron density matrix

$$^2 D_{rs}^{pq} = {}^1 D_r^{p1} D_s^q - {}^1 D_s^{p1} D_r^q. \tag{2.55}$$

For this wavefunction, the expectation value of any one- or two-electron operator may be obtained from the one-electron density matrix.

2.3.3 Density matrices in spin-orbital and coordinate representations

We can formally relate expectation values of one- and two-electron operators to first- and second-order reduced density matrices defined in terms of spatial (and spin) coordinates.

The first-order reduced density matrix is an integral of the N-electron density matrix over the coordinates of all but one electron. It can be written terms of spatial and spin coordinates as

$$\gamma_1(\mathbf{x}_1, \mathbf{x}_1^{'}) = N \int \Psi(\mathbf{x}_1, \mathbf{x}_2, \ldots, \mathbf{x}_N) \Psi^*(\mathbf{x}_1^{'}, \mathbf{x}_2, \ldots, \mathbf{x}_N) d\mathbf{x}_2 \ldots d\mathbf{x}_N. \tag{2.56}$$

In the same coordinate representation, we may write the expectation value of any one-electron operator as

$$\langle\Psi|\hat{O}_1|\Psi\rangle = \langle\Psi|\sum_i^N \hat{O}_{1i}(\mathbf{x}_i)|\Psi\rangle$$

$$= \sum_i^N \int \Psi^*(\mathbf{x}_1, \mathbf{x}_2, \ldots, \mathbf{x}_N)\hat{O}_{1i}(\mathbf{x}_i)\Psi(\mathbf{x}_1, \mathbf{x}_2, \ldots, \mathbf{x}_N)d\mathbf{x}_1 d\mathbf{x}_2 \ldots d\mathbf{x}_N. \tag{2.57}$$

It is fairly straightforward to show that the integral on the right hand side of 2.57 is the same for each electron so that

$$\langle\Psi|\hat{O}_1|\Psi\rangle = \sum_{pq}\langle\Psi|\hat{a}_p^\dagger\hat{a}_q|\Psi\rangle = N\int \Psi^*(\mathbf{x}_1, \mathbf{x}_2, \ldots, \mathbf{x}_N)\hat{O}_{11}\Psi(\mathbf{x}_1, \mathbf{x}_2, \ldots, \mathbf{x}_N)d\mathbf{x}_1 d\mathbf{x}_2 \ldots d\mathbf{x}_N. \tag{2.58}$$

It follows, from comparing left and right hand sides of 2.58, that

$$\langle\Psi|\hat{a}_p^\dagger\hat{a}_q|\Psi\rangle = \int \phi_q^*(\mathbf{x}_1)\gamma_1(\mathbf{x}_1, \mathbf{x}_1^{'})\phi_p(\mathbf{x}_1^{'})d\mathbf{x}_1 d\mathbf{x}_1^{'}. \tag{2.59}$$

The correspondence between the one-electron reduced density defined over spatial (and spin) coordinates, and the one-electron density matrix defined over spin orbitals is clear.

We now consider the second-order reduced density matrix, defined as the normalized integral of the N-electron density matrix over the coordinates of all but two electrons:

$$\gamma_2(\mathbf{x}_1, \mathbf{x}_2, \mathbf{x}_1^{'}, \mathbf{x}_2^{'}) = \frac{N(N-1)}{2}\int \Psi(\mathbf{x}_1, \mathbf{x}_2, \mathbf{x}_3, \ldots, \mathbf{x}_N)\Psi^*(\mathbf{x}_1^{'}, \mathbf{x}_2^{'}, \mathbf{x}_3, \ldots, \mathbf{x}_N)d\mathbf{x}_3 \cdots d\mathbf{x}_N. \tag{2.60}$$

For readability, we will skip the derivation, but it can be shown that

$$\gamma_2(\mathbf{x}_1, \mathbf{x}_2, \mathbf{x}_1^{'}, \mathbf{x}_2^{'}) = \frac{1}{2}\sum_{pqrs}{}^2D_{qs}^{pr}\phi_p^*(\mathbf{x}_1^{'})\phi_q(\mathbf{x}_1)\phi_r^*(\mathbf{x}_2^{'})\phi_s(\mathbf{x}_2), \tag{2.61}$$

and

$$\langle\Psi|\hat{a}_p^\dagger\hat{a}_r^\dagger\hat{a}_s\hat{a}_q|\Psi\rangle = 2\int \phi_q^*(\mathbf{x}_1)\phi_s^*(\mathbf{x}_2)\gamma_2(\mathbf{x}_1, \mathbf{x}_2, \mathbf{x}_1^{'}, \mathbf{x}_2^{'})\phi_p(\mathbf{x}_1^{'})\phi_r(\mathbf{x}_2^{'})d\mathbf{x}_1 d\mathbf{x}_2 d\mathbf{x}_1^{'} d\mathbf{x}_2^{'}, \tag{2.62}$$

demonstrating again the clear correspondence between a two-electron reduced density matrix defined over spatial (and spin) coordinates, and a two-electron density matrix defined over spin orbitals.

2.4 A brief history of reduced density matrix-based methods in quantum chemistry

2.4.1 The 1950s

The advent of reduced density matrix (RDM)-based approaches for quantum chemistry can be traced back to Coleman's realization, in the summer of 1951, that the ground state energy of a many-electron system could be written in terms of the 2-electron reduced density matrix. However, his attempt to demonstrate the utility of this approach for the Li atom using a two-electron RDM constrained to obey trace, anti-symmetry (with respect to particle exchange) and hermiticity conditions yielded a ground state energy that was 10% lower than the observed (experimental) value. He realized from this experience the need to impose some more limitations on the allowed 2RDM.

A similar approach to Coleman's was taken by Mayer in 1955 to compute the electron correlation energy of an electron gas by finding the elements of a two-electron density matrix that would yield the lowest energy. The two-electron density matrix that Mayer used was constrained to obey antisymmetry, hermiticity, as well as trace and contraction conditions. Even though his results showed some promise, in 1957, Tredgold[214] and Mizuno[145] proved that, for systems of more than two electrons, Mayer's approach could yield 2RDMs that were not N-representable, that is, not derivable from an antisymmetric N-particle wavefunction, and corresponded to ground state energies that were much too low. Both Mizuno and Tredgold conclude that further investigation into the properties of RDMs was necessary before they could be used as a basic variable in electronic structure calculations.

2.4.2 The 1960s-1980s

During the 1960s, it had become clear that the N-representability problem would have to be solved before the 2RDM could be used reliably to determine the ground state energy, The problem attracted the interest of mathematicians, theoretical physicists and chemists, and culminated in a series of conferences that sought to understand the properties of RDMs, and whether RDMs could indeed be variables in solving the many-electron problem. A

series of six conferences were held at different times between 1967-1985. According to an account by Rosina, the structure and symmetries of RDMs, as well as the possibility of variational calculations were of particular interest. During this period, several key works such as Garrod and Percus' *Reduction of the N-particle variational problem* [61], Garrod, Mihailović and Rosina's *Variational approach to the two-body densitry matrix*[60], Cohen and Frishberg's *Hierarchy of equations for reduced density matrices*[37] and Nakatsuji's *Equation for the direct determination of the density matrix*[152] were published. Garrod and Percus' paper pointed out that N-representability conditions on the two-electron operator implied positivity of an associated operator of the same rank. These rest of the works pointed out that the solution of Schrödinger's equation involving the a given RDM would have a dependence on higher order RDMs. In particular, solving the contracted Schrödinger equation involving the 2RDM would require knowledge of the 4RDM.

2.4.3 The 1990s

From the late 1970s to the early 1990s, research output on RDMs and their application to solving the many-electron problem appears to have waned, until in 1993 and soon after in 1994, when Colmenero and Valdemoro published two papers that turned out to motivate several publications, by Mazziotti particularly, in the latter half of the decade. The first paper demonstrated how approximate higher order RDMs could be obtained in terms of lower order ones[39], and the second demonstrated how the Schrödinger equation involving the 2RDM could be solved in a self-consistent field procedure[40]. During the latter part of the decade, Mazziotti published a number of papers on solving Schrödinger equations involving the 2- and 3-RDM, formulating and applying new techniques by which the 4- and 5-RDMs could be reconstructed from lower-order RDMs.

2.4.4 The 2000s to present

The 2000s saw significant progress in the advancement of RDM-based methods for many-electron systems. Perhaps the most significant of these was the generalization of the positivity conditions to a hierarchy of N-representability conditions[1]. With this form of N-

representability constraints, one could accurately determine, using variational means, the lower bound of an energy functional expressed in terms of the 2RDM. The variational determination of the energy with positivity constraints yields a semidefinite programming (SDP) problem which can be solved by applying semidefinite programming approaches. In fact, this period saw the application of semidefinite programming techniques[221], which included primal-dual interior-point methods[239, 5] and boundary-point methods[176, 123, 138] to the SDP problem. Implementations of the two-positivity conditions first published by Garrod and Percus[61], as well as that of various three- or partial three- positivity conditions[51, 139, 151, 24, 249] were reported and the accuracy of energies obtained with RDMs satisfying those constraints was found to be satisfactory for the various many-electron systems investigated. From 2010 onwards, we have the first publications of implementations of complete active space self-consistent field (CASSCF) methods where the full CI calculation in the active space is replaced with an RDM-driven procedure. We see the first such implementation from Mazziotti's group in 2011[167], and in 2016, a large scale implementation of this approach from the DePrince group[57].

CHAPTER 3

THE ELECTRON CORRELATION PROBLEM

The goal of most of quantum chemistry is to develop theoretical models and numerical algorithms with which molecular properties can be accurately determined. In electronic structure theory, one often works within the *non*-relativistic and Born-Oppenheimer[21] approximations, with the goal of solving the electronic Schrödinger equation:

$$\hat{H}_e \Psi_e(\mathbf{r}; \mathbf{R}) = E_e \Psi_e(\mathbf{r}; \mathbf{R}). \tag{3.1}$$

The solution of the electronic Schrödinger equation within the orbital approximation has been a major driver of research efforts in electronic structure theory over the last several decades. The challenge of accurately treating electron correlation in chemically relevant molecules has been at the center of these efforts. In order to define correlation effects more concretely, we need to look at two approaches that can be used to solve the electronic Schrödinger equation: the full configuration interaction (CI)[209, 73, 55, 198] and the Hartree-Fock (HF) [70, 54, 203] methods.

3.1 Full configuration interaction

Given a set of spin orbitals with which electronic configurations can be constructed, the exact solution to the electronic Schrödinger equation may be written as a linear combination of all possible electronic configurations that can be constructed from that set of spin orbitals. The full CI wavefunction is often expressed in terms of a reference electronic configuration, as well as other configurations generated from that same reference by rearranging the electrons. The full CI wavefunction may be written

$$|\Psi\rangle = \sum_i c_i |\Phi_i\rangle, \tag{3.2}$$

where c_i is an expansion coefficient associated with the configuration $|\Phi_i\rangle$. We can write down an energy functional in terms of the full CI wavefunction:

$$\langle\Psi|\hat{H}|\Psi\rangle = \sum_{ij} c_i^* c_j \langle\Phi_i|\hat{H}|\Phi_j\rangle. \tag{3.3}$$

This functional can be variationally minimized with the requirement that the wavefunction stays normalized, that is,

$$\langle\Psi|\Psi\rangle = \sum_{ij} c_i^* c_j \langle\phi_i|\phi_j\rangle = 1 \tag{3.4}$$

during the minimization. This can be done using Lagrange's method of multipliers. We start by defining a Lagrangian $\mathcal{L}$:

$$\mathcal{L} = \sum_{ij} c_i^* c_j \langle\Phi_i|\hat{H}|\Phi_j\rangle - E(\sum_{ij} c_i^* c_j \langle\phi_i|\phi_j\rangle - 1). \tag{3.5}$$

Here, E denotes a Lagrangian multiplier. Equation 3.5 can be rewritten more compactly as

$$\mathcal{L} = \sum_{ij} c_i^* c_j H_{ij} - E(c_i^* c_j S_{ij} - 1) \tag{3.6}$$

where

$$H_{ij} = \langle\Phi_i|\hat{H}|\Phi_j\rangle \tag{3.7}$$

and

$$S_{ij} = \langle\phi_i|\phi_j\rangle. \tag{3.8}$$

If we set the first variation in $\mathcal{L}$ to 0 we get

$$\delta\mathcal{L} = \sum_i \delta c_i^* \big[\sum_j H_{ij} c_j - E S_{ij} c_j\big] + \text{c.c.} = 0 \tag{3.9}$$

where "c.c." refers to the complex conjugate of the first term on the right hand side. $\delta\mathcal{L}$ can only be 0 if

$$\big[\sum_j H_{ij} c_j - E S_{ij} c_j\big] = 0. \tag{3.10}$$

This result can be written in matrix notation as

$$\mathbf{Hc} = E\mathbf{Sc} \tag{3.11}$$

If the basis functions $\{|\Phi_i\rangle\}$ are orthonormal, then $S_{ij} = \delta_{ij}$ and

$$\mathbf{Hc} = E\mathbf{c}. \tag{3.12}$$

It is apparent now that the full CI procedure involves the construction and diagonalization of $\mathbf{H}$ in the basis of Slater determinants $\{|\Phi_i\rangle\}$. In general, the number of determinants will be $\binom{N}{m}$, where N is the number of spin orbitals and m is the number of electrons. Solving the full CI eigenvalue problem would involve diagonalizing a matrix of dimension $\binom{N}{m}$ times $\binom{N}{m}$. The Slater-Condon rules can be applied to reduce the computational cost of computing elements of $\mathbf{H}$, since some of them will be 0. Special algorithms for solving full CI at a computational cost much less than that of diagonalizing the entire matrix $\mathbf{H}$ have been published [94, 161], but even these approaches can only be applied to modestly-sized many-electron systems, since the computational is dependent on the number of determinants, which grows exponentially. As an example, a calculation involving benzene in a correlation consistent polarized valence double zeta basis (cc-pVDZ) basis set[1] with full CI would involve over 10^{31} determinants!

Although it is conceptually simple, the full CI model is not commonly used because of its high computational cost. Calculations on most molecules relevant to chemistry are intractable, even with modestly-sized one-electron basis sets. However, for small-enough systems, it is the model against which other electronic structure theory methods are benchmarked.

3.2 The Hartree-Fock method

Hartree-Fock (HF) is the simplest wavefunction model in quantum chemistry. The HF wavefunction is a single configuration of spin-orbitals. Here, we briefly derive the equations of Hartree-Fock theory.

[1] Five basis functions for each hydrogen, two to describe the $1s$ orbital, and three functions for polarization ($2s1p$); and for 14 for each carbon: three to describe the 1s and 2s orbitals, two each for the three $2p$ orbitals, and five to describe polarization(3s2p1d)

The electronic Hamiltonian can be written in second quantization notation as

$$\hat{H} = \sum_{pq} h_{pq} \hat{a}_p^\dagger \hat{a}_q + \frac{1}{2} \sum_{pqrs} (pq|rs) \hat{a}_p^\dagger \hat{a}_r^\dagger \hat{a}_s \hat{a}_q, \tag{3.13}$$

where one- and two-electron operators are as described in Chapter 2, h_{pq} denotes a one-electron integral, and $(pq|rs)$ denotes a two-electron integral written in Mulliken notation. One can use the rules for obtaining matrix elements between one- and two-electron operators to show that the electronic energy can be written in terms of spin-orbitals, and the one- and two-electron integrals:

$$E_{HF} = \sum_{i}^{N} (i|\hat{h}|i) + \frac{1}{2} \sum_{ij}^{N} [(ii|jj) - (ij|ji)]. \tag{3.14}$$

The energy functional in HF theory is thus a function of spin-orbitals. The functional can be minimized with the constraint that the spin orbitals remain orthonormal:

$$\langle \phi_i | \phi_j \rangle = \delta_{ij}. \tag{3.15}$$

We can do this by defining a Lagrangian $\mathcal{L}$:

$$\mathcal{L}[\{\phi_i\}] = E_{HF}[\{\phi_i\}] - \sum_{ij} \epsilon_{ij} (\langle \phi_i | \phi_j \rangle - \delta_{ij}), \tag{3.16}$$

where

$$\langle \phi_i | \phi_j \rangle = \int \phi_i^*(\mathbf{x}) \phi_j(\mathbf{x}) d\mathbf{x}, \tag{3.17}$$

and ϵ_{ij} are Lagrange multipliers. By considering the change to the energy functional when ϕ_i changes by a small amount to $\phi_i + \delta\phi_i$, and then setting that change to 0, one obtains, after some algebraic manipulation, the following equation:

$$h(\mathbf{x}_1)\phi_i(\mathbf{x}_1) + \sum_{j \neq i} [\int d\mathbf{x}_2 \phi_j^*(\mathbf{x}_2) \phi_j(\mathbf{x}_2) r_{12}^{-1}] \phi_i(\mathbf{x}_1) - \sum_{j \neq i} [\int d\mathbf{x}_2 |\phi_j^*(\mathbf{x}_2) \phi_i(\mathbf{x}_2) r_{12}^{-1}] \phi_j(\mathbf{x}_1) = \epsilon_i \phi_i(\mathbf{x}_1), \tag{3.18}$$

with ϵ_i replacing ϵ_{ij} since ϵ_{ij} can be transformed so that only diagonal elements need to be picked for each orbital i

$$\epsilon_i = \epsilon_{ij} \delta_{ij}. \tag{3.19}$$

The second term on the left hand side of 3.18 contains the expression

$$\int d\mathbf{x}_2 \phi_j^*(\mathbf{x}_2)\phi_j(\mathbf{x}_2) r_{12}^{-1}, \tag{3.20}$$

which can be thought of as the Coulomb repulsion experienced by an electron in spin orbital ϕ_i at $\mathbf{x}_1$ due to the presence of another electron in ϕ_j and this repulsion is weighted with a probability density $\phi_j^*(\mathbf{x}_2)\phi_j(\mathbf{x}_2)$ that the electron in ϕ_j occupies the volume element $d\mathbf{x}_2$ at $\mathbf{x}_2$. Thus the sum in the second term can be considered to give the Coulomb interaction of an electron in spin-orbital ϕ_i with the average field of all of the other $N-1$ electrons. The third term looks similar to the second one, except that spin orbitals ϕ_i and ϕ_j are interchanged. It is thus known as the exchange term. At this point, a Coulomb operator $\mathcal{J}$ can be defined:

$$\mathcal{J}_j(\mathbf{x}_1) = \int d\mathbf{x}_2 \phi_j^*(\mathbf{x}_2)\phi_j(\mathbf{x}_2) r_{12}^{-1}], \tag{3.21}$$

and it gives the average potential at $\mathbf{x}_1$ due to the charge from the electron in orbital ϕ_j. The exchange operator $\mathcal{K}$, meanwhile, can be defined

$$\mathcal{K}_j(\mathbf{x}_1)\phi_i(\mathbf{x}_1) = [\int d\mathbf{x}_2 |\phi_j^*(\mathbf{x}_2)\phi_i(\mathbf{x}_2) r_{12}^{-1} \phi_i(\mathbf{x}_2)]\phi_j(\mathbf{x}_2). \tag{3.22}$$

The HF equations can now be written more compactly as

$$[h(\mathbf{x}_1) + \sum_{j\neq i} \mathcal{J}_j(\mathbf{x}_1) - \sum_{j\neq i} \mathcal{K}_j(\mathbf{x}_1)]\phi_i(\mathbf{x}_1) = \epsilon_i \phi_i(\mathbf{x}_1). \tag{3.23}$$

It is important to note that when $i = j$, $[\mathcal{J}_j(\mathbf{x}_1) - \mathcal{K}_j(\mathbf{x}_1)]\phi_i(\mathbf{x}_1) = 0$, so that the HF equations can be written as eigenvalue problems:

$$f(\mathbf{x}_1)\phi_i(\mathbf{x}_1) = \epsilon_i \phi_i(\mathbf{x}_1) \tag{3.24}$$

where f is defined

$$f(\mathbf{x}_1) = h(\mathbf{x}_1) + \sum_j \mathcal{J}_j(\mathbf{x}_1) - \mathcal{K}_j(\mathbf{x}_1), \tag{3.25}$$

and is the well-known Fock operator. The spin orbitals in these HF equations are usually expressed in terms atomic orbital basis functions

$$\phi_i = \sum_{\mu=1}^{K} C_{\mu i}\chi_\mu, \tag{3.26}$$

with μ being an atomic orbital label. As a result, 3.25 can be written

$$f(\mathbf{x}_1)\sum_{\nu} C_{\nu i}\chi_{\nu}(\mathbf{x}_1) = \epsilon_i \sum_{\nu} C_{\nu i}\chi_{\nu}(\mathbf{x}_1), \tag{3.27}$$

where ν is just another label for atomic orbitals. Left multiplication of 3.27 by χ_{μ}^* and integration yields the Hartree-Fock-Roothaan equations, the matrix form of which is:

$$\sum_{\nu} F_{\mu\nu}C_{\nu i} = \epsilon_i \sum_{\nu} S_{\mu\nu}C_{\nu i}, \tag{3.28}$$

where

$$S_{\mu\nu} = \int d\mathbf{x}_1 \chi_{\mu}^*(\mathbf{x}_1)\chi_{\nu}^*(\mathbf{x}_1), \tag{3.29}$$

and

$$F_{\mu\nu} = \int d\mathbf{x}_1 \chi_{\mu}^*(\mathbf{x}_1) f(\mathbf{x}_1)\chi_{\nu}^*(\mathbf{x}_1). \tag{3.30}$$

Effectively, the HF approach in an orbital basis reduced to an eigenvalue problem, solved self-consistently. The rate determining step in HF is usually the computation of two-electron integrals, which are needed in order to construct the Fock matrix. The formal scaling of the approach is $\mathcal{O}(N^4)$, where N is the size of the number of atomic-orbital centered basis functions used to describe the atomic orbitals.

In order to assess the performance of HF, we generate the potential energy curve of the ${}^1\Sigma_g^+$ state in molecular H_2 by plotting the total molecular energy computed at various interatomic/H-H distances, and we compare it to the curve obtained from full CI, as is illustrated in Figure 3.1.[2] We can see that full CI predicts qualitatively correctly the dissociation of molecular H_2 into atomic fragments, while restricted Hartree-Fock (RHF) fails. A comparison of the full CI and the RHF wavefunctions provides an explanation for why RHF fails. In full CI, the ${}^1\Sigma_g^+$ is a linear combination of two determinants: $|\sigma_{\mathbf{g}}\bar{\sigma}_{\mathbf{g}}\rangle$ and $|\sigma_{\mathbf{u}}\bar{\sigma}_{\mathbf{u}}\rangle$, with the bar (or lack thereof) representing β (α) spin, whereas the RHF wavefunction consists of the single determinant $|\sigma_{\mathbf{g}}\bar{\sigma}_{\mathbf{g}}\rangle$. At short bond lengths, the two configurations $|\sigma_{\mathbf{g}}\bar{\sigma}_{\mathbf{g}}\rangle$ and $|\sigma_{\mathbf{u}}\bar{\sigma}_{\mathbf{u}}\rangle$ are well separated in terms of energy, so the single configuration $|\sigma_{\mathbf{g}}\bar{\sigma}_{\mathbf{g}}\rangle$ is not a bad approximation to the ground state wavefunction. However, at long bond lengths, the

[2]Note that the results presented in the figure are within the accuracy afforded by the STO-3G basis set, which assigns one basis function per atomic orbital.

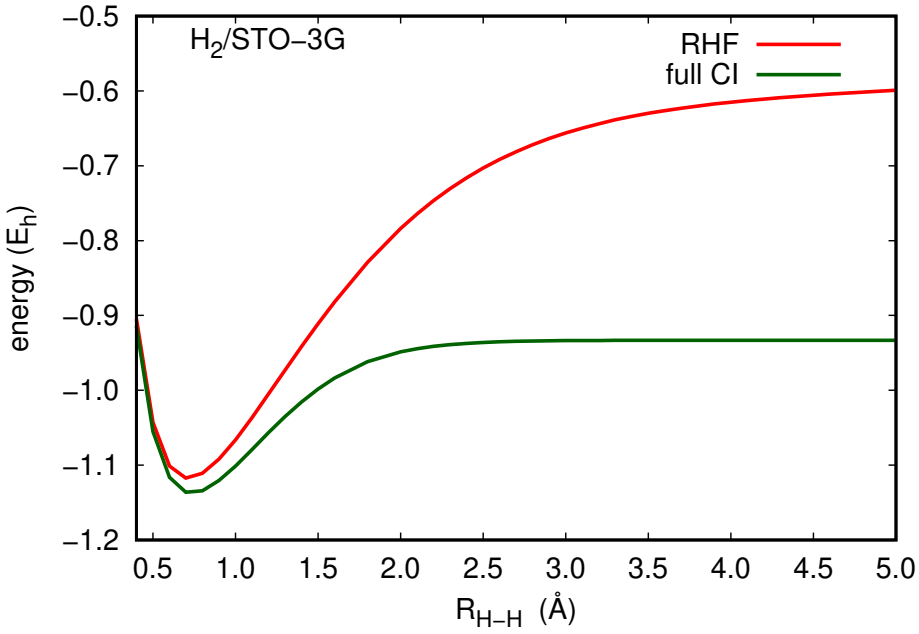

Figure 3.1: Potential energy curves from full CI and RHF of the ${}^1\Sigma_g^+$ state of H_2 undergoing symmetric dissociation.

configurations $|\sigma_{\mathbf{g}}\bar{\sigma}_{\mathbf{g}}\rangle$ and $|\sigma_{\mathbf{u}}\bar{\sigma}_{\mathbf{u}}\rangle$ become degenerate, so the single configuration that defines the RHF wavefunction is then no longer a good approximation to the full CI wavefunction. More generally, RHF fails to model bond dissociation processes due to near-degeneracies of electronic configurations that comprise the wavefunction. The difference between an energy computed by full CI and another by RHF at dissociation is said to arise due to the failure of the single configuration to account for correlation effects arising from near-degeneracies in electronic configurations that comprise the wavefunction. Such correlation effects are termed *non*-dynamical, to differentiate them from so-called *dynamical* correlation effects, whose origin is quite different and can be rationalized as the insufficient treatment by RHF of short range, instantaneous electron-electron interactions. To make this notion more apparent, we note that the minimum energy predicted by restricted Hartree-Fock (RHF) is higher than that predicted by full CI by nearly 20 mE_h, a significant difference for a two-electron sys-

tem. Furthermore, RHF predicts an equilibrium bond length that is shorter than the one predicted by full CI. A method such as full CI, which includes the determinant $|\sigma_{\mathbf{u}}\bar{\sigma}_{\mathbf{u}}\rangle$, which is made up of orbitals that have nodes at the center of the molecule, amounts to a reduction in the repulsion between electrons. In general, a multiconfigurational description of the wavefunction is needed to account for correlation effects. Such a description is particularly important in accounting for non-dynamical correlation effects. We can see, for instance, that the difference between the full CI and RHF energies at longer H-H distances is nearly an order of magnitude higher than it is near the equilibrium.

3.3 Electron correlation energy

The electron correlation energy of a molecule, E_{corr}, is defined as the difference between its exact energy and the HF energy computed in a complete basis:

$$E_{corr} = E_{exact} - E_{HF}^{\infty}, \tag{3.31}$$

where E_{HF}^{∞} denotes the HF energy computed with an infinitely large or complete basis set. Usually, the exact energy of a molecule is not known, but an estimate can be computed from a full CI calculation using a finite basis set. For this reason, it is generally easier to calculate a basis set correlation energy, which is defined

$$E_{corr}^{basis} = E_{FCI}^{basis} - E_{HF}^{basis}, \tag{3.32}$$

where E_{FCI}^{basis} and E_{HF}^{basis} are the full CI and HF energies, respectively, calculated within some basis set approximation.

The electron correlation energy can be considered to be a measure of the errors of HF theory. Electron correlation effects contribute an error of roughly 23 kcal/mol per electron pair[179, 81]. Therefore, the development of theoretical models and computational algorithms to compute accurate correlation energies [179, 81, 16, 191, 235, 178, 243] has been a major focus in quantum chemistry since the 1950s. Two broad classes of methods can be defined in the context of electron correlation in molecular systems:

- methods designed specifically to treat correlation where a single electronic configuration dominates, such as in the bonding region of the $^1\Sigma_g^+$ state of H_2, and
- multiconfigurational methods that attempt to treat electron correlation over the entire extent of a potential energy curve or surface.

This dissertation will describe work done to develop a complete active space (CAS) approach which is suited to addressing the electron correlation problem in general, over the entire extent of a potential energy curve or surface.

3.4 Complete active space self-consistent field approaches

It is well acknowledged that a good model for molecular electronic structure ought to be variational, and size consistent, that is, the sum of the energies of separate fragments should equal the energy computed when they are all considered together but at large separations. A good model for the electronic wavefunction ought to reproduce the energy correctly over the entire potential energy surface. Approaches based on multiple configurations have been applied to the electronic structure problem for both ground and excited states. Since full CI is not always feasible, one must select beforehand the configurations whose linear combination defines the wavefunction. This is often done by identifying a subset of orbitals (an *active* space) important to the electronic structure and including all the determinants or configuration state functions[3]. We can write down the energy as an expectation value of the Hamiltonian operator. This yields

$$E = \sum_{IJ} c_I^* c_J H_{IJ}, \tag{3.33}$$

where c_I and c_J are expansion coefficients and

$$H_{IJ} = \langle \Phi_I | \hat{H} | \Phi_J \rangle. \tag{3.34}$$

Using unitary group generators[196]

$$\hat{E}_{pq} = \hat{a}_{p\alpha}^\dagger \hat{a}_{q\alpha} + \hat{a}_{p\beta}^\dagger \hat{a}_{q\beta}, \tag{3.35}$$

[3]These are eigenfunctions of the $\hat{S}^2$ operator

where $\hat{a}^\dagger_{p\alpha}$ is an operator whose action is to create an electron in orbital p with α spin, and $\hat{a}_{q\alpha}$ is an operator whose action is to annihilate from orbital p an electron with α spin, the Hamiltonian can be written in terms of the unitary group generators as

$$\hat{H} = \sum_{pq}(p|h|q)\hat{E}_{pq} + \frac{1}{2}\sum_{pqrs}(pq|rs)(\hat{E}_{pq}\hat{E}_{rs} - \delta_{qr}\hat{E}_{ps}), \tag{3.36}$$

so that each matrix element $H_{IJ} = \langle\Phi_I|\hat{H}|\Phi_J\rangle$ can be written

$$H_{IJ} = \sum_{pq} {}^1D^{p,IJ}_q h_{pq} + \frac{1}{2}\sum_{pqrs} {}^2D^{pr,IJ}_{qs}(pq|rs), \tag{3.37}$$

where ${}^1D^{p,IJ}_q$ and ${}^2D^{pr,IJ}_{qs}$ are coupling coefficients

$${}^1D^{p,IJ}_q = \langle\Phi_I|\hat{E}_{pq}|\Phi_J\rangle, \tag{3.38}$$

and

$${}^2D^{pr,IJ}_{qs} = \langle\Phi_I|\hat{E}_{pq}\hat{E}_{rs} - \delta_{qr}\hat{E}_{ps}|\Phi_J\rangle. \tag{3.39}$$

These coupling coefficients have the same properties as the density matrices discussed in Chapter 2. For instance,

$${}^1D^{p,IJ}_q = ({}^1D^{q,IJ}_p)^* \tag{3.40}$$

and

$${}^2D^{pr,IJ}_{qs} = {}^2D^{rp,IJ}_{sq} = ({}^2D^{sq,IJ}_{rp})^* = ({}^2D^{qs,IJ}_{pr})^* \tag{3.41}$$

Using these properties of the coupling coefficients, we can write down the energy as

$$E = \sum_{IJ} c^*_I c_J \big[\sum_{pq} {}^1D^{p,IJ}_q \cdot h_{pq} + \frac{1}{2}\cdot {}^2D^{pr,IJ}_{qs}\cdot(pq|rs)\big], \tag{3.42}$$

or, even more compactly,

$$E = \sum_{pq} h_{pq}\cdot {}^1D^p_q + \frac{1}{2}\cdot {}^2D^{pr}_{qs}\cdot(pq|rs), \tag{3.43}$$

with

$${}^1D^p_q = \sum_{IJ} c^*_I c_J \cdot {}^1D^{p,IJ}_q, \tag{3.44}$$

and

$$ {}^2D^{pr}_{qs} = \sum_{IJ} c^*_I c_J \cdot {}^2D^{pr,IJ}_{qs}. \tag{3.45} $$

${}^1D^p_q$ and ${}^2D^{pr}_{qs}$ define elements of one and two-particle density matrices, respectively. Since the energy functional in the complete active space complete active space self-consistent field (CASSCF) method depends on the configuration interaction (CI) coefficients as well as molecular orbitals, its variational minimization occurs in two steps

- The determination of CI coefficients by diagonalization, similar to the procedure for full CI.
- Optimization of the initial set of orbitals by a unitary transformation.

Overall, the feasibility of CASSCF depends on the size of the active space since a full CI expansion in the active space is necessary. The size of the active space that can be treated with CASSCF has grown larger with improvements in computer algorithms and hardware, but, due to its steeply scaling computational cost, application has been limited to active spaces of less than 18 electrons in 18 orbitals. Even though an (18e, 18o) active space is small when compared to the number of valence electrons and orbitals in common molecules, the CASSCF approach has been applied to the study of large systems using much smaller active spaces. As long as the chemically relevant orbitals are all included in the active space, a CASSCF wavefunction will provide a good qualitative description of the electronic structure.

Yet active space selection remains a challenge, particularly with CI-driven CASSCF. One needs not only have the chemical intuition of the many-electron system to be investigated– they also need to make sure the active space size is small enough to allow for tractable computations. Attempts to automate active space selection[204, 190, 205, 13] have not done away with these challenges. To make matters worse, an active space larger than a full valence active space is seldom needed to properly correlate the motion of electrons, for example, in cases where most of the valence orbitals are occupied. This is exemplified by $[Cu_2O_2]^{2+}$ [127, 101, 241, 14], a compound in which the valence orbitals of the Cu atoms are filled. In this system, one needs to include the $4s$ as well as the $4d$ orbitals in the active space to get a

good qualitative description of the wavefunction. Another example for which a full valence active space may not suffice is the CAS treatment of molecular fluorine, F_2. For this system, the molecular orbitals from the $3p$ atomic orbitals need to be included in the active space. Given the challenge of active space selection as well as the fact that active spaces larger than (18e,18o) are simply necessary in some cases has led to the development of active space solvers based on the density matrix renormalization group (DMRG)[62, 240, 241, 237, 208, 120] and the variational two-electron reduced density matrix (v2RDM-)[64, 57] approaches.

3.5 Dynamical correlation energy

Since the CASSCF method can be considered to be an incomplete configuration interaction, further correction of the CASSCF wavefunction and the energy is usually needed in order to achieve quantitative agreement with full CI. If the active space is carefully selected, CASSCF presumably accounts for all non-dynamical correlation effects. Any subsequent corrections to the CASSCF wavefunction or the CASSCF energy would then seek to address dynamical correlation effects. To illustrate how important the correction for dynamical correlation is, one can look at the rather extreme case of the potential energy curve of the ${}^1\Sigma_g^+$ state of Cr_2, for which the CASSCF energy needs to be corrected by a large amount of dynamical correlation energy in order to obtain a bound potential curve[29, 6, 144, 102]. Probably the most popular approach to correct for dynamical correlation energy for CAS references is multireference perturbation theory[7, 88, 8, 9, 108, 68]. Other less popular approaches include multireference configuration interaction (MRCI)[25, 26, 69, 230], multireference coupled-cluster (MRCC)[118, 97, 171, 79, 17, 78, 174, 173, 172, 45, 122, 121, 202, 33, 163, 110, 109, 111, 164, 149]. and multireference pair-density functional theory (MC-PDFT)[59, 112, 146]. Recently, another approach to account for dynamical correlation effects for CAS references was published by Pernal and coworkers[166, 170]. This approach is based on an adiabatic connection (AC) approach between a system of electrons described at the CASSCF level of theory, and another described by full CI.

CHAPTER 4

THE VARIATIONAL TWO-ELECTRON REDUCED DENSITY MATRIX COMPLETE ACTIVE SPACE SELF-CONSISTENT FIELD METHOD

The derivation outlined in this chapter follows that from Refs. 57 and 126. In this chapter, the convention for orbital index labels in complete active space self-consistent field (CASSCF) methods is followed: the indices i, j, k, and l represent inactive, doubly occupied orbitals; t, u, v, w, x, and y represent active orbitals; a, b, c, and d correspond to external (empty) orbitals; and p, q, r, and s represent general orbitals.

4.1 The active space energy

In the CASSCF method, the active space Hamiltonian can be written in the notation of second quantization as

$$\hat{H} = \sum_{tu} h_{tu} E^t_u + \frac{1}{2} \sum_{tuvw} (tv|uw)(E^t_v E^u_w - \delta_{vu} E^t_w), \tag{4.1}$$

where E^t_u is a unitary group generator[196].

$$E^t_u = \hat{a}^\dagger_{t_\alpha} \hat{a}_{u_\alpha} + \hat{a}^\dagger_{t_\beta} \hat{a}_{u_\beta}, \tag{4.2}$$

$\hat{a}^\dagger$ and $\hat{a}$ represent creation and annihilation operators, and the Greek indices α and β denote up and down spin. The symbol $(tv|uw)$ represents a two-electron repulsion integral, and h_{tu} represents the sum of electron kinetic energy integrals (T_{tu}), electron-nuclear potential energy integrals (V_{tu}), and the Coulomb and exchange contributions from electrons in orbitals that are restricted to be doubly occupied.

$$h_{tu} = T_{tu} + V_{tu} + \sum_i [2(ii|tu) - (iu|ti)]. \tag{4.3}$$

The active space electronic energy $E_{act} = \langle\Psi|\hat{H}|\Psi\rangle$ can then be written:

$$E_{\text{act}} = \sum_{tu} h_{tu}\, {}^1D_u^t + \frac{1}{2}\sum_{tuvw}(tv|uw)\, {}^2D_{vw}^{tu}, \tag{4.4}$$

where

$${}^1D_u^t = \langle\Psi|\hat{a}_t^\dagger \hat{a}_u|\Psi\rangle, \tag{4.5}$$

and

$${}^2D_{vw}^{tu} = \langle\Psi|\hat{a}_t^\dagger \hat{a}_u^\dagger \hat{a}_w \hat{a}_v|\Psi\rangle, \tag{4.6}$$

define the elements of the active-space 1- and 2-RDM, respectively.

In the v2RDM approach to CASSCF, the active space energy functional is minimized with respect to variations the elements of the active space 1- and 2-RDM. The variable 1- and 2-RDMs are constrained to satisfy known ensemble N-representability constraints during the minimization. If N-representability conditions are exactly satisfied, ground-state v2RDM- and CI-based CASSCF are equivalent. However, when the N-representability conditions are only approximately satisfied, say, from the application of a subset of the N-representability conditions, v2RDM-CASSCF provides a lower bound to the ground-state CI-CASSCF energy.

4.2 N-representability conditions

The active space 2RDM needs to have the same properties as the two-electron density matrices discussed in Chapters 2 and 3. One of the properties of two-electron density matrices is hermiticity, so the variable 2RDM in v2RDM-CASSCF needs to be constrained to be hermitian

$${}^2D_{vw}^{tu} = {}^2D_{tu}^{vw}. \tag{4.7}$$

The 2RDM should also obey antisymmetry with respect to the exchange of orbital indices

$${}^2D_{vw}^{tu} = -{}^2D_{vw}^{ut} = -{}^2D_{wv}^{tu} = {}^2D_{wv}^{ut}, \tag{4.8}$$

as well as trace constraints that preserve the number of pairs of electrons. For each spin block of the 2RDM,

$$\sum_{tu} {}^2D^{t_\alpha u_\alpha}_{t_\alpha u_\alpha} = N_\alpha(N_\alpha - 1), \tag{4.9}$$

$$\sum_{tu} {}^2D^{t_\beta u_\beta}_{t_\beta u_\beta} = N_\beta(N_\beta - 1), \tag{4.10}$$

$$\sum_{tu} {}^2D^{t_\alpha u_\beta}_{t_\alpha u_\beta} = N_\alpha N_\beta, \tag{4.11}$$

where α and β denote up or down spin, N_α and N_β represent the number of electrons of α or β spin, respectively, in the active space. Each spin block of the 2RDM should map correctly to the 1RDM,

$$(N_\alpha - 1)^1D^{t_\alpha}_{u_\alpha} = \sum_v {}^2D^{t_\alpha v_\alpha}_{u_\alpha v_\alpha}, \tag{4.12}$$

$$(N_\beta - 1)^1D^{t_\beta}_{u_\beta} = \sum_v {}^2D^{t_\beta v_\beta}_{u_\beta v_\beta}, \tag{4.13}$$

$$N_\beta {}^1D^{t_\alpha}_{u_\alpha} = \sum_v {}^2D^{t_\alpha v_\beta}_{u_\alpha v_\beta}, \tag{4.14}$$

$$N_\alpha {}^1D^{t_\beta}_{u_\beta} = \sum_v {}^2D^{v_\alpha t_\beta}_{v_\alpha u_\beta}. \tag{4.15}$$

The 2-RDM is also constrained to ensure a well-defined expectation value of $\hat{S}^2$, where S is the total spin angular momentum operator property of N-representable 2RDMs

$$\sum_{tu} {}^2D^{t_\alpha u_\beta}_{u_\alpha t_\beta} = \frac{1}{2}(N_\alpha + N_\beta) + \frac{1}{4}(N_\alpha - N_\beta)^2 - S(S+1), \tag{4.16}$$

since a well-defined $\hat{S}^2$ is a property of N-representable 2RDMs.[169, 63, 220]

Less trivial constraints on the N-representability of the 2-RDM include positivity constraints that ensure that particle probabilities or the eigenvalues of the RDMs remain non-negative. For the 2RDM, we can write

$${}^{\mathbf{2}}\mathbf{D} \succeq 0, \tag{4.17}$$

and for the 1-RDM

$${}^{\mathbf{1}}\mathbf{D} \succeq 0. \tag{4.18}$$

Positivity constraints are also enforced on the one-hole ($\mathbf{^1Q}$), the two-hole ($\mathbf{^2Q}$), and the electron-hole ($\mathbf{^2G}$) RDMs. The elements of these RDMs are defined

$$ {}^1Q^t_u = \langle\Psi|\hat{a}_t\hat{a}^\dagger_u|\Psi\rangle, \tag{4.19} $$

$$ {}^2Q^{tu}_{vw} = \langle\Psi|\hat{a}_t\hat{a}_u\hat{a}^\dagger_w\hat{a}^\dagger_v|\Psi\rangle, \tag{4.20} $$

and

$$ {}^2G^{tu}_{vw} = \langle\Psi|\hat{a}^\dagger_t\hat{a}_u\hat{a}^\dagger_w\hat{a}_v|\Psi\rangle. \tag{4.21} $$

Each of these RDMs must also correctly map to one another according to the anticommutation relations. These constraints on the two-body RDMs are the "PQG" constraints of Garrod and Percus.[61]. One can also consider the nonnegativity of the partial three-body RDM, $\mathbf{T2}$, [48, 249] defined as

$$ \mathbf{T2} = {}^3\mathbf{E} + {}^3\mathbf{F}, \tag{4.22} $$

where

$$ {}^3E^{tuv}_{wxy} = \langle\Psi|\hat{a}^\dagger_t\hat{a}^\dagger_u\hat{a}_v\hat{a}^\dagger_y\hat{a}_x\hat{a}_w|\Psi\rangle, \tag{4.23} $$

and

$$ {}^3F^{tuv}_{wxy} = \langle\Psi|\hat{a}^\dagger_t\hat{a}_u\hat{a}_v\hat{a}^\dagger_y\hat{a}^\dagger_x\hat{a}_w|\Psi\rangle. \tag{4.24} $$

The spin structures of the RDMs just described are:

$$ \mathbf{^1D} = \begin{pmatrix} {}^1D^\alpha_\alpha & 0 \\ 0 & {}^1D^\beta_\beta \end{pmatrix}. \tag{4.25} $$

The 1-hole RDM ($\mathbf{^1Q}$) has the same spin structure. The particle-particle RDM has three spin blocks expressed in the basis of two-particle basis functions (geminals) of $\alpha\alpha$, $\beta\beta$, and $\alpha\beta$ spin symmetry:

$$ \mathbf{^2D} = \begin{pmatrix} {}^2D^{\alpha\alpha}_{\alpha\alpha} & 0 & 0 \\ 0 & {}^2D^{\beta\beta}_{\beta\beta} & 0 \\ 0 & 0 & {}^2D^{\alpha\beta}_{\alpha\beta} \end{pmatrix}, \tag{4.26} $$

the hole-hole RDM ($\mathbf{^2Q}$) has the same structure, and the particle-hole RDM ($\mathbf{^2G}$) is given by:

$$ \mathbf{^2G} = \begin{pmatrix} {}^2G^{\alpha\alpha}_{\alpha\alpha} & {}^2G^{\alpha\alpha}_{\beta\beta} & 0 & 0 \\ {}^2G^{\beta\beta}_{\alpha\alpha} & {}^2G^{\beta\beta}_{\beta\beta} & 0 & 0 \\ 0 & 0 & {}^2G^{\alpha\beta}_{\alpha\beta} & 0 \\ 0 & 0 & 0 & {}^2G^{\beta\alpha}_{\beta\alpha} \end{pmatrix}. \tag{4.27} $$

. The partial three-body RDM, as defined in 4.22 has the following spin structure:

$$\mathbf{T2} = \begin{pmatrix} \mathbf{T2}^{\alpha\alpha\alpha}_{\alpha\alpha\alpha} & \mathbf{T2}^{\alpha\beta\beta}_{\alpha\alpha\alpha} & 0 & 0 & 0 & 0 \\ \mathbf{T2}^{\alpha\alpha\alpha}_{\alpha\beta\beta} & \mathbf{T2}^{\alpha\beta\beta}_{\alpha\beta\beta} & 0 & 0 & 0 & 0 \\ 0 & 0 & \mathbf{T2}^{\beta\alpha\alpha}_{\beta\alpha\alpha} & \mathbf{T2}^{\beta\beta\beta}_{\beta\alpha\alpha} & 0 & 0 \\ 0 & 0 & \mathbf{T2}^{\beta\alpha\alpha}_{\beta\beta\beta} & \mathbf{T2}^{\beta\beta\beta}_{\beta\beta\beta} & 0 & 0 \\ 0 & 0 & 0 & 0 & \mathbf{T2}^{\alpha\alpha\beta}_{\alpha\alpha\beta} & 0 \\ 0 & 0 & 0 & 0 & 0 & \mathbf{T2}^{\beta\beta\alpha}_{\beta\beta\alpha} \end{pmatrix}. \tag{4.28}$$

4.3 Semidefinite optimization

We minimize the energy given by Eq. (4.4) with respect to variations in the 1- and 2-RDM, subject to the constraints outlined above. Such a constrained optimization, involving both equality and inequality constraints, is a semidefinite programming (SDP) problem. The primal form of this problem can be written as:

$$\begin{aligned} \text{minimize} \quad & E_{\text{primal}} = \mathbf{c}^T \cdot \mathbf{x}, \\ \text{such that} \quad & \mathbf{Ax} = \mathbf{b}, \\ \text{and} \quad & M(\mathbf{x}) \succeq 0, \end{aligned} \tag{4.29}$$

where $\mathbf{x}$ is the primal solution vector, E_{primal} is the primal energy, ($\mathbf{A}$) is a matrix that maps the primal solution vector onto the set of constraints in vector ($\mathbf{b}$). The set of constraints is defined by the N-representability conditions described in section 4.2. The primal solution vector maps onto various RDMs according to

$$M(\mathbf{x}) = \begin{pmatrix} {}^1\mathbf{D} & 0 & 0 & 0 & 0 & 0 \\ 0 & {}^1\mathbf{Q} & 0 & 0 & 0 & 0 \\ 0 & 0 & {}^2\mathbf{D} & 0 & 0 & 0 \\ 0 & 0 & 0 & {}^2\mathbf{Q} & 0 & 0 \\ 0 & 0 & 0 & 0 & {}^2\mathbf{G} & 0 \\ 0 & 0 & 0 & 0 & 0 & \mathbf{T2} \end{pmatrix}. \tag{4.30}$$

The vector, $\mathbf{c}$, contains the one- and two-electron components of the Hamiltonian such that the primal energy and the energy given by Eq. (4.4) are equivalent. The SDP problem can also be written in its dual (complementary) form. Denoting the dual solution vectors as $\mathbf{y}$

and $\mathbf{z}$, the SDP problem can be restated:

$$\begin{aligned} \text{maximize} \quad & E_{\text{dual}} &&= \mathbf{b}^T \cdot \mathbf{y}, \\ \text{such that} \quad & \mathbf{z} &&= \mathbf{c} - \mathbf{A}^T\mathbf{y}, \\ \text{and} \quad & M(\mathbf{z}) &&\succeq 0, \end{aligned} \tag{4.31}$$

with E_{dual} representing the dual energy.

A boundary-point semidefinite optimization algorithm[176, 123, 138] is used to compute the primal and dual solutions. This happens iteratively, and for each iteration, the following is done:

1. The equation $\mathbf{A}\mathbf{A}^T\mathbf{y} = \mathbf{A}(\mathbf{c} - \mathbf{z}) + \mu(\mathbf{b} - \mathbf{A}\mathbf{x})$ is solved for $\mathbf{y}$ by conjugate gradient methods.

2. The primal and dual solution vectors $\mathbf{x}$ and $\mathbf{z}$ are updated by separating $\mathbf{U} = M(\mu\mathbf{x} + \mathbf{A}^T\mathbf{y} - \mathbf{c})$ into its positive and negative components (by diagonalization), then updating $\mathbf{x}$ and $\mathbf{z}$ by $M(\mathbf{x}) = \mathbf{U}(+)/\mu$ and $M(\mathbf{z}) = -\mathbf{U}(-)$.

Here, μ is a penalty parameter that controls how strictly the primal or dual constraints are enforced.[138]. The algorithm is considered converged when the primal error $||\mathbf{A}\mathbf{x} - \mathbf{b}||$, the dual error $||\mathbf{A}^T\mathbf{y} - \mathbf{c} + \mathbf{z}||$, and the primal/dual energy gap $|E_{\text{primal}} - E_{\text{dual}}|$ fall below specified thresholds.

The diagonalization step in step 2 is usually the most computationally demanding part of the SDP algorithm. That step determines the formal scaling of the v2RDM-CASSCF method. Storage requirements of the computer implementation of the method depend on the number of active orbitals as well as the number of N-representability constraints enforced. Table 4.1 summarizes the computational scaling of the v2RDM-CASSCF in terms of floating point operations and storage requirements for the two commonly enforced ensemble N-representability constraints.

4.4 Orbital optimization

There are two contributions to the v2RDM-CASSCF energy: one from the electrons in the active space, and another from electrons in spin (spatial) orbitals restricted to be

Table 4.1: Computational complexity of v2RDM-CASSCF

	N-representability condition	
	PQG	PQG+T2
[a] n	$\mathcal{O}(N_{act}^6)$	$\mathcal{O}(N_{act}^9)$
storage	$\mathcal{O}(N_{act}^4)$	$\mathcal{O}(N_{act}^6)$

[a] n: number of floating point operations.
N_{act} denotes the number of orbitals in the active space.

singly (doubly) occupied. The active space 2RDM is optimized *via* the SDP procedure. This optimization changes the elements of the 2RDM, making it necessary to minimize the total v2RDM-CASSCF energy with respect to all molecular orbitals. The optimization of RDMs and molecular orbitals can be done in a two-step fashion, with the optimization of the elements of the RDMs preceding that of the molecular orbitals, or in a quasi one-step fashion where orbitals are optimized after a specified number of iterations of the boundary-point algorithm. More details concerning the orbital optimization can be found in Ref. 57, but it suffices for now to be aware that orbital optimization is carried out by a unitary matrix that rotates non-redundant pairs of orbitals.

CHAPTER 5

ANALYTIC GRADIENTS FOR THE VARIATIONAL TWO-ELECTRON REDUCED DENSITY MATRIX COMPLETE ACTIVE SPACE SELF-CONSISTENT FIELD METHOD

5.1 Introduction

The complete active space self-consistent field (CASSCF) approach[184, 200, 201, 183] is an enormously important method in quantum chemistry. It enables the description of electronic states dominated by more than one electronic configuration. In the conventional formulation of CASSCF, the electronic structure of the active space is described by a full configuration interaction (CI) wave function. However, the size of the active space that can be routinely employed within CI-driven CASSCF is limited by the extremely unfavorable scaling of full CI. In practice, the exponential cost of full CI limits its application to active spaces comprised of at most 18 electrons in 18 orbitals. As a result, substantial effort has been dedicated to the development of alternative representations of the electronic structure of the active space. Some CI-based approaches include the restricted active space self-consistent field[161, 124], the generalized active space (GAS) self-consistent field[53, 119], the split GAS[113], the occupation-restricted multiple active spaces self-consistent field[83], and the full configuration interaction quantum Monte Carlo self-consistent field[212, 114].

On the other hand, methods that avoid CI altogether can lead to formally polynomially-scaling descriptions of the electronic structure of the active space. One of the most successful alternatives to CI-based CASSCF is that in which the active-space wave function is expressed as a matrix-product state as is done in the density-matrix renormalization group (DMRG) approach[233, 234, 194, 195, 143, 30, 127, 247, 101, 160, 210, 238, 93]. Less well known are methods based on the variational optimization of the two-electron reduced-density matrix (2-RDM)[61, 60, 141, 186, 49, 50, 151, 139, 133, 136, 249, 58, 27, 223, 56, 222]. Both DMRG-driven[62, 240, 241, 237, 208, 120] and variational 2-RDM (v2RDM)-driven[64, 57] CASSCF methods are capable of modeling active spaces as large or larger than 50 electrons in 50 orbitals.

We extend the applicability of v2RDM and v2RDM-CASSCF methods to the determination of analytic energy gradients. The semidefinite programming (SDP) algorithm utilized to obtain the ground-state 2-RDM provides a Lagrangian that is stationary with respect to variations in the elements of the 2-RDM. Hence, no additional response equations are required to determine the response of the 2-RDM to geometric perturbations, and orbital response contributions to the gradient are the same as those that arise in CI-based CASSCF methods.

This chapter is organized as follows. In section 5.2 the v2RDM Lagrangian is introduced and the procedures used to obtain the active-space 2-RDM are described. We then provide expressions for v2RDM-CASSCF analytic energy gradients, including orbital response contributions. In Sec. 5.3, we verify the correctness of our gradient implementation numerically, and we use the method to compute the equilibrium geometries for a set of twenty small molecules as well as pentacene.

5.2 Theory

In this Section we discuss the key aspects of our implementation of analytic gradients for v2RDM-CASSCF. We begin with a brief overview of the v2RDM approach that includes the minimization of the v2RDM energy subject to approximate N-representability conditions

and the orbital optimization. For a detailed discussion of our implementation of v2RDM-CASSCF the reader is referred to Ref. 57. We conclude this Section with the details of our implementation of analytic energy gradients within the framework of v2RDM-CASSCF. Throughout the paper, we follow the usual conventions for orbital index labels in CASSCF: the indices i, j, k, and l represent inactive (doubly occupied) orbitals; the indices t, u, v, w, x, and y span the active (partially occupied) orbitals; the indices a, b, c, and d correspond to external (empty) orbitals; and the indices p, q, r, and s represent general orbitals.

5.2.1 The active space energy

The relevant expressions for the active-space energy have been presented in 4.1.

5.2.2 Semidefinite optimization and the v2RDM Lagrangian

Our goal is to minimize the energy given by Eq. (4.4) with respect to variations in the 1- and 2-RDM, subject to N-representability constraints. Since the SDP procedure is a constrained optimization, the active-space energy is not stationary with respect to variations in the primal or dual solutions. For the evaluation of analytic energy gradients, we seek some active-space Lagrangian that is stationary with respect to all variable parameters. Fortunately, the boundary-point SDP algorithm we employ[176, 123, 138] provides just that; the procedure maximizes an augmented Lagrangian for the dual problem

$$\mathcal{L}_{\text{act}} = \mathbf{b}^T\mathbf{y} - \mathbf{x}^T(\mathbf{A}^T\mathbf{y} - \mathbf{c} + \mathbf{z}) - \frac{1}{2\mu}||\mathbf{A}^T\mathbf{y} - \mathbf{c} + \mathbf{z}||^2 \tag{5.1}$$

with respect to the dual solution. Here, we have introduced a penalty parameter, μ, which controls how strictly the primal and dual constraints are enforced; Ref. 138 provides a prescription for updating the penalty parameter during the course of the optimization. Differentiation of Eq. (5.1) with respect to the elements of $\mathbf{y}$ leads to

$$\frac{\partial\mathcal{L}_{\text{act}}}{\partial\mathbf{y}} = \mathbf{b} - \mathbf{A}\mathbf{x} + \frac{1}{\mu}\mathbf{A}(\mathbf{A}^T\mathbf{y} - \mathbf{c} + \mathbf{z}) \ . \tag{5.2}$$

By setting the right-hand side of Eq. (5.2) to zero and rearranging terms, we obtain the set of equations used in the boundary-point SDP procedure to determine $\mathbf{y}$

$$\mathbf{A}\mathbf{A}^T\mathbf{y} = \mathbf{A}(\mathbf{c} - \mathbf{z}) + \mu(\mathbf{A}\mathbf{x} - \mathbf{b}) \ . \tag{5.3}$$

Hence, when Eq. (5.3) is satisfied, the Lagrangian is stationary to variations in $\mathbf{y}$. Differentiation of Eq. (5.1) with respect to the elements of $\mathbf{x}$ leads to the system of equations

$$\frac{\partial \mathcal{L}_{\text{act}}}{\partial \mathbf{x}} = \mathbf{A}^T\mathbf{y} - \mathbf{c} + \mathbf{z} \ . \tag{5.4}$$

At convergence, when the dual constraints are satisfied, the right-hand side of Eq. (5.4) is zero. The vectors $\mathbf{z}$ and $\mathbf{y}$ are not independent, and we have

$$\frac{\partial \mathcal{L}_{\text{act}}}{\partial \mathbf{z}} = \frac{\partial \mathcal{L}_{\text{act}}}{\partial \mathbf{y}} \frac{\partial \mathbf{y}}{\partial \mathbf{z}}, \tag{5.5}$$

which vanishes when Eq. (5.3) is satisfied. Lastly, the Lagrangian is also stationary with respect to variations in the penalty parameter, provided that the dual constraints are satisfied. The only contributions to the energy gradient, aside from the orbital response contributions discussed below, are those from the derivatives of the one- and two-electron integrals that comprise the vector $\mathbf{c}$.

5.2.3 Orbital optimization

Details concerning orbital optimization techniques are presented in Ref. 57.

5.2.4 Analytic energy gradient expressions

Expressions for analytic energy gradients are most compactly written in terms of the spin-free 2-RDM ($^{\mathbf{2}}\mathbf{D}$) and 1-RDM ($^{\mathbf{1}}\mathbf{D}$). Density matrix elements with one or more external orbital indices or an odd number of doubly-occupied and/or active orbital indices vanish. Thus, the non-zero elements of the spin-free density matrices may be grouped according to the number of active and doubly-occupied orbital labels.

The active-active block of $^{\mathbf{1}}\mathbf{D}$ contains the elements

$${}^1D^t_u = {}^1D^{t_\alpha}_{u_\alpha} + {}^1D^{t_\beta}_{u_\beta}, \tag{5.6}$$

and the remaining non-zero elements of the full-space 1-RDM are simply

$${}^1D^i_j = 2\delta_{ij} \ . \tag{5.7}$$

The elements of $^{\mathbf{2}}\mathbf{D}$ with only active orbital indices are

$$ {}^2D^{tv}_{uw} = \frac{1}{2}({}^2D^{t_\alpha v_\alpha}_{u_\alpha w_\alpha} + {}^2D^{t_\alpha v_\beta}_{u_\alpha w_\beta} + {}^2D^{t_\beta v_\alpha}_{u_\beta w_\alpha} + {}^2D^{t_\beta v_\beta}_{u_\beta w_\beta}) \tag{5.8} $$

while the elements involving only doubly-occupied orbitals are given by

$$ {}^2D^{ik}_{jl} = 2\delta_{ij}\delta_{kl} - \delta_{il}\delta_{jk} \ . \tag{5.9} $$

Lastly, the elements with two active labels are

$$ {}^2D^{it}_{ju} = {}^2D^{ti}_{uj} = {}^1D^t_u\delta_{ij}, \tag{5.10} $$

and

$$ {}^2D^{it}_{uj} = {}^2D^{ti}_{ju} = -\frac{1}{2}\cdot {}^1D^t_u\delta_{ij}. \tag{5.11} $$

The total energy is then given by

$$ E = \sum_{pq}(T_{pq} + V_{pq}){}^1D^p_q + \sum_{pqrs}(pq|rs)\cdot {}^2\tilde{D}^{pr}_{qs}, \tag{5.12} $$

where the orbital labels span all doubly occupied and active orbitals, and the symmetrized 2-RDM, $^2\tilde{\mathbf{D}}$, which has the same eight-fold permutational symmetry as the two-electron integrals, is defined as

$$ {}^2\tilde{D}^{pr}_{qs} = \frac{1}{2}({}^2D^{pr}_{qs} + {}^2D^{qr}_{ps}). \tag{5.13} $$

We can now define the Lagrangian for the full molecular orbital space as

$$ \mathcal{L} = E_{\text{core}} + \mathcal{L}_{\text{act}}, \tag{5.14} $$

where $E_{\text{core}} = E - E_{\text{act}}$. Note that this Lagrangian is stationary with respect to variations in the active-space 1- and 2-RDM, as these quantities directly map onto the primal solution vector for the SDP problem described above. Thus, the gradient of the energy with respect to an arbitrary perturbation χ is

$$ \frac{dE}{d\chi} = \frac{\partial\mathcal{L}}{\partial\chi} = \sum_{pq}(T^\chi_{pq} + V^\chi_{pq}){}^1D^p_q + \sum_{pqrs}(pq|rs)^\chi\ {}^2\tilde{D}^{pr}_{qs} - \sum_{pq}X_{pq}S^\chi_{pq}, \tag{5.15} $$

where the symbols T^{χ}_{pq}, V^{χ}_{pq}, S^{χ}_{pq}, and $(pq|rs)^{\chi}$ represent the skeleton kinetic energy, electron-nucleus potential energy, overlap, and electron repulsion derivative integrals, respectively. The last term arises from the orbital response to the perturbation. It can be shown[181] that, for a CASSCF wave function with an energy that is stationary with respect to rotations between all non-redundant orbital pairs, the orbital response depends only on the overlap derivative integrals and the orbital Lagrangian, $\boldsymbol{X}$, with matrix elements

$$X_{pq} = \sum_{r} (T_{pr} + V_{pr})^1 D^r_q + 2 \sum_{rst} (pr|st)^2 \tilde{D}^{qs}_{rt} \; . \tag{5.16}$$

Note that, in our implementation, the gradient is not evaluated in the molecular orbital basis, as implied by Eq. (5.15). Rather, $^{\mathbf{1}}\mathbf{D}$, $^{\mathbf{2}}\mathbf{D}$, and $\boldsymbol{X}$ are back transformed to the atomic orbital basis and contracted against atomic orbital basis derivative integrals.

5.3 Results and discussion

5.3.1 Numerical validation of gradients

The v2RDM-CASSCF analytic energy gradients were implemented as a plugin to the Psi4 electronic structure package.[165] We validated the implementation by computing analytic and numerical gradients for the twenty small molecules given in Table 5.1 at the full-valence v2RDM-CASSCF/cc-pVDZ level of theory. The number of orbitals per irreducible representation that comprise the restricted doubly occupied and active orbital spaces are provided in Table 5.1. For each molecule, the active spaces are defined for the case where the principal axis is aligned with the z axis, and we employ the highest Abelian subgroup of the full molecular point group. For the validation, gradients were computed at the experimentally-determined geometries tabulated in the Computational Chemistry Comparison and Benchmark Database (CCCBDB) [85], and the RDMs in the v2RDM-CASSCF computations satisfied the PQG N-representability conditions.

Tight convergence thresholds were employed in both numerical and analytic energy gradient evaluations. The SDP algorithm that determines the active space 2-RDM was considered converged when the primal ($||\mathbf{Ax} - \mathbf{b}||$) and dual ($||\mathbf{A}^T\mathbf{y} - \mathbf{c} + \mathbf{z}||$) errors fell below 10^{-9}

Table 5.1: Small molecules and corresponding active spaces used in the present benchmarking studies.

molecule	active space	restricted doubly occupied	active
CH_2	(6e, 6o)	[1, 0, 0, 0]	[3, 0, 1,2]
C_2H_2	(10e, 10o)	[1, 0, 0, 0, 0, 1, 0, 0]	[3, 0, 1, 1, 0, 3, 1, 1]
C_2H_4	(12e, 12o)	[1, 0, 0, 0, 0, 1, 0, 0]	[3, 0, 1, 2, 0, 3, 2, 1]
CH_2O	(12e, 10o)	[2, 0, 0, 0]	[5, 0, 2, 3]
CH_4	(8e, 8o)	[1, 0, 0, 0]	[4, 0, 2, 2]
CO_2	(12e, 12o)	[2, 0, 0, 0, 0, 1, 0, 0]	[3, 0, 1, 1, 0, 3, 2, 2]
CO	(10e, 8o)	[2, 0, 0, 0]	[4, 0, 2, 2]
F_2	(14e, 8o)	[1, 0, 0, 0, 0, 1, 0, 0]	[2, 0, 1, 1, 0, 2, 1, 1]
H_2	(2e, 2o)	[0, 0, 0, 0, 0, 0, 0, 0]	[1, 0, 0, 0, 0, 1, 0, 0]
H_2O_2	(14e, 10o)	[1, 1]	[5, 5]
H_2O	(8e, 6o)	[1, 0, 0, 0]	[3, 0, 1, 2]
HCN	(10e, 9o)	[2, 0, 0, 0]	[5, 0, 2, 2]
HF	(8e, 5o)	[1, 0, 0, 0]	[3, 0, 1, 1]
HNC	(10e, 9o)	[2, 0, 0, 0]	[5, 0, 2, 2]
HNO	(12e, 9o)	[2, 0]	[7, 2]
HOF	(14e, 9o)	[2, 0]	[7, 2]
N_2	(10e, 8o)	[1, 0, 0, 0, 0, 1, 0, 0]	[2, 0, 1, 1, 0, 2, 1, 1]
N_2H_2	(12e, 10o)	[1, 0, 0, 1]	[4, 1, 1, 4]
O_3	(18e, 12o)	[2, 0, 0, 1]	[5, 1, 2, 4]
NH_3	(8e, 7o)	[1, 0]	[5, 2]

and the primal/dual energy gap ($|E_{\text{primal}} - E_{\text{dual}}|$) fell below 10^{-9} E_h. The orbital optimization procedure was considered converged when the orbital gradient fell below 10^{-9} E_h and the energy change produced by orbital rotations fell below 10^{-12} E_h. These thresholds are referred to as "tight" below. Numerical gradients were evaluated using a five-point stencil with a step size of 0.005 a_0. We compared the analytic and numerical gradients of the energy with respect to perturbations of each atom in each molecule in the x, y, and z directions; when considering all non-zero gradients, the mean unsigned deviation between the analytic and numerical gradients is 7.5 $\times 10^{-8}$ $E_h a_0^{-1}$, and the maximum unsigned deviation is 9.3 $\times 10^{-7}$ $E_h a_0^{-1}$. We further validated the correctness of the analytic gradients for the CO and N_2 molecules using tighter convergence criteria in the v2RDM-CASSCF optimizations: primal/dual errors of $\leq 10^{-12}$, a primal/dual energy gap of $\leq 10^{-12}$ E_h, an orbital gradient of $\leq 10^{-12}$ E_h, and energy changes due to orbital rotations of $\leq 10^{-14}$ E_h. With these tighter convergence criteria, analytic and numerical gradients differ by 5.4 $\times 10^{-10}$ $E_h a_0^{-1}$ and 2.4

$\times 10^{-13}$ $E_h a_0^{-1}$ for N_2 and CO, respectively.

For general systems, it is difficult to converge v2RDM-CASSCF as tightly as was done in this validation study; in practice, we employ considerably more loose thresholds. Here, we determine the error incurred when using more typical convergence criteria: primal/dual errors of $\leq 10^{-5}$, a primal/dual energy gap of $\leq 10^{-4}$ E_h, an orbital gradient of $\leq 10^{-5}$ E_h, and energy changes due to orbital rotations of $\leq 10^{-9}$ E_h (denoted "loose" below). For the same set of molecules, analytic gradients with these loose thresholds deviate on average from analytic gradients evaluated with the tight thresholds used above by 3.0×10^{-6} $E_h a_0^{-1}$; the maximum observed deviation is 1.9×10^{-5} $E_h a_0^{-1}$. These errors are much smaller than the default convergence criterion for the gradient in a conventional geometry optimization in Psi4 (a maximum force of 3.0 $\times 10^{-4}$ $E_h a_0^{-1}$). In the geometry optimizations below, we employ the "`GAU_TIGHT`" convergence criteria: a maximum force of 1.5 $\times 10^{-5}$ $E_h a_0^{-1}$ and a root-mean-square force of 1.0 $\times 10^{-5}$ $E_h a_0^{-1}$. When using loose tolerances in v2RDM-CASSCF, the maximum error in the gradient we observe is comparable to these thresholds, but, on average, the errors incurred are much smaller. We experienced no difficulties tightly converging geometry optimizations with the analytic gradients from loosely converged v2RDM-CASSCF.

We also explore the effects that changes to the orbital optimization procedure have on the total energy and analytic energy gradient. The present v2RDM-CASSCF procedure can be classified as a two-step optimization. In a true two-step v2RDM-CASSCF optimization, the active-space 2-RDM is fully optimized, and the orbitals are then varied to minimize the energy. This procedure is repeated until the orbitals and active-space 2-RDM are self-consistent. In practice, our algorithm does not fully converge the active-space 2-RDM before varying the orbitals. Instead, we perform the orbital optimization every few hundred v2RDM iterations. Prior work[57] indicates that this strategy can significantly reduce the total wall time for two-step v2RDM-CASSCF. We find here that the energy and gradients are, in some cases, sensitive to the frequency with which the orbital optimization is performed. Table 5.2 provides the total energy and analytic energy gradient for one of the molecules given in Table 5.1, HNC. The full-valence v2RDM-CASSCF energy and gradient were evaluated at

Table 5.2: Energies (E_h) energy gradients ($E_h a_0^{-1}$) for HNC computed at the full-valence v2RDM-CASSCF/cc-pVDZ level of theory for different orbital update frequencies. A frequency of ∞ refers to a true two-step optimization.

frequency	E	$\frac{\partial E}{\partial z_H}$	$\frac{\partial E}{\partial z_N}$	$\frac{\partial E}{\partial z_C}$
250	–93.026290	–0.030340	–0.019795	0.050135
500	–93.026290	–0.030340	–0.019795	0.050135
1000	–93.026290	–0.030340	–0.019795	0.050135
5000	–93.026278	–0.030466	–0.019726	0.050192
∞	–93.026278	–0.030466	–0.019726	0.050191

the experimentally-obtained equilibrium geometry for HNC tabulated in the CCCBDB using the cc-pVDZ basis set and five different orbital update frequencies, and the active-space 2-RDM satisfied the PQG N-representability conditions. Somewhat surprisingly, the energy and gradient vary in the fifth decimal place, despite the fact that the v2RDM-CASSCF optimization was performed using the tight thresholds given above.

After extensive numerical testing, we conclude that the sensitivity of the final energy to the orbital optimization procedure is due to the presence of closely-spaced minima in the v2RDM-CASSCF energy landscape, and we note that both of the solutions satisfy the two-body N-representability conditions to the same degree. We also note that we only locate multiple minima when initializing the v2RDM-CASSCF computation with certain guess-types. For example, if the computation is seeded with Hartree-Fock 1- and 2-RDMs, we find only one solution; if the computation is seeded with randomly-generated RDMs, we can find multiple solutions. This behavior is essentially the same when employing point-group symmetry or not, as well as when employing density-fitting approximation to the two-electron repulsion integrals. We have also explored the role of three-particle conditions in this issue. When employing the PQG+T2 N-representability conditions and different orbital update frequencies, the final energies in each case agree to within the specified convergence criteria. However, it is difficult to draw definitive conclusions regarding the presence of multiple minima when enforcing the T2 condition because we cannot converge the optimization procedure as tightly in this case.

Before we apply our analytic energy gradient implementation to the equilibrium geometries of full set of twenty molecules given in Table 5.1, we demonstrate that these slight differences in energies and gradients when enforcing the PQG conditions lead to quite similar equilibrium geometries for HNC. Table 5.3 provides the equilibrium H–N (r_{HN}) and N–C (r_{NC}) bond lengths using both tight and loose v2RDM-CASSCF convergence thresholds, the "`GAU_TIGHT`" geometry optimization convergence thresholds, and the five different orbital update frequencies considered above. For this case, the optimized equilibrium bond lengths obtained using different orbital update frequencies agree to 0.0001 Å. As will be shown below, variations in the bond lengths stemming from this issue are more than an order of magnitude smaller than the errors associated with the approximate N-representability of the v2RDM-CASSCF active space 2-RDM.

Table 5.3: Equilibrium bond lengths (Å) computed at the full-valence v2RDM-CASSCF/cc-pVDZ level of theory for different orbital update frequencies. A frequency of ∞ refers to a true two-step optimization.

	r_{HN}		r_{NC}	
frequency	tight	loose	tight	loose
250	1.018985	1.018978	1.197653	1.197652
500	1.018985	1.018979	1.197653	1.197650
1000	1.018985	1.019062	1.197653	1.197671
5000	1.019000	1.019062	1.197656	1.197675
∞	1.019059	1.018978	1.197669	1.197652

5.3.2 v2RDM-CASSCF equilibrium geometries

Here, we assess the accuracy of v2RDM-CASSCF relative to CI-CASSCF for the equilibrium geometries of the twenty small molecules introduced above. The v2RDM-CASSCF optimizations were carried out in Psi4 using the "`GAU_TIGHT`" geometry convergence thresholds and the loose thresholds defined above within v2RDM-CASSCF. CI-CASSCF geometry optimizations were carried out in the GAMESS electronic structure package,[193] using the same geometry convergence criteria. Figure 5.3.2 compares CI- and v2RDM-CASSCF

bond lengths. When enforcing the PQG N-representability conditions, the v2RDM- and

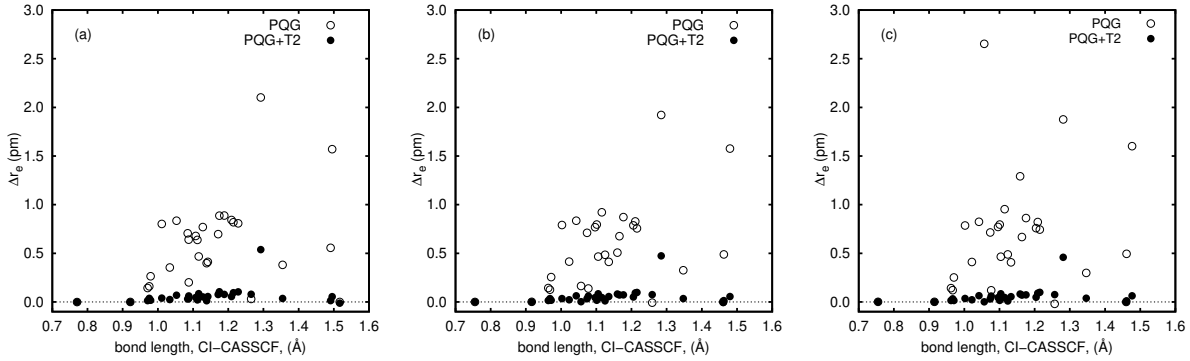

Figure 5.1: The difference in equilibrium bond lengths (Δr_e, pm)[a] obtained from full-valence v2RDM- and CI-CASSCF using the (a) cc-pVDZ, (b) cc-pVTZ, and (c) cc-pVQZ basis sets.

[a] $\Delta r_e = r_e^{\mathrm{v2RDM}} - r_e^{\mathrm{CI}}$.

CI-CASSCF bond lengths are in reasonable agreement, differing on average by 0.0059 Å, 0.0056 Å, and 0.0067 Å in the cc-pVDZ, cc-pVTZ, and cc-pVQZ basis sets, respectively. The maximum deviations are 0.021 Å, 0.019 Å, and 0.027 Å in the same basis sets. The v2RDM-CASSCF-optimized bond lengths are almost universally longer than those from CI-CASSCF. This result is not too surprising; with incomplete N-representability conditions, electrons in the active space are over correlated, and, for these simple molecules, that over-correlation manifests itself in a lengthening of molecular bonds. Figure 5.3.2 also compares CI-CASSCF bond lengths to those from v2RDM-CASSCF computations that enforce the T2 condition in addition to the PQG conditions. The T2 condition leads to a dramatic improvement in the quality of the v2RDM-CASSCF bond lengths. The maximum deviation between v2RDM- and CI-CASSCF-optimized bond lengths falls to 0.0054 Å, 0.0047 Å, and 0.0046 Å in the cc-pVDZ, cc-pVTZ, and cc-pVQZ basis sets, respectively, while the mean unsigned deviation is reduced to only 0.0006 Å in all three basis sets.

The performance of v2RDM-CASSCF relative to CI-CASSCF for bond angles is similar. When enforcing the PQG conditions, v2RDM-CASSCF angles differ from those from CI-

CASSCF on average by approximately 0.5 degrees in each basis set, and the maximum deviation ranges from 1.1–1.5 degrees throughout the three basis sets. Angles from v2RDM-CASSCF with the PQG+T2 conditions are essentially equivalent to those from CI-CASSCF. The average deviation is less than 0.1 degrees, and the maximum deviation across the three basis sets is only 0.1 degrees.

Table 5.4 shows the deviation in CI- and v2RDM-CASSCF equilibrium bond lengths (r_e^{CASSCF}) from experimentally determined values (r_e). CASSCF computations were performed in the cc-pVQZ basis (cc-pVDZ and cc-pVTZ data can be found in Appendix A). With the exception of molecular hydrogen, all r_e values were taken from Ref. 72 and the references therein. For H_2, the equilibrium bond length was taken from Ref. 74. Mean unsigned errors (MUE) for v2RDM-CASSCF bond lengths are 0.017 Å and 0.011 Å when imposing the PQG or PQG+T2 N-representability conditions, while CI-CASSCF bond lengths display an MUE of 0.010 Å. In this basis set, the maximum error observed for both CI- and v2RDM-CASSCF was 0.048 Å. In general, CI-CASSCF tends to overestimate bond lengths; this observation is consistent with previous multiconfigurational self-consistent field computations on the same set of molecules.[197] Here, we find that the over-correlation of the active-space electrons in v2RDM-CASSCF with two-body conditions amplifies this tendency. Fortunately, the additional error associated with the incompleteness of the PQG conditions appears to be slightly smaller than that of the CASSCF approach itself. The accuracy of v2RDM-CASSCF with the T2 conditions is essentially equivalent to that of CI-CASSCF.

Equilibrium structure of pentacene. We now consider the equilibrium geometry of a larger system for which CI-CASSCF is intractable: pentacene with an active space comprised of 11 π bonding orbitals and 11 π^* antibonding orbitals [a (22e,22o) active space]. This system is easily within the reach of the v2RDM-CASSCF approach when employing the PQG N-representability conditions, but it is somewhat too large to treat with our current implementation of the T2 conditions. The practical limit for our implementation of the T2 conditions is more similar to that for CI; the largest systems for which we have imposed partial three-particle conditions involved a (16e,16o) active space.[57] Figure 5.3.2 compares the symmetry-unique carbon-carbon bond lengths obtained at the v2RDM-CASSCF/cc-

Table 5.4: Errors in equilibrium bond lengths (Δr_e, pm)[a] optimized using CI- and v2RDM-CASSCF in the cc-pVQZ basis set. Computed bond lengths are compared to experimentally-obtained bond lengths (r_e, Å).

		Δr_e			
Molecule	Bond	PQG	PQG+T2	CI	r_e
C_2H_2	C-H	1.9	1.2	1.2	1.062
C_2H_2	C-C	1.9	1.3	1.2	1.203
C_2H_4	C-H	2.3	1.5	1.5	1.081
C_2H_4	C-C	1.6	1.3	1.3	1.334
CH_2	C-H	2.1	1.7	1.7	1.107
CH_2O	C-O	0.8	0.1	0.1	1.203
CH_2O	C-H	2.5	1.6	1.6	1.099
CH_4	C-H	2.3	1.5	1.5	1.086
CO_2	C-O	1.1	0.5	0.4	1.160
CO	C-O	0.9	0.5	0.5	1.128
F_2	F-F	4.8	4.8	4.8	1.412
H_2	H-H	1.3	1.3	1.3	0.741
H_2O_2	O-H	0.1	0.0	0.0	0.967
H_2O_2	O-O	3.7	2.2	2.1	1.456
H_2O	O-H	0.7	0.6	0.5	0.957
HCN	C-H	1.8	–0.8	–0.8	1.065
HCN	C-N	1.8	0.6	0.6	1.153
HF	H-F	–0.2	–0.2	–0.2	0.917
HNC	C-N	1.5	0.7	0.6	1.169
HNC	N-H	1.6	0.9	0.8	0.994
HNO	N-H	1.5	1.4	1.3	1.063
HNO	N-O	0.5	–0.2	–0.3	1.212
HOF	O-H	0.7	0.5	0.5	0.966
HOF	F-O	3.1	2.6	2.6	1.435
N_2	N-N	1.1	0.7	0.6	1.098
N_2H_2	N-N	0.5	0.6	0.5	1.252
N_2H_2	N-H	2.2	1.4	1.4	1.028
O_3	O-O	2.8	1.4	0.9	1.272
NH_3	N-H	1.4	1.0	1.0	1.012
	MSE[b]	1.7	1.1	1.0	-
	MUE[c]	1.7	1.1	1.1	-
	Max[d]	4.8	4.8	4.8	-

[a] $\Delta r_e = r_e^{\mathrm{CASSCF}} - r_e$. [b] mean signed error. [c] mean unsigned error. [d] maximum unsigned error.

pVDZ level of theory to those derived from a crystal structure.[192] The experimentally

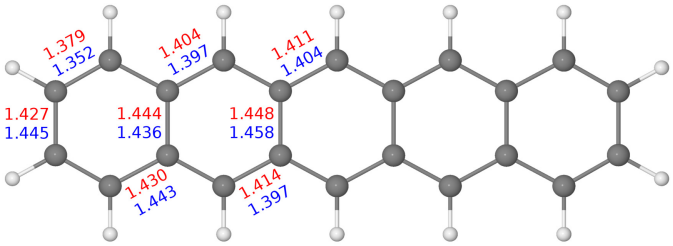

Figure 5.2: Symmetry-unique carbon-carbon bond lengths (Å) obtained at the v2RDM-CASSCF/cc-pVDZ level of theory (red) and derived from experiment[192] (blue). The RDMs in the v2RDM-CASSCF optimization satisfied the PQG N-representability conditions.

obtained bond lengths that correspond to what would be symmetry-equivalent bonds in the gas-phase molecule were averaged for comparison with the computed values. We find that v2RDM-CASSCF with the PQG conditions yields bond lengths for pentacene that are comparable in quality to those obtained for the smaller systems considered above. The mean and maximum deviation in the v2RDM-CASSCF-optimized bond lengths relative to those derived from the crystal structure are 0.015 Å and 0.027 Å, respectively, and, unlike in the case of the smaller molecules considered above, the bond lengths here are no longer systematically overestimated.

Lastly, the computational cost of v2RDM-CASSCF relative to that of CI-CASSCF merits some discussion. The number of floating point operations in v2RDM-CASSCF increases polynomially with the size of the active space. Enforcing the PQG or T2 conditions requires computational effort that scales with the sixth or ninth power of the size of the active space, respectively. Despite these nice scaling properties, the cost of v2RDM-CASSCF for small systems is considerable, as compared to that of CI-CASSCF. For example, consider a full-valence CASSCF computation on CH_2 [a (6e,6o) active space] within the cc-pVDZ basis set. For this system, a CI-CASSCF optimization in GAMESS requires only a few seconds, but v2RDM-CASSCF requires about three minutes when enforcing the PQG conditions and almost an hour when enforcing the PQG+T2 conditions, when the code is executed on six cores of an Intel Core i7-5930k CPU. The usefulness of v2RDM-CASSCF becomes apparent

once active space sizes approach the practical limits of CI-based CASSCF. For example, the computational cost of a v2RDM-CASSCF computation that enforces the PQG conditions for a molecule like pentacene is quite modest, while the corresponding CI-CASSCF computation is impossible. Using the (22e,22o) active space described above, one full step of the v2RDM-CASSCF geometry optimization required less than three hours when using six cores of an Intel Core i7-5930k processor; this time includes that required for the initial SCF procedure, as well as for the generation of the two-electron and derivative two-electron integrals.

5.4 Conclusions

We have presented and benchmarked an implementation of analytic first-order energy gradients for variational two-electron reduced-density-matrix- (v2RDM)-driven CASSCF methods. The Lagrangian formulation of the semidefinite problem corresponding to the active-space v2RDM optimization simplifies analytic energy gradient evaluation, and no additional response equations need to be solved once the active-space 1- and 2-RDM have been determined. The gradient expression, including the orbital response contribution, is identical to that for CI-based CASSCF methods.

We have verified numerically the correctness of the analytic gradients and applied them to the computation of equilibrium geometries for a set of twenty small molecules. When using two-particle N-representability conditions, v2RDM-CASSCF-optimized bond lengths and angles are in reasonable agreement with those from CI-CASSCF. Bond lengths are systematically overestimated, relative to those from CI-CASSCF, due to the over-correlation of the active-space electrons when the active-space 2RDM is only approximately N-representable. Relative to CI-CASSCF, enforcing partial three-particle constraints significantly improves the quality of v2RDM-CASSCF-optimized bond lengths and angles for these systems.

Lastly, we note that the v2RDM-CASSCF approach described herein is similar to state-specific CASSCF, but with a more narrow domain of applicability. Without additional constraints that differentiate ground- and excited-state 2-RDMs, which are unknown, v2RDM-CASSCF can only model the lowest-energy state of a given spin symmetry. Hence, neither

energy optimizations nor analytic energy gradients are currently available for state-specific excited-state or state-averaged (SA) v2RDM-CASSCF, as described herein.

CHAPTER 6

EXCITED STATE APPROACHES FOR THE VARIATIONAL TWO-ELECTRON REDUCED DENSITY MATRIX COMPLETE ACTIVE SPACE SELF-CONSISTENT FIELD METHOD

6.1 Introduction

A range of advances in semidefinite programming algorithms have made it possible to evaluate the ground state two-electron reduced density matrix (2RDM) directly, without requiring knowledge of the N-electron wavefunction. However, as explained in Chapter 4, the optimization of the 2RDM depends on the variational minimization of an energy functional. This means that the energy obtained corresponds to the lowest energy state of a specified spin symmetry. In order to obtain higher-lying states of that same spin symmetry, further constraints in a form that allows optimization of the excited state 2RDM by variational means are needed. Such constraints are at present unknown, and here we describe non-variational approaches for calculating excited states.

A general excited state can be expressed as a configuration interaction of determinants that describe the ground state. To compute the energy of excited states, one constructs and diagonalizes the Hamiltonian in the space of m-particle excitations and deexcitations from the ground state wavefunction. It can be shown that this requires knowledge of the ground state $(2m + 2)$-RDM. For a case where only single excitations and deexcitations are considered in describing the excited state wavefunction, knowledge of the ground state four-electron reduced density matrix (4RDM) is required. The 4RDM is typically not known at the end of a ground state calculation, since the energy is minimized with respect to elements of the 2-, and sometimes the 3RDM.

The 3- and the 4RDM of the ground state can be obtained, for instance, from a ground state calculation using an iterative solution of the contracted Schrödinger equation where the 3- and the 4RDMs are constrained *via* cumulant theory.[38, 39, 153, 245, 130, 128, 244, 131, 35, 132]. It is more convenient, however, to evaluate the elements of the Hamiltonian matrix from only a knowledge of the ground state 2RDM. We will note in this context two methods, both of which eliminate dependence on the ground state 4RDM. In the first, the cumulant method, the 3RDM is constructed from the 2RDM via its cumulant expansion[129, 131, 132] whereas in the Hermitian- or antiHermitian-operator methods, dependence on the 3RDM is eliminated by constraining basis functions to be in a Hermitian subspace of the space of single excitations and deexcitations from the ground state.

At the end of this chapter, we consider another approach from which excited states can be obtained from a knowledge and manipulation of only the ground state 2RDM. This is an approach based on Rowe's equation of motion (EOM)[187] as well as the extended random phase approximation (ERPA) [32, 219, 46, 166, 125], which amounts to an excited state ansatz modeled from single excitations and deexcitations out of a correlated ground state wavefunction. In this approach, the assumption that the ground state is an exact eigenfunction of the Hamiltonian is made, and the double commutator form of Rowe's EOM makes it possible to have a calculation that depends on only the ground state 2RDM.

We also consider, in this chapter, explicitly time-dependent approaches, where a time-dependent 2RDM is used to model an N-electron system driven by a time-dependent potential. The solution of the EOM of the 2RDM can provide excited state information. However, because the EOM of a time-dependent p-RDM depends on the $p+1$-RDM, according to the Born-Bogoliubov-Green-Kirkwood-Yvon hierarchy[98], the determination of higher-order RDMs is necessary for such approaches.

6.2 The Hermitian and anti-Hermitian operator methods

In this section, we largely follow the derivation and notation in Ref. 134. We restrict our description of this method to the space of single excitations and deexcitations out of the

ground state. That is

$$|\Psi_n\rangle = \sum_{ij} c_{ij}^n \hat{a}_i^\dagger \hat{a}_j |\Psi_g\rangle, \tag{6.1}$$

where i, j, k, and l are orbital labels, c_{ij}^n is an expansion coefficient, $|\Psi_g\rangle$ the ground state wavefunction and $\hat{a}_i^\dagger \hat{a}_j |\Psi_g\rangle$ the basis of single excitations and deexcitations. The overlap matrix between these basis functions can be written

$${}^2G_{kl}^{ij} = \langle \Psi_g | (\hat{a}_i^\dagger \hat{a}_j)^\dagger \hat{a}_k^\dagger \hat{a}_l | \Psi_g \rangle. \tag{6.2}$$

Similarly, the Hamiltonian can be written

$$H_{kl}^{ij} = \langle \Psi_g | (\hat{a}_i^\dagger \hat{a}_j)^\dagger \hat{H} \hat{a}_k^\dagger \hat{a}_l | \Psi_g \rangle. \tag{6.3}$$

It is clear than the Hamiltonian, itself a two-electron operator, is a functional of the ground state 4RDM. If the Hamiltonian could be constructed in the basis of the single excitations and deexcitations, one could obtain excited state energies $E_n, n > 0$ by solving the generalized eigenvalue problem

$$H_{kl}^{ij} c_{kl}^n = E_n {}^2G_{kl}^{ij} c_{kl}^n. \tag{6.4}$$

To remove the functional dependence of the Hamiltonian on the ground state 4RDM, it is important to note that matrix elements of the Hamiltonian can be written as

$$H_{kl}^{ij} = \langle \Psi_g | \hat{a}_i^\dagger \hat{a}_j)^\dagger [\hat{H}, \hat{a}_k^\dagger \hat{a}_l] | \Psi_g \rangle + \langle \Psi_g | \hat{a}_i^\dagger \hat{a}_j)^\dagger \hat{a}_k^\dagger \hat{a}_l | \Psi_g \rangle. \tag{6.5}$$

If $|\Psi_g\rangle$ is an eigenfunction of the Hamiltonian, the second term on the right hand side of 6.5 can be simplified by applying the following relation from the formulation of the contracted Schrödinger equation:

$$\langle \Psi_g | \hat{a}_i^\dagger \hat{a}_j)^\dagger \hat{a}_k^\dagger \hat{a}_l \hat{H} | \Psi_g \rangle = E_g \langle \Psi_g | \hat{a}_i^\dagger \hat{a}_j)^\dagger \hat{a}_k^\dagger \hat{a}_l | \Psi_g \rangle \tag{6.6}$$

so that

$$H_{kl}^{ij} = \langle \Psi_g | \hat{a}_i^\dagger \hat{a}_j)^\dagger [\hat{H}, \hat{a}_k^\dagger \hat{a}_l] | \Psi_g \rangle + E_g \langle \Psi_g | \hat{a}_i^\dagger \hat{a}_j)^\dagger \hat{a}_k^\dagger \hat{a}_l | \Psi_g \rangle. \tag{6.7}$$

Since the commutator reduces the overall particle rank of the operators in it, the Hamiltonian can now be expressed with knowledge of only the ground state 3RDM.

Further, if the basis of excitations is restricted to be in a Hermitian or anti-Hermitian subspace:

$$^{\pm}\Gamma_{ij} = \hat{a}_i^\dagger \hat{a}_j + \hat{a}_j^\dagger \hat{a}_i, \tag{6.8}$$

then the Hamiltonian could be written as

$$^{S}H_{kl}^{ij} = \pm\frac{1}{4}\langle\Psi_g|[^{\pm}\Gamma_{ij},[\hat{H},^{\pm}\Gamma_{kl}]]|\Psi_g\rangle \pm \frac{1}{4}\langle\Psi_g|[^{\pm}\Gamma_{kl},[\hat{H},^{\pm}\Gamma_{ij}]]|\Psi_g\rangle \pm E_g\langle\Psi_g|^{\pm}\Gamma_{ij}{}^{\pm}\Gamma_{kl}|\Psi_g\rangle. \tag{6.9}$$

The double commutators reduce overall particle rank by 2, so the Hamiltonian can be written in terms of the ground state 2RDM. This constitutes the Hermitian operator method (HOM)[22, 141, 185, 134, 52, 65, 218], which may be implemented with either Hermitian or anti-Hermitian basis functions[137, 147, 135]

6.3 Explicitly time-dependent reduced density matrix methods

The equation of motion for the full N-electron density matrix is given by the von-Neumann-Liouville equations as:

$$i\frac{\partial}{\partial t}{}^{N}\mathbf{D} = [\hat{H},{}^{N}\mathbf{D}], \tag{6.10}$$

where ${}^{N}\mathbf{D}$ is the N-electron density matrix. For reduced density matrices, the equation of motion is a coupled set of equations known as the quantum Bogoliubov-Born-Green-Kirkwood-Yvon (BBGKY) hierarchy[103]. These give the equation of motion for a 2RDM as

$$i\frac{\partial}{\partial t}{}^{2}\mathbf{D} = [\hat{H},{}^{2}\mathbf{D}] + C_2[{}^{3}\mathbf{D}], \tag{6.11}$$

where the operator $C_2[{}^{3}\mathbf{D}]$ describes the interaction of electron pairs with the other $N-2$ electrons, and the equation of motion for the 1RDM as

$$i\frac{\partial}{\partial t}{}^{1}\mathbf{D} = [\hat{H},{}^{1}\mathbf{D}] + C_1[{}^{2}\mathbf{D}], \tag{6.12}$$

where the operator $C_1[{}^{2}\mathbf{D}]$ describes the interaction of an electron with the other $N-1$ electrons. It is clear from this formulation that the propagation of a 2RDM requires knowledge of the 3RDM, and that that of the 1RDM requires the 2RDM.

Explicitly time-dependent schemes for reduced density matrices have been published[84, 103, 104]. In Ref. 84, the molecular response to an external time-dependent field is modeled by a time-dependent 1RDM whose time-dependent response contains information about excited state properties. The 2RDM to be used in the EOM is obtained by searching the space of all N-representable 2RDMs which contract to the time-dependent 1RDM:

$$(N-1)^1 D^i_j = \sum_P {}^2D^{iP}_{jP}. \tag{6.13}$$

This approach was successful in computing the potential energy curves for the excited states of small molecules in good agreement with full CI. However, excited states of the same symmetry as the ground state are not well described. The excited state energies computed are practically equivalent to those computed from real-time time-dependent Hartree-Fock (RTTDHF). Also, this approach fails to describe Rabi oscillations, which are considered a good measure of a time-dependent method's ability to model long-term electron dynamics. In Refs. 103 and 104, the time-dependent 2RDM is propagated. N-representability of the time-dependent 2RDM is enforced by projecting the time dependent 2RDM onto the subspace of N-representable 2RDMs.

$${}^2\mathbf{D}(t+\Delta t) = \hat{\mathbf{P}}\,{}^2\underline{\mathbf{D}}(t+\Delta t)\hat{\mathbf{P}}. \tag{6.14}$$

Here, the projector $\hat{\mathbf{P}}$ projects ${}^2\underline{\mathbf{D}}$ onto the space of 2RDMs that satisfy specified N-representability constraints. The 3RDM is reconstructed from the Valdemoro functional,[39, 153, 131, 35] but in such a way that it ensures spin and energy conservation. With this approach, both single and pair-electron observables were in good agreement with respective values from multiconfigurational time-dependent Hartree-Fock theory for the four electron system (LiH) studied. The study envisions the application of this method to larger systems.

6.4 The extended random phase approximation

The last approach we will discuss involves the application of Rowe's equation of motion. The derivation outlined here has been adapted from Refs. 125 which draws from Ref. 187.

Similar derivations can also be found in Refs. 32 and 219. The ERPA is derived as a specific case of Rowe's equation of motion[187].

We start by defining excitation and deexcitation operators $\hat{O}_n^\dagger$ and $\hat{O}_n$ such that an excited state $|\Psi_n\rangle$ results from the action of $\hat{O}_n^\dagger$ on a ground state $|\Psi_0\rangle$

$$|\Psi_n\rangle = \hat{O}_n^\dagger|\Psi_0\rangle \text{ for any } n > 0, \tag{6.15}$$

and 0 results from the action of $\hat{O}_n$ on the ground state

$$\hat{O}_n|\Psi_0\rangle = 0. \tag{6.16}$$

This suggests

$$\hat{O}_n^\dagger = |\Psi_n\rangle\langle\Psi_0| \tag{6.17}$$

as a possible form for the excitation operator. Since $|\Psi_0\rangle$ and $|\Psi_n\rangle$ are eigenstates of the Hamiltonian, which we will denote $\hat{H}$, with E_0 and E_n being their respective eigenvalues

$$\begin{aligned} \hat{H}|\Psi_0\rangle &= E_0|\Psi_0\rangle \\ \hat{H}|\Psi_n\rangle &= E_n|\Psi_n\rangle \end{aligned} \tag{6.18}$$

we can write

$$\begin{aligned} [\hat{H}, \hat{O}_n^\dagger]|\Psi_0\rangle &= \omega_n \hat{O}_n^\dagger|\Psi_0\rangle, \\ [\hat{H}, \hat{O}_n]|\Psi_0\rangle &= -\omega_n \hat{O}_n|\Psi_0\rangle \equiv 0, \end{aligned} \tag{6.19}$$

where ω_n is defined

$$\omega_n = E_n - E_0. \tag{6.20}$$

Using equations Eq. (6.19), one can show that

$$\begin{aligned} \langle\Psi_0|[\delta\hat{O}_n, [\hat{H}, \hat{O}_n^\dagger]]\Psi_0\rangle &= \omega_n \langle\Psi_0|[\hat{\delta}\hat{O}_n, \hat{O}_n^\dagger]|\Psi_0\rangle, \\ \langle\Psi_0|[\delta\hat{O}_n^\dagger, [\hat{H}, \hat{O}_n]]\Psi_0\rangle &= -\omega_n \langle\Psi_0|[\hat{\delta}\hat{O}_n^\dagger, \hat{O}_n]|\Psi_0\rangle, \end{aligned} \tag{6.21}$$

where δO_n and $\delta O_n^\dagger$ are variations in the operators O_n and $O_n^\dagger$, respectively.

The ERPA introduces the approximation that the excitation operator includes only single excitations and deexcitations of the ground state wavefunction,

$$\hat{O}_n^\dagger = \sum_{ij, i\neq j} c_{ij}^n \hat{a}_j^\dagger \hat{a}_i \tag{6.22}$$

so that excited states can be expressed as

$$|\Psi_n\rangle = \sum_{ij,i\neq j} c_{ij}^n \hat{a}_j^\dagger \hat{a}_i |\Psi_0\rangle, \tag{6.23}$$

where $\hat{a}_j^\dagger$ and $\hat{a}_i$ are creation and annihilation operators, respectively, and c_{ij}^n is an expansion coefficient for $|\Psi_n\rangle$.

Using the first of the two equations defined in Eq. (6.21), one can write

$$\begin{aligned} \sum_{ij,i\neq j} c_{ij}^n \langle\Psi_0|[\hat{a}_k^\dagger \hat{a}_l, [\hat{H}, \hat{a}_j^\dagger \hat{a}_i]]|\Psi_0\rangle = \\ \omega_n \sum_{ij,i\neq j} c_{ij}^n \langle\Psi_0|[\hat{a}_k^\dagger \hat{a}_l, \hat{a}_j^\dagger \hat{a}_i]|\Psi_0\rangle. \end{aligned} \tag{6.24}$$

The double commutator in Eq. (6.24) results in a particle operator of rank two, such that the left hand side defines a sum over elements of the ground state 2RDM, while the single commutator on the right hand side results in particle operator of rank one, and the right hand side of Eq. (6.24) defines a sum over elements of a ground state 1RDM.

From Eq. (6.21), one can deduce that the left and right hand sides of Eq. (6.24) have the following symmetry properties

$$\begin{aligned} \langle\Psi_0|[\hat{a}_k^\dagger \hat{a}_l, [\hat{H}, \hat{a}_j^\dagger \hat{a}_i]]|\Psi_0\rangle = \langle\Psi_0|[\hat{a}_j^\dagger \hat{a}_i, [\hat{H}, \hat{a}_k^\dagger \hat{a}_l]]|\Psi_0\rangle, \\ \langle\Psi_0|[\hat{a}_k^\dagger \hat{a}_l, \hat{a}_j^\dagger \hat{a}_i]|\Psi_0\rangle = \langle\Psi_0|[\hat{a}_j^\dagger \hat{a}_i, \hat{a}_k^\dagger \hat{a}_l]|\Psi_0\rangle \end{aligned} \tag{6.25}$$

and

$$\begin{aligned} \langle\Psi_0|[\hat{a}_k^\dagger \hat{a}_l, [\hat{H}, \hat{a}_j^\dagger \hat{a}_i]]|\Psi_0\rangle = \langle\Psi_0|[\hat{a}_l^\dagger \hat{a}_k, [\hat{H}, \hat{a}_i^\dagger \hat{a}_j]]|\Psi_0\rangle, \\ \langle\Psi_0|[\hat{a}_k^\dagger \hat{a}_l, \hat{a}_j^\dagger \hat{a}_i]|\Psi_0\rangle = -\langle\Psi_0|[\hat{a}_l^\dagger \hat{a}_k, \hat{a}_i^\dagger \hat{a}_j]|\Psi_0\rangle \end{aligned} \tag{6.26}$$

and that excitation energies occur in pairs $(\omega_n, -\omega_n)$.

Using Eq.(6.16), the matrix element of any operator $\hat{W}$ between the ground and the excited state $|\Psi_n\rangle$ can be written

$$\langle\Psi_n|\hat{W}|\Psi_0\rangle = \langle\Psi_0|[\hat{O}_n, \hat{W}]|\Psi_0\rangle. \tag{6.27}$$

CHAPTER 7

MODELING CORE-LEVEL EXCITATIONS WITH VARIATIONALLY-OPTIMIZED REDUCED DENSITY MATRICES AND THE EXTENDED RANDOM PHASE APPROXIMATION

7.1 Introduction

The development of powerful x-ray sources and sophisticated measurement technology over the years has enhanced the utility of near-edge x-ray absorption fine structure (NEXAFS) [207] as a tool for probing local chemical information. Near-edge features contain a wealth of information about electronic structure, providing insight into oxidation state, coordination number, and covalency, [115, 142] while time-resolved NEXAFS can even be used to follow reaction intermediates with elemental specificity. [159] The interpretation of experimental data from NEXAFS is often aided through the use of quantum-chemical computations. Many electronic structure methods have been applied to this problem, including time-dependent density functional theory (TDDFT) [115, 142, 248, 213, 4, 116, 105], linear response[95, 150, 41, 42, 89] and equation-of-motion[158, 168, 43, 155] coupled-cluster theory, second-order algebraic diagrammatic construction [ADC(2)] [175, 228, 229, 157], and active-space-based multiconfigurational approaches [242, 182, 86, 231, 100, 232, 20, 99]. While TDDFT is often the method of choice, owing to its relatively low computational cost, quantitative agreement with experimental data can require a sophisticated treatment of both static and dynamical correlation effects, as well as relativistic effects. [31] Unfortunately, standard approaches for capturing static correlation, such as the complete active space self-consistent field (CASSCF) method, [184, 200, 201, 183] are associated with steep computational costs that limit their application to small systems.

The limitations of configuration-interaction (CI)-based CASSCF stem from the exponential complexity of the active-space wave function. In contrast, the number of unknowns in the active-space two-electron reduced-density matrix (2-RDM) grows only quartically with the size of the active space. For this reason, variational 2-RDM (v2RDM)-driven CASSCF [64, 57] algorithms can be applied to much larger active spaces than can be considered with CI-based CASSCF. For example, most CI-based algorithms are limited to active spaces comprised of at most 18 electrons in 18 orbitals, although active spaces as large as 22 electrons in 22 orbitals have recently been realized using massively parallel algorithms. [224] On the other hand, an active space as large as 50 electrons in 50 orbitals can routinely be considered with a v2RDM-driven algorithm. Unfortunately, despite its nice scaling properties, v2RDM-CASSCF is not directly applicable to the NEXAFS problem, as v2RDM-based methods can only describe ground electronic states of a given spin symmetry. In light of this issue, several strategies have been proposed to extract excited-state information from ground-state reduced-density matrices (RDMs), including the Hermitian operator method [23, 185, 218, 65, 134] explicitly time-dependent RDM methods, [84, 103] and the extended random phase approximation (ERPA). [32, 219, 46] The present work focuses on the application of ERPA to the NEXAFS problem.

The ERPA is a specific application of Rowe's equation of motion [187, 188] to the case in which excited-state wave functions are assumed to be well described by single excitations out of the ground state. The ERPA leads to a nonsymmetric generalized eigenvalue problem that can be formulated in terms of the ground-state one-electron reduced-density matrix (1-RDM) and the 2-RDM, making it an ideal candidate for computing excitation energies from variationally obtained RDMs. While Rowe's equation of motion is itself formally exact, the accuracy of excitation energies computed from its application within the ERPA will depend on (i) how well ground state 1- and 2-RDMs resemble those of the exact ground state and (ii) how well the actual excited-state wave functions are represented by single excitations out of the ground state.

We explore the utility of the ERPA for describing core-level excitations out of ground states described at the v2RDM-CASSCF level of theory. In Section 7.2, we present the

working equations for the ERPA and discuss the computational cost associated with solving the ERPA equations when using a CASSCF reference. We also derive a set of killer conditions that must be considered for a reliable description of core-level excitations. These conditions can be satisfied by removing all excitations that do not involve a core orbital (i.e. within the core-valence separation [CVS] approximation [28, 15, 215, 206, 43]). Section 7.3 then provides the details of our computations. In Section 7.4, we assess the quality of the core-level spectra obtained from the ERPA and examine the effects of electron correlation, N-representability, core-valence separation, and the choice of orbital basis (i.e. canonical versus energy-optimized orbitals) on the excitation energies.

7.2 Theory

Following Refs. 32 and 219, the ERPA is easily derived as a specific case of Rowe's equation of motion [187]. First, consider the ground electronic state, $|\Psi_0\rangle$, and an excited state, $|\Psi_n\rangle$ ($n > 0$), both of which are eigenfunctions of the Hamiltonian

$$\hat{H}|\Psi_0\rangle = E_0|\Psi_0\rangle, \tag{7.1}$$

$$\hat{H}|\Psi_n\rangle = E_n|\Psi_n\rangle, \tag{7.2}$$

with eigenvalues E_0 and E_n, respectively. We introduce an excitation operator, $\hat{O}_n^\dagger$, that defines the excited state as

$$|\Psi_n\rangle = \hat{O}_n^\dagger|\Psi_0\rangle, \tag{7.3}$$

and a deexcitation operator, $\hat{O}_n$, the action of which on the ground state yields zero

$$\hat{O}_n|\Psi_0\rangle = 0. \tag{7.4}$$

Equation 7.4 is the well-known "killer condition.' We reexpress Eq. 7.2 as

$$[\hat{H}, \hat{O}_n^\dagger]|\Psi_0\rangle = \omega_n \hat{O}_n^\dagger|\Psi_0\rangle, \tag{7.5}$$

where $\omega_n = E_n - E_0$, and subsequently left-multiply Eq. 7.5 by $\langle\Psi_0|\hat{A}$ to obtain

$$\langle\Psi_0|\hat{A}[\hat{H}, \hat{O}_n^\dagger]|\Psi_0\rangle = \omega_n \langle\Psi_0|\hat{A}\hat{O}_n^\dagger|\Psi_0\rangle. \tag{7.6}$$

Here, $\langle\Psi_0|\hat{A}$ represents an arbitrary state within the manifold of states defined by $\langle\Psi_0|\hat{O}_n$. If the killer condition is satisfied, Eq. 7.6 can be reexpressed in the more convenient form

$$\langle\Psi_0|[\hat{A},[\hat{H},\hat{O}_n^\dagger]]|\Psi_0\rangle = \omega_n\langle\Psi_0|[\hat{A},\hat{O}_n^\dagger]|\Psi_0\rangle, \tag{7.7}$$

which is Rowe's formally exact equation of motion.

Within the ERPA, the excitation operator is restricted to include only single excitations out of the ground state. We choose the singlet spin-adapted excitation operator

$$\hat{O}_n^\dagger = \frac{1}{\sqrt{2}}\sum_{pq,p\neq q} c_{pq}^n(\hat{a}_q^\dagger\hat{a}_p + \hat{a}_{\bar{q}}^\dagger\hat{a}_{\bar{p}}), \tag{7.8}$$

where $\hat{a}_q^\dagger$ and $\hat{a}_p$ represent fermionic creation and annihilation operators, respectively, the indices p and q are spatial orbital labels (specifically, the natural orbitals of the ground state), and an overbar (or lack thereof) represents an electron of β (or α) spin. Note that the summation includes excitations between all orbitals; this structure contrasts with that of the more familiar random phase approximation (RPA), which involves only particle/hole and hole/particle transitions. Further, the excitation operator excludes terms where $p = q$, which is a consequence of the killer condition. [32] Specifically, it is the consequence of the following constraint implied by, but weaker, than Eq. 7.4

$$\langle\Psi_0|\hat{O}_n|\Psi_0\rangle = 0. \tag{7.9}$$

In the natural orbital basis, Eq. 7.9 can be satisfied by restricting the labels in Eq. 7.8 so that $p \neq q$. [32]

To obtain the working equations of the ERPA, the arbitrary excitation operator, $\hat{A}$, is chosen to be

$$\hat{A} = \frac{1}{\sqrt{2}}(\hat{a}_r^\dagger\hat{a}_s + \hat{a}_{\bar{r}}^\dagger\hat{a}_{\bar{s}}). \tag{7.10}$$

Using Eqs. 7.7, 7.8, and 7.10, we arrive at the nonsymmetric generalized eigenvalue equation

$$\sum_{pq,p\neq q} c_{pq}^n\langle\Psi_0|[\hat{a}_r^\dagger\hat{a}_s + \hat{a}_{\bar{r}}^\dagger\hat{a}_{\bar{s}},[\hat{H},\hat{a}_q^\dagger\hat{a}_p + \hat{a}_{\bar{q}}^\dagger\hat{a}_{\bar{p}}]]|\Psi_0\rangle = 2\omega_n(n_r - n_s)c_{rs}^n. \tag{7.11}$$

The double commutator on the left-hand side (LHS) of Eq. 7.11 is a two-particle operator, the expectation value of which is expressible as a sum over the elements of the ground state

2-RDM, and the right-hand side depends on only the natural orbital occupation numbers ($n_r = \langle\Psi_0|\hat{a}_r^\dagger\hat{a}_r^\dagger|\Psi_0\rangle = \langle\Psi_0|\hat{a}_{\bar{r}}^\dagger\hat{a}_{\bar{r}}^\dagger|\Psi_0\rangle$). In this form, the construction of the LHS of Eq. 7.11 should scale as the sixth power of the size of the one-electron basis set, and the solution of the generalized eigenvalue equation for all states shares the same scaling.

The excitation operator given by Eq. 7.8 is the most general operator for the ERPA problem. In practice, the actual form of the operator depends upon the choice of the ground-state wave function. For example, in the case that the ground-state is a restricted Hartree-Fock wave function, the ERPA reduces to the usual RPA, with $\hat{O}_n^\dagger$ comprised of only particle/hole and hole/particle transitions. The present work is concerned with the case that the ground-state wave function is obtained from CASSCF, so we partition our orbitals into restricted (doubly occupied), active (partially occupied), and external (empty) orbitals, and we note that excitations among restricted or external orbitals cannot contribute to any excited-state wave function. An appropriate excitation operator for CASSCF-specific ERPA is then

$$\begin{aligned}\hat{O}_n^\dagger = \frac{1}{\sqrt{2}} \Bigg(& \sum_{ia}[c_{ia}^n(\hat{a}_a^\dagger\hat{a}_i + \hat{a}_{\bar{a}}^\dagger\hat{a}_{\bar{i}}) + c_{ai}^n(\hat{a}_i^\dagger\hat{a}_a + \hat{a}_{\bar{i}}^\dagger\hat{a}_{\bar{a}})] \\ + & \sum_{it}[c_{it}^n(\hat{a}_t^\dagger\hat{a}_i + \hat{a}_{\bar{t}}^\dagger\hat{a}_{\bar{i}}) + c_{ti}^n(\hat{a}_i^\dagger\hat{a}_t + \hat{a}_{\bar{i}}^\dagger\hat{a}_{\bar{t}})] \\ + & \sum_{at}[c_{at}^n(\hat{a}_t^\dagger\hat{a}_a + \hat{a}_{\bar{t}}^\dagger\hat{a}_{\bar{a}}) + c_{ta}^n(\hat{a}_a^\dagger\hat{a}_t + \hat{a}_{\bar{a}}^\dagger\hat{a}_{\bar{t}})] \\ + & \sum_{tu,t\neq u} c_{tu}^n(\hat{a}_u^\dagger\hat{a}_t + \hat{a}_{\bar{u}}^\dagger\hat{a}_{\bar{t}})\Bigg),\end{aligned} \tag{7.12}$$

where the orbital labels i and a correspond to restricted and external orbitals, respectively, and the labels t and u correspond to orbitals belonging to the active space. The application of ERPA with this excitation operator can be thought of as an uncontracted multireference configuration interaction method limited to single-electron transitions, with the exception that the ERPA also includes deexcitations. With this operator, the evaluation of the LHS of Eq. 7.11 and the solution of the generalized eigenvalue problem still scale as the sixth power with system size, but the prefactor is significantly reduced, relative to the general case. The dimension of the matrix representation of the LHS of Eq. 7.11 is $2k_rk_a + 2k_rk_e + 2k_ak_e + k_a(k_a - 1)$, where k_r, k_a, and k_e represent the number of restricted, active, and external

orbitals, respectively; the solution of the generalized eigenvalue problem scales as the cube of this number.

As will be discussed in Section 7.4, the last term in Eq. 7.12, which involves active/active-type excitations, can lead to severe violations in the killer condition (Eq. 7.4) that degrade the quality of the ERPA excitation energies. We therefore consider an additional class of killer conditions beyond Eq. 7.9 that can be derived by the projection of Eq. 7.4 onto an arbitrary state $\langle\Psi_0|\hat{a}_r^\dagger\hat{a}_s$:

$$\langle\Psi_0|\hat{a}_r^\dagger\hat{a}_s\hat{O}_n|\Psi_0\rangle = 0. \tag{7.13}$$

These constraints, combined with Eq. 7.9, are stronger than Eq. 7.9 alone, but they are still weaker than the killer condition itself. In the case that the ground-state wave function has the form of a CASSCF wave function, we consider nine separate constraints defined by the space to which the operators $\hat{a}_r^\dagger$ and $\hat{a}_s$ belong, four of which are not trivially satisfied. The constraints

$$\forall t,u: \quad \langle\Psi_0|\hat{a}_t^\dagger\hat{a}_u\hat{O}_n|\Psi_0\rangle = 0, \tag{7.14}$$

imply

$$\forall t,u: \quad (1-\delta_{tu})n_t c_{ut}^n + \sum_{v\neq w}({}^2D_{uw}^{tv} + {}^2D_{u\bar{w}}^{t\bar{v}})c_{vw}^n = 0, \tag{7.15}$$

where ${}^2D_{uw}^{tv}$ and ${}^2D_{u\bar{w}}^{t\bar{v}}$ represent elements of the active-space 2-RDM, defined as

$${}^2D_{uw}^{tv} = \langle\Psi_0|\hat{a}_t^\dagger\hat{a}_v^\dagger\hat{a}_w\hat{a}_u|\Psi_0\rangle, \tag{7.16}$$

$${}^2D_{u\bar{w}}^{t\bar{v}} = \langle\Psi_0|\hat{a}_t^\dagger\hat{a}_{\bar{v}}^\dagger\hat{a}_{\bar{w}}\hat{a}_u|\Psi_0\rangle. \tag{7.17}$$

Additionally, the constraints

$$\forall i,a: \quad \langle\Psi_0|\hat{a}_i^\dagger\hat{a}_a\hat{O}_n|\Psi_0\rangle = 0, \tag{7.18}$$

$$\forall i,t: \quad \langle\Psi_0|\hat{a}_i^\dagger\hat{a}_t\hat{O}_n|\Psi_0\rangle = 0, \tag{7.19}$$

and

$$\forall t,a: \quad \langle\Psi_0|\hat{a}_t^\dagger\hat{a}_a\hat{O}_n|\Psi_0\rangle = 0, \tag{7.20}$$

lead to

$$\forall a, i: \quad c^n_{ai} = 0, \tag{7.21}$$

$$\forall t, i: \quad (1 - n_t) c^n_{ti} = 0, \tag{7.22}$$

and

$$\forall a, t: \quad n_t c^n_{at} = 0. \tag{7.23}$$

Equation 7.21 is identical to the condition that would be obtained from the same considerations in the case that the reference wave function was a Hartree-Fock wave function (i.e. within the RPA). The only way to satisfy this condition is to set all restricted/external deexcitation weights to zero; if these terms are eliminated from the excited-state operator expansion for RPA, that method reduces to the Tamm-Dancoff approximation (TDA) or CI with single excitations (CIS). Equations 7.22 and 7.23 are generalizations of this condition for CASSCF reference functions that can only be satisfied by eliminating the relevant deexcitations from the operator expansion. These conditions both reduce to Eq. 7.21 in the limit of zero electron correlation within the active space (when $n_t \to 0$ or $n_t \to 1$) and can thus be classified as TDA-like restrictions on deexcitations.

We ignore the TDA-like restrictions of Eqs. 7.21–7.23 and focus on Eq. 7.15. As will be shown in Section 7.4, we observe large violations of Eq. 7.15 for some K-edge features in small molecules. An ERPA procedure that explicitly enforces these conditions could improve the description of these states, but we find that reasonable results can be obtained simply by invoking the CVS approximation, removing from the ERPA expansion all transitions that do not involve a core orbital. Assuming that all valence electrons reside within the active space, the CVS-ERPA excitation operator can be defined as

$$\begin{aligned} \hat{O}^\dagger_n = \frac{1}{\sqrt{2}} \Bigg(& \sum_{ia} [c^n_{ia}(\hat{a}^\dagger_a \hat{a}_i + \hat{a}^\dagger_{\bar{a}} \hat{a}_{\bar{i}}) + c^n_{ai}(\hat{a}^\dagger_i \hat{a}_a + \hat{a}^\dagger_{\bar{i}} \hat{a}_{\bar{a}})] \\ + & \sum_{it} [c^n_{it}(\hat{a}^\dagger_t \hat{a}_i + \hat{a}^\dagger_{\bar{t}} \hat{a}_{\bar{i}}) + c^n_{ti}(\hat{a}^\dagger_i \hat{a}_t + \hat{a}^\dagger_{\bar{i}} \hat{a}_{\bar{t}})] \Bigg). \end{aligned} \tag{7.24}$$

In addition to automatically satisfying the conditions given by Eq. 7.15 (and Eq. 7.23), the CVS approximation prevents accidental degeneracies between core-excited states and valence excitations that lie far above the ionization threshold.

Before moving on, we should highlight two important properties of Eq. 7.11. First, the excitation energies obtained from this equation are size intensive. We have verified this property numerically for the system of non-interacting LiH molecules described in Ref. 96. For these tests, the ground-state was treated at the full-valence v2RDM-driven CASSCF level of theory, and the excitation operator employed within the ERPA was that given in Eq. 7.12. Second, for a stable ground-state reference function, Eq. 7.11 can be recast as a symmetric eigenvalue problem with real, positive eigenvalues. In the case that the orbitals are optimized for the reference state, the stability condition is satisfied. However, should one employ a different orbital basis, the stability condition could be violated. In principle, the lack of symmetry in the LHS could then lead to complex eigenvalues, as well as to matrix defects relevant to the description of conical intersections. [91, 92]

7.3 Computational details

Table 7.1: Active spaces employed using the C_{2v} ([A_1, A_2, B_1, B_2]) and D_{2h} ([A_g, B_{1g}, B_{2g}, B_{3g}, A_u, B_{1u}, B_{2u}, B_{3u}]) point groups.

			active orbitals		
molecule	point group	restricted orbitals	f.v.[a]	f.v.+3s[b]	f.v.+3s3p[c]
CO	C_{2v}	[2, 0, 0, 0]	[4, 0, 2, 2]	[6, 0, 2, 2]	[8, 0, 4, 4]
H_2CO	C_{2v}	[2, 0, 0, 0]	[5, 0, 2, 3]	[7, 0, 2, 3]	[9, 0, 4, 5]
HCN	C_{2v}	[2, 0, 0, 0]	[5, 0, 2, 2]	[7, 0, 2, 2]	[9, 0, 4, 4]
N_2O	C_{2v}	[3, 0, 0, 0]	[6, 0, 3, 3]	[9, 0, 3, 3]	[10, 0, 7, 7]
CH_4	C_{2v}	[1, 0, 0, 0]	[4, 0, 2, 2]	[5, 0, 2, 2]	[6, 0, 3, 3]
C_2H_2	D_{2h}	[1, 0, 0, 0, 0, 1, 0, 0]	[3, 0, 1, 1, 0, 3, 1, 1]	[4, 0, 1, 1, 0, 4, 1, 1]	[5, 0, 2, 2, 0, 5, 2, 2]
N_2	D_{2h}	[1, 0, 0, 0, 0, 1, 0, 0]	[2, 0, 1, 1, 0, 2, 1, 1]	[3, 0, 1, 1, 0, 3, 1, 1]	[4, 0, 2, 2, 0, 4, 2, 2]

[a] the full valence space
[b] f.v. plus orbitals of the symmetry of the 3s orbital on each heavy atom
[c] f.v. plus orbitals of the symmetry of the 3s and 3p orbitals on each heavy atom

In Sec. 7.4, we compare ERPA excitation energies to those obtained from the usual RPA, TDDFT (with the B3LYP functional), and time-dependent equation of motion (EOM) second-order approximate coupled cluster theory (TD-EOM-CC2). [154] RPA and TDDFT excitation energies were computed using the GAMESS electronic structure package, [193] and TD-EOM-CC2 computations were performed using a plugin to the Psi4 package. [165] TD-EOM-CC2 computations employed Cholesky-decomposed electron repulsion integral (ERI)

tensors with a tight decomposition threshold of 10^{-12} E_h. The molecular geometries employed within all computations were optimized for the ground state using density functional theory (with the B3LYP functional [18]) and the cc-pVQZ basis set.[87] All other ground and excited state computations were performed using the cc-pVTZ, cc-pCVTZ,[236] aug-cc-pVTZ,[90] and cc-pVQZ basis sets.

The ground-state 1- and 2-RDMs entering the ERPA equations were obtained from v2RDM-driven CASSCF computations, as implemented in a plugin [57] to Psi4. Table 8.1 provides the active spaces employed within these computations. Optimized RDMs satisfy either two-particle (PQG) N-representability conditions [61] or two-particle and partial three-particle (T2) conditions. [249, 48] All v2RDM-CASSCF computations employed the density fitting approximation to the ERI tensor. Computations within the cc-pVTZ, aug-cc-pVTZ, and cc-pVQZ basis sets used the corresponding jk-type fitting basis,[226] while computations within the cc-pCVTZ basis used the def2-QZVpp-jkfit fitting basis. [227] The DF approximation reduces the scaling of the orbital optimization step in v2RDM-CASSCF from $\mathcal{O}(k^5)$ to $\mathcal{O}(k^4)$, where k represents the dimension of the one-electron basis. All ERPA computations also employed the DF approximation, which reduces the formal scaling of the construction of some terms that contribute to the matrix representation of the double commutator on the LHS of Eq. 7.11 from $\mathcal{O}(k^6)$ to $\mathcal{O}(k^5)$. Even within the DF approximation, though, the overall scaling of the construction of this matrix and of the solution to the ERPA eigenvalue problem is unchanged from that described in Sec. 7.2.

7.4 Results and discussion

7.4.1 Principal K-edge features

Experimentally obtained K-edge features corresponding to $1s \rightarrow \pi^*$-type excitations are provided in Table 7.2 for a set of small molecules containing π bonds (CO, H_2CO, HCN, C_2H_2, N_2, and N_2O). Also provided are errors in excitation energies obtained from TD-EOM-CC2, TDDFT, RPA, ERPA, and CVS-ERPA; ERPA computations employed RDMs generated from full-valence v2RDM-CASSCF. All computed results reported here were obtained using

Table 7.2: Core-level ($1s \rightarrow \pi^*$) excitation energies (eV) obtained from experiment and errors in computed excitation energies determined in the cc-pCVTZ basis set.

						ERPA		CVS-ERPA	
molecule	transition	exp.	CC2	TDDFT	RPA	PQG	PQG+T2	PQG	PQG+T2
CO	C $1s \rightarrow \pi^*$	287.4[a]	2.2	-11.3	7.0	5.6	5.6	5.2	5.0
	O $1s \rightarrow \pi^*$	533.6[b]	2.0	-13.8	16.5	8.3	8.8	6.9	6.9
H_2CO	C $1s \rightarrow \pi^*$	285.6[c]	3.1	-10.4	8.8	7.2	7.2	7.0	7.2
	O $1s \rightarrow \pi^*$	530.8[c]	2.0	-14.1	15.1	7.7	8.1	6.6	6.7
C_2H_2	C $1s \rightarrow \pi^*$	285.8[d]	2.7	-10.5	10.2	6.9	6.9	6.8	6.9
HCN	C $1s \rightarrow \pi^*$	286.4[e]	2.7	-10.6	9.6	6.7	6.6	6.5	6.6
	N $1s \rightarrow \pi^*$	399.7[e]	2.4	-12.1	12.3	7.4	7.5	7.0	7.0
N_2	N $1s \rightarrow \pi^*$	401.0[f]	2.3	-12.5	11.2	6.8	6.9	6.4	6.4
N_2O	N_t $1s \rightarrow \pi^*$	401.1[g]	2.5	-12.2	12.4	7.1	7.4	6.6	6.9
	N_c $1s \rightarrow \pi^*$	404.7[g]	2.8	-12.4	11.4	6.6	6.9	6.6	6.9
	O $1s \rightarrow \pi^*$	534.8[g]	1.4	-14.3	18.5	9.3	9.9	8.2	8.8
	mean unsigned error		2.0	12.2	12.1	7.2	7.4	6.7	6.9
	maximum unsigned error		2.7	14.3	18.5	9.3	9.9	8.2	8.8

[a−g] Experimental results are taken from Refs. [162], [177], [180], [216], [76], [82] and [217], respectively.

the cc-pCVTZ basis. We first consider the results obtained with the excitation operator of Eq. 7.12 and discuss the role of the CVS approximation below.

We find that RPA and TDDFT consistently overestimate and underestimate, respectively, the position of the K-edge features considered; the mean unsigned error in the excitation energies computed using these approaches are 12.1 eV for RPA and 12.2 eV for TDDFT. The maximum unsigned error obtained with RPA (18.5 eV) is slightly larger than that of TDDFT (14.3 eV). The ERPA improves upon the RPA for all molecules. The mean unsigned errors are reduced to 7.2 eV and 7.4 eV when enforcing the PQG or PQG+T2 N-representability conditions, respectively, while the maximum errors are reduced to only 9.3 eV (PQG) and 9.9 eV (PQG+T2). Interestingly, the ERPA excitation energies appear to be insensitive to the degree to which the ground-state RDMs are N-representable, as evidenced by the similar performance of the approach when enforcing two- or three-particle N-representability conditions in the underlying v2RDM-CASSCF computations. Aside from the modest improvement in the magnitudes of the excitation energies, the ERPA also appears to provide a more balanced description of multiple K-edges within a given molecule than is obtained with RPA or TDDFT. For example, in H_2CO, the errors in the carbon and oxygen $1s \rightarrow \pi^*$ excitation energies predicted by RPA are 8.8 eV and 15.1 eV, respectively,

while those predicted by ERPA with PQG constraints are 7.2 eV and 7.7 eV. The basis set dependence of the $1s \rightarrow \pi^*$ excitation energies is quite small, and the conclusions drawn from the data in Table 7.2 are unchanged when considering the cc-pVTZ, cc-pVQZ, and aug-cc-pVTZ basis sets. The errors in the $1s \rightarrow \pi^*$ excitation energies computed in these basis sets can be found in Appendix B.

We note that TD-EOM-CC2 consistently outperforms all other methods considered here; the mean unsigned error in the TD-EOM-CC2 energies is only 2.0 eV in the cc-pCVTZ basis set. Even greater accuracy could be obtained from a higher level of coupled cluster (CC) theory [e.g. CC with single and double excitations (CCSD)]. EOM and linear-response CCSD typically yield K-edge features for second-row atoms that are accurate to roughly 1–2 eV, [155, 41] and the inclusion of triple excitations can reduce errors to less than 1 eV [41].

The performance of the ERPA appears promising, but some problematic cases reveal a shortcoming of the method that is related to the CASSCF-specific excitation operator defined in Eq. 7.12; these cases can be identified by violations in the killer condition. For example, consider N_2O described by the cc-pCVTZ basis set. ERPA computations with RDMs that satisfy PQG conditions predict two features whose wave functions contain significant $1s \rightarrow \pi^*$ contributions at similar energies (544.1 eV and 542.1 eV), which is problematic for two reasons. First, the spectrum is only expected to have one such feature. Second, the dominant term in both expansions corresponds to a $\sigma\rightarrow \pi$-type excitation; this transition is one between orbitals that are active in the full-valence CASSCF reference function, with similar occupation numbers ($n_\sigma = 0.988$ and $n_\pi = 0.985$). It is entirely possible that this transition contributes to the true wave function, but it is unlikely that it would be the dominant term in the expansion. The large expansion coefficients [Eq. 7.8] associated with this transition indicate a breakdown in the ERPA; the expansion coefficients are approximately 16 and 7 for the states at 542.1 eV and 544.1 eV, respectively.

The breakdown of the ERPA in this case may stem from the near-degeneracy of the occupations of the orbitals in question. Regardless of its precise cause, the breakdown is easily identifiable by large violations in the killer condition. We can quantify the degree to which the killer condition is violated with the root mean squared (RMS) error in Eq. 7.15

for all possible operators, $\hat{a}_t^\dagger \hat{a}_u$. For the two problematic states at the oxygen K-edge in N_2O, the RMS errors in Eq. 7.15 are 1.9×10^{-1} (at 542.0 eV) and 8.6×10^{-3} (at 544.1 eV). These errors are substantially larger than those observed in other molecules; the RMS errors in Eq. 7.15 at the oxygen K-edge in CO and H_2CO are 6.5×10^{-6} and 1.1×10^{-4}, respectively. Unlike the wave functions for K-edge states in N_2O, those in CO and H_2CO are dominated by core excitations, as expected. We therefore conclude that the difficulty in assigning the edge in N_2O reflects violations in the killer condition and a breakdown in the ERPA, perhaps caused by the near-degeneracy of the occupations of the active orbitals.

Table 7.2 includes errors in excitation energies computed using CVS-ERPA, which should reduce killer-condition violations by excluding all active/active-type excitations. The CVS approximation yields improved excitation energies for all molecules, reducing the error from ERPA by as much as 1.8 eV in the case of the oxygen K-edge in CO (with RDMs that satisfy the PQG+T2 conditions). The mean and maximum errors for CVS-ERPA with RDMs that satisfy two-particle N-representability conditions are reduced to only 6.7 eV and 8.2 eV, respectively, while those for CVS-ERPA with RDMs that satisfy partial three-particle conditions are reduced to 6.9 eV and 8.8 eV. We again find that the CVS-ERPA provides a more consistent description of multiple features within a given molecule than that afforded by other methods. Consider, for example, the $1s \rightarrow \pi^*$ transitions of the central and terminal nitrogen atoms in N_2O (denoted N_t and N_c in Table 7.2, respectively). Using the CVS-ERPA and RDMs that satisfy the PQG conditions, the error in both of the excitation energies is 6.6 eV, meaning that CVS-ERPA exactly predicts the separation between the features. No other method considered here predicts a separation between these features that agrees with experiment to this degree. Lastly, and perhaps most importantly, by disregarding all non-core excitations, the K-edge can be more clearly identified in all molecules, including in the problematic case of the oxygen K-edge of N_2O discussed above. The consideration of the killer condition is thus extremely important in the framework of the ERPA, and all remaining ERPA-derived results discussed use the CVS-ERPA excitation operator given by Eq. 7.24.

Table 7.3: Core-level ($1s \rightarrow 3s$ and $1s \rightarrow 3p$) excitation energies (eV) obtained from experiment and errors in computed excitation energies determined in the cc-pCVTZ basis set.

					CVS-ERPA	
molecule	transition	exp.	TDDFT	RPA	PQG	PQG+T2
CO	C $1s \rightarrow 3s$	292.4[a]	-6.1	14.9	12.7	12.9
	O $1s \rightarrow 3s$	538.9[b]	-12.8	25.5	17.2	17.5
H_2CO	C $1s \rightarrow 3s$	290.2[c]	-10.9	12.2	10.2	10.3
	O $1s \rightarrow 3s$	535.4[c]	-12.1	21.2	15.0	15.3
C_2H_2	C $1s \rightarrow 3s$	287.7[d]	-10.4	12.6	10.4	10.0
HCN	C $1s \rightarrow 3s$	289.1[e]	-11.4	11.3	9.3	8.8
	N $1s \rightarrow 3s$	401.8[e]	-11.6	19.1	13.9	15.2
N_2	N $1s \rightarrow 3s$	406.2[f]	-4.5	24.4	20.1	20.2
N_2O	N_t $1s \rightarrow 3s$	404.0[g]	-10.8	17.8	12.7	13.2
	N_c $1s \rightarrow 3s$	407.5[g]	-11.4	16.9	12.0	11.1
	O $1s \rightarrow 3s$	536.7[g]	-13.1	24.7	10.1	10.2
CH_4	C $1s \rightarrow 3s$	287.1[d]	-10.9	13.0	10.8	9.8
	C $1s \rightarrow 3p$	288.0[d]	-10.2	11.9	8.5	8.6
	mean unsigned error		10.5	17.4	12.5	12.6
	maximum unsigned error		13.1	25.5	20.1	20.2

[a−g] Experimental results are taken from Refs. [162], [177], [180], [216], [76], [82] and [217], respectively.

7.4.2 Rydberg features

We now consider Rydberg-type K-edge features in the small molecules considered above, as well as in CH_4. Table 7.3 provides experimentally-obtained excitation energies and errors in computed excitation energies for $1s \rightarrow 3s$ features in all molecules and the $1s \rightarrow 3p$ feature in methane. Again, all ERPA computations employed RDMs generated from full-valence v2RDM-CASSCF. As measured by the mean and maximum unsigned errors, TDDFT performs slightly better for this set of excitations than it does for the $1s \rightarrow \pi^*$ transitions; the mean and maximum unsigned errors for TDDFT are 10.4 and 13.1 eV, respectively. On the other hand, RPA and CVS-ERPA perform considerably worse. The mean and maximum unsigned errors for RPA are 17.4 eV and 25.5 eV, respectively. The CVS-ERPA improves over RPA by almost 5 eV for the mean unsigned error [12.5 eV (PQG) and 12.6 eV (PQG+T2)], and CVS-ERPA reduces the maximum error observed to 20.1 (20.2) eV when the procedure employs RDMs that satisfy the PQG (PQG+T2) conditions.

It is unclear exactly why the performance of the CVS-ERPA is so different for Rydberg-type features than for $1s \rightarrow \pi^*$ transitions. What is clear, however, is that this difference

Table 7.4: Mean unsigned errors (eV) and maximum errors (eV) in computed gaps between the $1s \rightarrow \pi^*$ and Rydberg features at the K-edge, as compared to experimentally obtained values. Mean and maximum errors in the excitation energies for $1s \rightarrow \pi^*$ transitions are provided in parentheses.

				CVS-ERPA[a]		
	basis set	TDDFT	RPA	f.v.[b]	f.v.+3s[c]	f.v.+3s3p[d]
mean	cc-pVTZ	1.8 (12.1)	5.5 (12.1)	6.4 (6.7)	6.7 (7.3)	6.1 (8.9)
	cc-pCVTZ	2.0 (12.2)	6.2 (12.1)	6.3 (6.7)	6.7 (7.3)	6.0 (8.9)
	aug-cc-pVTZ	1.4 (12.5)	4.2 (12.1)	5.9 (6.8)	5.7 (7.5)	4.9 (8.9)
	cc-pVQZ	0.9 (12.3)	5.5 (12.1)	6.4 (6.7)	6.4 (7.3)	5.7 (9.0)
maximum	cc-pVTZ	9.6 (14.3)	10.1 (18.5)	14.1 (8.2)	11.6 (8.3)	11.2 (12.4)
	cc-pCVTZ	8.0 (14.3)	13.1 (18.5)	13.7 (8.2)	11.5 (8.4)	10.7 (12.4)
	aug-cc-pVTZ	3.4 (15.3)	6.1 (18.5)	10.9 (8.3)	9.7 (9.3)	8.4 (12.3)
	cc-pVQZ	2.7 (14.4)	7.9 (18.4)	12.4 (8.2)	10.8 (8.4)	9.9 (12.4)

[a] CVS-ERPA computations employed RDMs that satisfied the PQG N-representability conditions
[b] a full valence active space
[c] f.v. plus orbitals of the symmetry of the 3s orbital on each heavy atom
[d] f.v. plus orbitals of the symmetry of the 3s and 3p orbitals on each heavy atom

directly impacts the utility of ERPA for evaluating the relative positions of these features at the K-edge. Indeed, while CVS-ERPA yields slightly better absolute excitation energies than those provided by RPA, the overall spectral shape predicted by CVS-ERPA and RPA are similar. As a measure of the shape of the absorption curve, we present in Table 7.4 the errors in computed gaps between the $1s \rightarrow \pi^*$ and Rydberg features tabulated above, as compared to those from experiment. According to this metric, neither RPA nor CVS-ERPA perform particularly well, with slightly worse results obtained from CVS-ERPA. Mean errors for both methods are on the order of 5–6 eV, depending on the choice of the basis set. On the other hand, TDDFT provides much more reasonable results; the B3LYP functional yields the gaps between these features with an accuracy of roughly 1–2 eV, on average.

One factor that potentially contributes to the poor performance of CVS-ERPA observed here is that the full-valence active space does not include the $3s$ and $3p$ orbitals. Table 7.4 also provides errors in the spacing between the $1s \rightarrow \pi^*$ and Rydberg features obtained from CVS-ERPA with two slightly larger active spaces consisting of the full valence space plus orbitals of the symmetry of the 3s or 3s and 3p orbitals on each heavy atom (see Table 8.1 for details). The errors in the excitation energies for $1s \rightarrow \pi^*$ transitions are also provided in parentheses. We find that the CVS-ERPA predictions for the relative positions of the K-

edge features improve slightly with the larger active spaces, and the accuracy of CVS-ERPA approaches that of the usual RPA with the largest active space. However, the quality of the description of the $1s \rightarrow \pi^*$ transitions decreases with increasing size of the active space size.

7.4.3 The role of orbital basis

The data discussed to this point demonstrate that the CVS-ERPA and RPA approaches offer comparable descriptions of K-edge features in small molecules. CVS-ERPA provides a modest improvement in absolute excitation energies for both $1s \rightarrow \pi^*$ and Rydberg-type excitations, but the methods predict similar relative positions of the excitations. Two features of the CVS-ERPA framework distinguish it from RPA, which lead to the small differences in the numerical performance of the approaches. Both distinctions are rooted in the underlying v2RDM-CASSCF-based description of the ground state. First, the RDMs that enter CVS-ERPA contain nondynamical correlation information lacking in RPA based on a Hartree-Fock reference. Second, the orbitals employed within CVS-ERPA are optimized for the correlated ground state. We can differentiate between the effects of correlation and orbital optimization within the CVS-ERPA by employing RDMs generated from ground-state active-space v2RDM computations that do not involve any orbital optimization [i.e. v2RDM-driven complete active space (CAS) CI]. Figure 7.4.3 illustrates the mean unsigned errors for RPA and CVS-ERPA in several basis sets, and CVS-ERPA computations either employed v2RDM-CASSCF or v2RDM-CASCI references [labeled CVS-ERPA(CASSCF) and CVS-ERPA(CASCI), respectively]. In all basis sets, orbital optimization leads to a significant improvement in the quality of the CVS-ERPA excitation energies. Interestingly, in the case of the aug-cc-pVTZ basis set, it appears that an ERPA that accounts for static correlation alone offers essentially no advantage over the usual RPA.

The fact that the performance of CVS-ERPA is coupled to the choice of orbital basis is not surprising; it is well known that orbital relaxation effects are considerable for core-excited states. In principle, the performance of CVS-ERPA could be improved by choosing a more appropriate set of orbitals than the those obtained from Hartree-Fock or v2RDM-CASSCF.

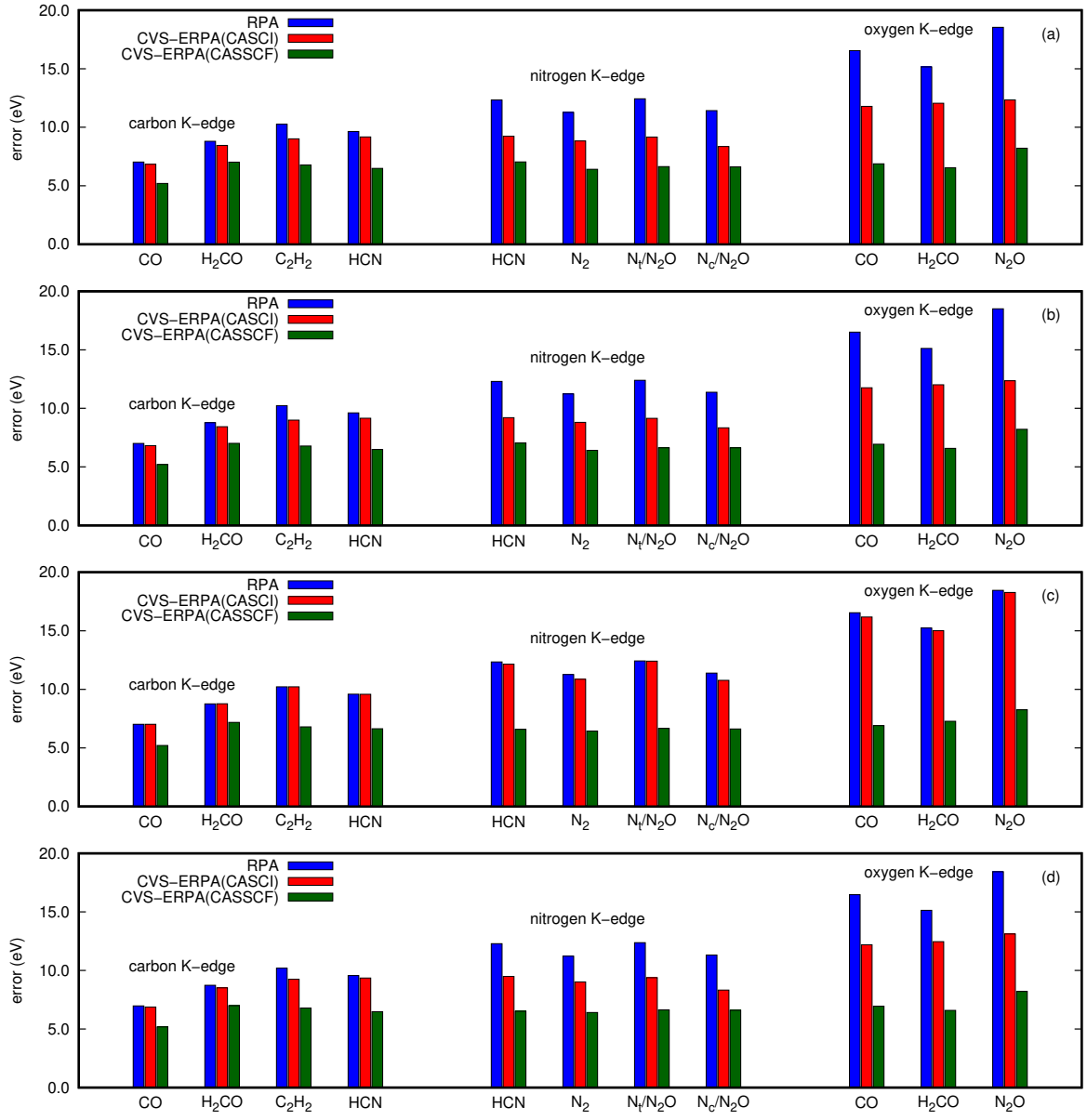

Figure 7.1: Mean unsigned errors (eV) in computed excitation energies for K-edge features in small molecules described by the (a) cc-pVTZ, (b) cc-pCVTZ, (c) aug-cc-pVTZ, and (d) cc-pVQZ basis sets.

From the perspective of CASSCF, the most obvious strategy would be to employ a state-averaged (SA) [106, 31, 77] v2RDM-CASSCF procedure that optimizes the orbitals for the ground and target excited states simultaneously. Excited-state RDMs required for such a procedure are accessible within the equation of motion framework. Alternatively, one could pre-relax the orbitals as is done within the static exchange (STEX) approximation [3, 2, 47] or employ CIS natural orbitals as approximation to SA-CASSCF. [199] While each of these strategies may yield improved orbitals for the description of core excitations, within the context of the ERPA, they all share the same potential shortcoming. As mentioned above, the ERPA problem is nonsymmetric, but it can be recast as a symmetric problem, provided that the reference is stable. Unfortunately, a guarantee of stability requires that the orbitals be optimized for the ground state, and the use of STEX or (approximate) SA-CASSCF orbitals could lead to instabilities in the ERPA equations.

7.4.4 Oscillator strengths

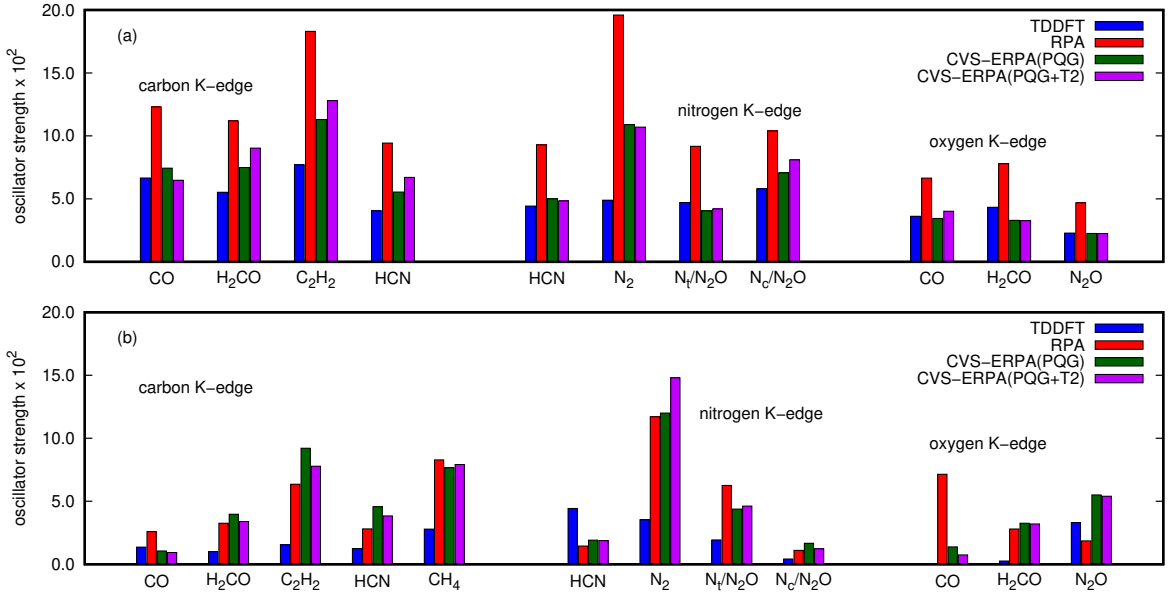

Figure 7.2: Computed oscillator strengths for (a) $1s \rightarrow \pi^*$ and (b) $1s \rightarrow 3s$ excitations in small molecules described by the cc-pCVTZ basis set. In panel (b), the oscillator strength for CH_4 corresponds to the $1s \rightarrow 3p$ transition.

Lastly, we consider the quality of CVS-ERPA-derived oscillator strengths. Within Rowe's equation of motion formalism and the ERPA, the transition dipole moment that defines the oscillator strength is given by

$$\langle \Psi_n | \hat{\mu}_\xi | \Psi_0 \rangle = \langle \Psi_0 | [\hat{O}_n, \hat{\mu}_\xi] | \Psi_0 \rangle, \tag{7.25}$$

where $\hat{\mu}_\xi$ is the ξ-component of the dipole operator ($\xi \in x, y, z$). Figure 7.4.4 illustrates the oscillator strengths computed at the TDDFT, RPA, and CVS-ERPA levels of theory within the cc-pCVTZ basis set; CVS-ERPA computations employed RDMs from full-valence v2RDM-CASSCF that satisfied either PQG or PQG+T2 N-representability conditions. For $1s \rightarrow \pi^*$ excitations [Fig. 7.4.4 (a)] CVS-ERPA oscillator strengths resemble those from TDDFT more than those from RPA. In particular, when using RDMs that satisfy PQG N-representability conditions, CVS-ERPA oscillator strengths tend to agree with those from TDDFT to a greater degree than when using RDMs that satisfy PQG and T2 conditions. On the other hand, oscillator strengths for Rydberg-type excitations [Fig. 7.4.4 (b)] computed using CVS-ERPA appear to resemble those from RPA more than those from TDDFT.

7.5 Conclusions

We have developed a procedure for computing core-level excitation energies using a combination of the variational optimization of the ground-state 2-RDM and the extended random phase approximation. Because we lack N-representability conditions that differentiate between ground- and excited-state RDMs, the direct optimization of an excited-state 2-RDM is still an open problem. As a result, several non-variational approaches have been proposed that can extract excited-state information from variationally obtained ground-state RDMs. The ERPA is one such method.

We have benchmarked the quality of ERPA- and CVS-ERPA-derived $1s \rightarrow \pi^*$, $1s \rightarrow 3s$, and $1s \rightarrow 3p$ excitations in a set of small molecules for the case that the ground-state 2-RDMs are obtained from a v2RDM-driven CASSCF procedure. In general, we find that CVS-ERPA offers a modest improvement over its uncorrelated limit, the RPA, when considering absolute

excitation energies. In particular, the description of $1s \rightarrow \pi^*$-type transitions that the CVS-ERPA offers is somewhat better than that provided by both RPA and TDDFT (with the B3LYP functional). However, the CVS-ERPA appears to be a less promising approach for the description of Rydberg-type excitations. In this case, CVS-ERPA absolute excitation energies are still slightly better than those from RPA, but mean and maximum unsigned errors from CVS-ERPA are larger than those from TDDFT. Further, CVS-ERPA is slightly less accurate than RPA for predicting the relative positions of the principal and Rydberg features. Similar conclusions can be drawn from the inspection of oscillator strengths. For $1s \rightarrow \pi^*$-type excitations, CVS-ERPA-derived oscillator strengths are in better agreement with those from TDDFT than with those from RPA (presumably, the TDDFT oscillator strengths are the more reliable ones). However, the CVS-ERPA does not consistently offer any improvement over RPA for oscillator strengths corresponding to $1s \rightarrow 3s$ and $1s \rightarrow 3p$ excitations.

Interestingly, we have shown that the (CVS-)ERPA appears to be insensitive to the degree to which the ground-state 2-RDMs are N-representable. In terms of both excitation energies and oscillator strengths, results from the (CVS-)ERPA are quite similar when utilizing RDMs that satisfy either the two-particle (PQG) constraints or two-particle plus partial three-particle (PQG+T2) constraints. This result suggests that the imposition of computationally demanding higher-order N-representability conditions on RDMs that enter the (CVS-)ERPA may not be as crucial as it is for the ground-state problem itself.

We derived new conditions implied by the killer condition that should be fulfilled by ERPA-derived excited-state wave functions. One subset of these conditions can be satisfied by removing active/active-type excitations from the ERPA excitation operator. We showed that the CVS-ERPA excitation operator (which removes all active/active-type excitations) consistently yields excitation energies that are superior to those obtained with the original CASSCF-specific ERPA excitation operator. The truncated operator also simplifies the assignment of K-edge features in some molecules.

Lastly, we demonstrated that the EOM-CC2 framework provides a description of $1s \rightarrow \pi^*$ excitations that is clearly superior to that from TDDFT, RPA, or CVS-ERPA, and we note

that even more accurate results could be obtained by considering higher levels of CC theory. Along these lines, the success of the CC hierarchy suggests a clear route to improving CVS-ERPA. The inclusion of double excitations within the ERPA will undoubtedly improve the description of the core-excited states. Without any additional approximations, an ERPA procedure that includes doubles could be devised with knowledge of the ground-state four-electron reduced-density matrix. Further, the present formulation of the ERPA could be improved by accounting for orbital relaxation effects, either through the STEX approximation or a combined SA-CASSCF/ERPA procedure.

CHAPTER 8

A DYNAMICAL CORRELATION MODEL FOR THE VARIATIONAL TWO-ELECTRON REDUCED DENSITY MATRIX COMPLETE ACTIVE SPACE SELF-CONSISTENT FIELD METHOD

8.1 Introduction

An accurate description of molecular electronic structure ought to include a mixing of all possible electronic states of the molecule. This is effectively done within a finite orbital basis by representing the wavefunction as a configuration interaction (CI) of all the determinants that can be defined within that basis. However, this representation of the wavefunction presents immense computational hurdles for all but the smallest many-electron systems. For larger systems, one typically expresses the wavefunction as a linear combination of select configurations. This is the basis of the multiconfigurational self-consistent field (MCSCF) approach [71, 44, 36, 107, 189, 225, 80, 75, 19, 12, 11, 34, 117, 246]. While this approach overcomes the expense of a full CI, one needs to know beforehand the important configurations to include in the description of the wavefunction. Probably the most widely used formulation of MCSCF is the complete active space (CAS) approach. Here, a subspace of chemically important orbitals is defined, and the wavefunction represented as a linear combination involving all determinants that can be made from all possible excitations within that subspace. Since only a subset of the determinants that define the full CI wavefunction comprise the wavefunction, energies computed using CAS approaches are upper bounds to the full CI energy. If the space of chemically important orbitals is large enough, one accounts sufficiently for *nondynamical* correlation effects, and the deviation of the energy from full CI

can be attributed to the inadequacy of the CAS wavefunction in accounting for *dynamical* correlation.

In order to account for the remaining correlation in a CAS framework, the wavefunction is often corrected to the desired order by perturbation theory. This defined the complete active space perturbation theory (CASPT) approaches. Typically, the wavefunction is corrected to first order, and the energy to second order, as in the complete active space second-order perturbation theory (CASPT2)[7, 88] and second order n-electron perturbation theory (NEVPT2)[8, 9], and driven similarity renormalization group second-order perturbation theory (DSRG-PT2). [108, 68]. Other approaches include multireference configuration interaction (MRCI) [25, 26, 69, 230] and multireference coupled-cluster (MRCC)[118, 97, 171, 79, 17, 78, 174, 173, 172, 45, 122, 121, 202, 33, 163, 110, 109, 111, 164, 149]. These methods can generally be applied quite successfully to a range of many-electron systems, but their ability to tackle larger systems can be limited. For instance, in the CASPT2 and NEVPT2 methods, one needs to evaluate the active space three- and four-electron reduced density matrix (3- and 4-RDM), which can be quite costly when the active space being considered is large. In DSRG-PT2, one needs to compute the three-body density cumulant of the reference. In the MRCI method, scaling with respect to excitation level is steep, and truncation at lower excitation levels is often necessary. The same can be said for MRCC methods. Additionally, a final and generally acceptable MRCC theory is still lacking.[97].

Recently, a different approach for computing the remaining dynamical correlation for state specific CAS wavefunctions was presented by Pernal and coworkers. [166] By employing an adiabatic connection (AC) between two Hamiltonians describing a non-interacting limit/system defined by the CASSCF wavefunction, and the fully interacting limit defined by full CI. They show that the approximate remaining dynamical correlation energy can be computed as an integral of a function of the elements of 1RDMs of the reference, and transition density matrices. We obtain approximate transition density matrices using excited state information obtained by applying Rowe's equation of motion (EOM) and the extended random phase approximation (ERPA)[32, 46]. As we will show, this is convenient in the case where the variational two-electron reduced density matrix (v2RDM-) CASSCF method

[57, 56] is used to compute references. First of all, reference 1- and 2RDMs are readily available for calculations of excited states needed to compute transition density matrices and more significantly, the remaining dynamical correlation energy can be computed for references involving active-spaces larger than those that can be tackled with configuration interaction (CI-) driven CASSCF.

This chapter is organized as follows. In section II, we briefly summarize the theory of the AC for CAS wavefunctions, and we show how the ERPA makes it possible to compute the remaining dynamical correlation using 1- and 2-RDMs from a reference calculated at the CASSCF level of theory. In sections III and IV, we present, respectively, computational details and numerical examples that illustrate the performance of this corrected v2RDM-CASSCF (hereafter, the v2RDM-CASSCF+AC) approach. In section V, we present some conclusions.

8.2 Theory

Here, we summarize the derivation outlined in Ref. 166. The remaining correlation energy not accounted for by a CASSCF wavefunction can be written

$$E_{corr} = E_{exact} - \langle \Psi | \hat{H} | \Psi \rangle. \tag{8.1}$$

where Ψ denotes the CASSCF wavefunction and $\hat{H}$ the full interaction Hamiltonian. The many-electron system as described by the CASSCF wavefunction can now be considered to represent a non-interacting limit. This system is connected to the fully-interacting limit by an adiabatic connection Hamiltonian, H^{α}, defined

$$\forall \ 0 \leq \alpha \leq 1, \quad \hat{H}^{\alpha} = \hat{H}^{(0)} + \alpha(\hat{H} - \hat{H}^{(0)}) \tag{8.2}$$

Here, $\hat{H}^{(0)}$ is a Hamiltonian whose expectation value defines the CASSCF energy, $\hat{H}$ is the full-interaction Hamiltonian, and α is a parameter such that when it is varied from 0 to 1, one smoothly switches between the uncorrelated limit defined by CASSCF, and the full interaction limit. From the exact relationship between the ground state two-electron reduced

density matrix, defined here in terms of natural spin orbitals p, q, r and s

$$^2D^{pq}_{rs} = \langle\Psi_0|\hat{a}^\dagger_p\hat{a}^\dagger_q\hat{a}_r\hat{a}_s|\Psi_0\rangle, \tag{8.3}$$

the one-electron reduced density matrix

$$^1D^{p}_{r} = \langle\Psi_0|\hat{a}^\dagger_p\hat{a}_r|\Psi_0\rangle, \tag{8.4}$$

and transition density matrices[140]

$$\gamma^{0\nu}_{pr} = \langle\Psi_0|\hat{a}^\dagger_p\hat{a}_r|\Psi_\nu\rangle, \tag{8.5}$$

$$\gamma^{\nu 0}_{qs} = \langle\Psi_\nu|\hat{a}^\dagger_q\hat{a}_s|\Psi_0\rangle, \tag{8.6}$$

an expression for the approximate value of E_{corr} can be derived

$$E^{AC}_{corr} = \int_0^1 W^\alpha \mathrm{d}\alpha, \tag{8.7}$$

where W^α involves transition density matrices $\gamma^{\alpha,0\nu}$ and $\gamma^{\alpha,\nu 0}$ evaluated along the path of the adiabatic connection

$$W^\alpha = \frac{1}{2}{\sum_{pqrs}}' \big(\sum_\nu \gamma^{\alpha,0\nu}_{pr}\gamma^{\alpha,\nu 0}_{qs} + (^1D^p_p - 1)(^1D^q_q)\delta_{rq}\delta_{ps}\big)(pr|qs) \tag{8.8}$$

with the prime symbol indicating that all contributions involving cases where all four labels p, q, r, and s denote either active or inactive electrons, are excluded. In deriving the results in Equation 8.7, it has been assumed that the one-electron density matrix stays constant along the path of the adiabatic connection

$$\forall\, 0 \leq \alpha \leq 1,\ \ ^1D^{p,\alpha}_q = {}^1D^{p,\alpha=0}_q. \tag{8.9}$$

We compute approximate transition density matrices along the path of the adiabatic connection by applying the spin-adapted form of the extended random phase approximation (ERPA)

$$|\hat{\Psi}_\nu\rangle = \frac{1}{\sqrt{2}}\sum_{pq} c^\nu_{pq}(\hat{a}^\dagger_p\hat{a}_q\ + \hat{a}^\dagger_{\bar{p}}\hat{a}_{\bar{q}})|\Psi_0\rangle \tag{8.10}$$

and Rowe's equation of motion (EOM) approach to obtain the following generalized eigenvalue problem

$$\sum_{pq,p\neq q} c_{pq}^{\nu} \langle\Psi_0|[\hat{a}_r^\dagger \hat{a}_s + \hat{a}_{\bar{r}}^\dagger \hat{a}_{\bar{s}}, [\hat{H}^\alpha, \hat{a}_p^\dagger \hat{a}_q + \hat{a}_{\bar{p}}^\dagger \hat{a}_{\bar{q}}]]|\Psi_0\rangle = \omega_\nu \sum_{pq,p\neq q} c_{pq}^{\nu} \langle\Psi_0|[\hat{a}_r^\dagger \hat{a}_s + \hat{a}_{\bar{r}}^\dagger \hat{a}_{\bar{s}}, \hat{a}_p^\dagger \hat{a}_q + \hat{a}_{\bar{p}}^\dagger \hat{a}_{\bar{q}}]|\Psi_0\rangle. \tag{8.11}$$

In equations 8.10 and 8.11, the overbar denotes a β spin orbital, and the lack thereof, an α spin orbital. The left hand side of equation 8.11 is a function of elements of the 2RDM computed at the v2RDM-CASSCF level of theory, and the right hand side that of elements of the 1RDM. The cost of solving this equation scales as the cube of the number of elements on the left hand side. Transition density matrix elements can subsequently be computed as a function of elements of the 1RDM and the set of excitation and deexcitation coefficients $\{c_{pq}^{\nu}\}$

$$\gamma_{ij}^{\alpha,0\nu} = \sum_{pq} c_{pq}^{\nu} \langle\Psi_0|[\hat{a}_p^\dagger \hat{a}_q, \hat{a}_j^\dagger \hat{a}_i]|\Psi_0\rangle \tag{8.12}$$

Lastly, a cheaper approximation for the remaining correlation energy can be derived for multireference wavefunctions such as CASSCF, for which coupling between active, inactive, and virtual orbitals can be assumed to be weak. In such a case, an approximate value of E_{corr}^{AC} can be computed as a function of $W^{(1)}$, the first order term in the perturbative expansion of W^α.

$$E_{corr}^{AC} \approx E_{corr}^{AC0} = \frac{W^{(1)}}{2} \tag{8.13}$$

We refer readers to Ref. 166 for more details on this derivation.

8.3 Computational details

We obtain reduced density matrices at the single root CASSCF level of theory using the v2RDM-CASSCF method. For these v2RDM-CASSCF calculations, full valence active spaces are used. Table 8.1 summarizes the molecules and active spaces used in the first part of this study. We also use full valence active spaces in computing single point energies pertinent to a set of 29 reactions for which CCSD(T) data is available. The reaction set

used is similar to the one used in the optimization of parameters for spin-component-scaled (SCS) MP2[66] and SCS-CCSD methods[211]. The geometries used for these calculations were obtained from the supporting information of Ref. 211.

For the molecules summarized in table 8.1, Dunning's cc-pVXZ basis sets (X = D, T, Q) [87] were used, whereas only the cc-pVQZ basis set was used for the calculation of reaction energies. was used. The evaluation of two-electron integrals is accelerated by making use of the density-fitting (DF) approximation. For calculations where the primary basis set is cc-pVXZ (X = D, T, Q), the cc-pVQZ-JKFIT[226] auxiliary basis set is used.

Table 8.1: Full-valence active spaces when using the C_{2v} ([A_1, A_2, B_1, B_2]) and D_{2h} ([A_g, B_{1g}, B_{2g}, B_{3g}, A_u, B_{1u}, B_{2u}, B_{3u}]) point groups.

molecule	point group	active space	restricted orbitals	active orbitals
H_2O	C_{2v}	(8e, 6o)	[1, 0, 0, 0]	[3, 0, 1, 2]
N_2	D_{2h}	(10e, 8o)	[1, 0, 0, 0, 0, 1, 0, 0]	[2, 0, 1, 1, 0, 2, 1, 1]
CO_2	D_{2h}	(16e, 12o)	[2, 0, 0, 0, 0, 1, 0, 0]	[3, 0, 1, 1, 0, 3, 2, 2]
H_2	D_{2h}	(2e, 2o)	[0, 0, 0, 0, 0, 0, 0, 0]	[1, 0, 0, 0, 0, 1, 0, 0]
H_4	D_{2h}	(4e, 4o)	[0, 0, 0, 0, 0, 0, 0, 0]	[2, 0, 0, 0, 0, 2, 0, 0]
H_6	D_{2h}	(6e, 6o)	[0, 0, 0, 0, 0, 0, 0, 0]	[3, 0, 0, 0, 0, 3, 0, 0]
H_8	D_{2h}	(8e, 8o)	[0, 0, 0, 0, 0, 0, 0, 0]	[4, 0, 0, 0, 0, 4, 0, 0]

In computing 1- and 2-RDMs using the v2RDM-CASSCF method, active-space 1- and 2-RDMs are constrained to be ensemble N-representable by requiring that they satisfy ensemble N-representability conditions. The N-representability constraints include those that ensure the RDMs have the correct spin, trace, as well as the correct relationship to lower order RDMs. Less trivial are the p-body conditions which ensure that joint probabilities associated with any sum total of p particles (electrons, holes) in the active space are non-negative, and a hierarchy of such conditions can be defined, depending on the number of electrons and orbitals in the active space. In practice, we enforce the two-body (PQG)[61] conditions, which are often good enough for a qualitative description of the electronic structure, or partial three-body (T2)[48] conditions, which are often necessary for quantitative (sub kcal/mol) agreement with configuration interaction- (CI-) driven CASSCF. We consider the ground state RDM calculations converged when the primal-dual error and the primal-

dual energy gap [57] fall below 1.0×10^{-5} (in certain cases 1.0×10^{-4}) and 1.0×10^{-4} E_h, respectively.

The integral in equation (8.7) is evaluated by numerical integration using the trapezium rule with 10 intervals. Except for the rare cases in which instabilities occur in equation (8.11), W^α is very nearly linear with respective to α, and numerical integration with only a few intervals yields a good approximation.

The code used to compute energies at the v2RDM-CASSCF+AC level of theory is implemented as a plugin to the Psi4[165] electronic structure package. In addition, Psi4 was used to compute the full-CI energies used as yardstick data in this study. The Orca [156] electronic structure package was used to compute ground state energies at the NEVPT2 level of theory. For calculations at the CASPT2 level of theory, the OpenMolcas[10] package was used, with the IPEA shift parameter set to 0.25 E_h.

8.4 Results and discussion

8.4.1 Potential energy curves

We start by considering potential energy curves for the singlet ground state of H_2O upon symmetric dissociation, as shown in Fig. 8.4.1. Visually, there is good agreement between v2RDM- and CI-based CASSCF. Numerically, the maximum unsigned errors of v2RDM-CASSCF with respect to CI-CASSCF are 7 mE_h and 0.7 mE_h when using the PQG and PQG+T2 constraints, respectively. Both these maximum errors occur at a bond length of about 1.8 Å, in the intermediate region between the weak and strong static correlation regimes. We also compare the NEVPT2 approach to v2RDM-CASSCF+AC, and we find that the v2RDM-CASSCF+AC method recovers more correlation energy, in absolute terms, than does NEVPT2. Now, when we compare v2RDM-CASSCF+AC where the RDMs used are from a v2RDM-CASSCF calculation where the PQG N-representability conditions are used, and another where the RDMs used are from a v2RDM-CASSCF calculation with the PQG+T2 condition, we find that comparable amounts of correlation energy are recovered, with v2RDM-CASSCF+AC (PQG) recovering slightly more of the correlation energy in

absolute terms. The maximum unsigned difference in the correlation energies recovered between these two curves is only 0.6 mE_h.

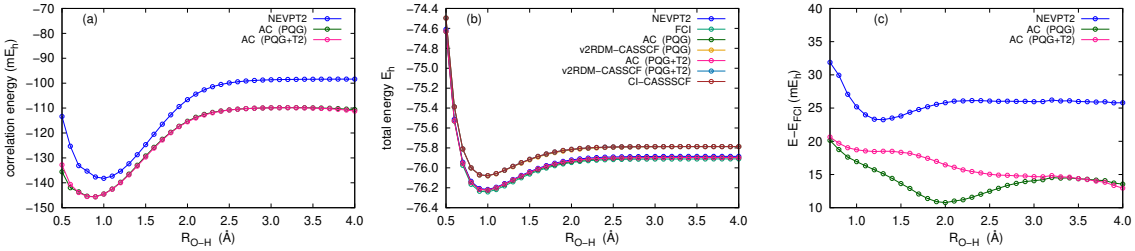

Figure 8.1: Correlation energy (a), total energy (b) and error relative to full CI (c) for the singlet ground state of H_2O computed with the cc-pVDZ basis set.

We also investigate the triple bond cleavage/dissociation of N_2. Here we see, from Fig. 8.4.1, good qualitative agreement in energies between CI- and v2RDM-CASSCF, and good quantitative agreement between CI- and v2RDM-CASSCF (PQG+T2). When we compare the v2RDM-CASSCF+AC approach to NEVPT2, we find once more that the AC approach recovers more dynamical correlation energy in comparison, and is closer to the yardstick potential energy curve from MRCISDTQ [67]. We note that between the two potential energy curves from v2RDM-CASSCF+AC, comparable amounts of electron correlation energy are recovered, whether the reference RDM used is from a v2RDM-CASSCF computation with PQG or PQG+T2 constraints. In the range of N-N distances presented here ($1.0 \leq R_{NN} \leq 5.3$ Å), the two curves differ by at most 0.8 mE_h.

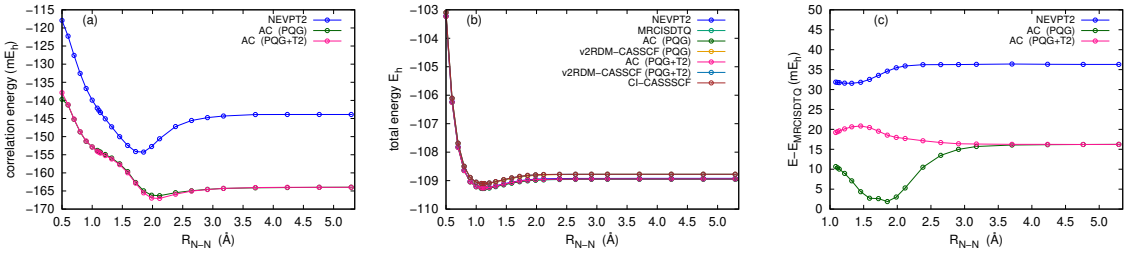

Figure 8.2: Correlation energy (a), total energy (b) and error relative to MRCISDTQ (c) for the singlet ground state of N_2 computed with the cc-pVDZ basis set.

We also look at the potential energy curves of the ground state of linear hydrogen chains, prototypical systems for strong correlation. Fig. 8.4.1 shows the potential energy curves of the singlet ground states of H_2, H_4 and H_6 calculated at various levels of theory. For H_2, there is perfect agreement at all bond lengths between CI-based and v2RDM-based CASSCF. This is because the two-body (PQG) constraints used in the v2RDM-CASSCF calculation guarantee ensemble N-representability of the ground state RDM. In such a case, the two approaches to CASSCF are equivalent. Since there are no inactive electrons in this case, the remaining dynamical correlation energy is computed from an integrand whose calculation involves summing over active and virtual orbital labels. We find that the v2RDM-CASSCF+AC-based approach recovers a larger amount of correlation energy, particularly at shorter bond lengths, when compared with NEVPT2. For this reason, the v2RDM-CASSCF+AC approach produces potential energy curves closer to full-CI. For H_4 and H_6, we see similar qualitative results. However, for these cases, total energies computed from RDMs using v2RDM-CASSCF with the PQG conditions can fall below their full-CI values at bond lengths between those that define weak and strong static correlation. This is remedied by using references computed from v2RDM-CASSCF calculations with the PQG+T2 conditions.

In order to assess the performance of the v2RDM-CASSCF+AC approach over entire potential energy curves, we compute nonparallelity errors relative to full CI (for H_2O and H_n, n=2,4,6) and MRCISDTQ (for N_2). These are summarized in Table 8.2. For H_2, nonparallelity errors are 6.4 and 3.5 mE_h, respectively, for NEVPT2 and v2RDM-CASSCF (PQG). For H_4, they are 12.2, 10.4, and 8.8 mE_h with respect to NEVPT2, v2RDM-CASSCF+AC (PQG), and v2RDM-CASSCF+AC (PQG+T2), and for H_6, 14.0, 13.6, and 10.0 mE_h. For H_2O, nonparallelity errors are 8.6, 9.4, and 7.7 mE_h with respect to NEVPT2, v2RDM-CASSCF+AC (PQG) and v2RDM-CASSCF+AC (PQG+T2). For N_2, they are 4.8, 14.4, and 4.8 mE_h.

Lastly, for these test systems, we compute estimates of bond strengths based on the depths of the potential energy curves. We find that the v2RDM-CASSCF+AC approach deviates from full CI by 2.1 kcal/mol in its estimate of the H−H bond strength in H_2,

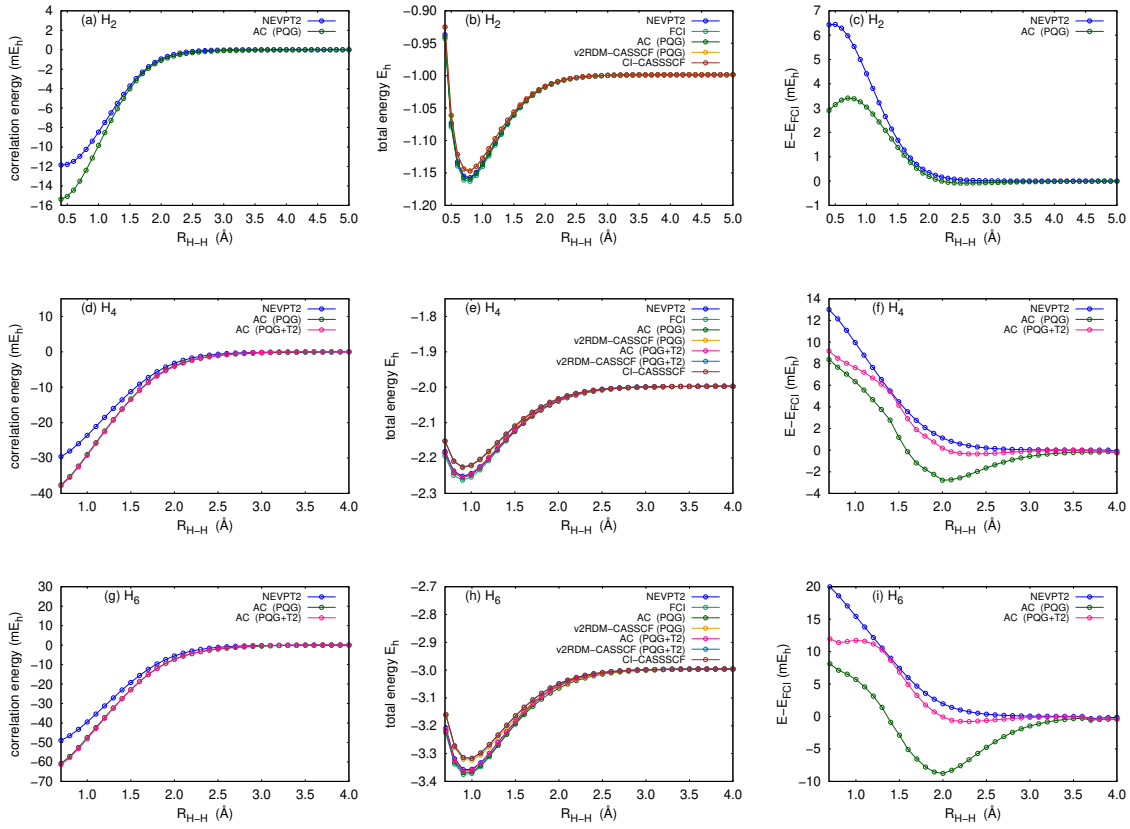

Figure 8.3: Correlation energy (a), (d), and (g), total energy (b), (e), and (h), and error relative to full CI (c), (f), and (i) for the singlet ground state of H_n, $n = 2, 4, 6$ computed with the cc-pVDZ basis set.

Table 8.2: Nonparallelity errors (mE_h) computed within the cc-pVDZ basis set approximation.

		v2RDM-CASSCF+AC	
molecule	NEVPT2	PQG	PQG+T2
H_2	6.4	3.5	†
H_4	12.2	10.4	8.8
H_6	18.9	15.9	12.5
H_2O	8.6	9.4	7.7
N_2	4.8	14.4	4.8

† PQG provides exact ensemble N-representability

Table 8.3: Estimated bond strengths (kcal/mol).

			v2RDM-CASSCF+AC	
molecule	ref.[a]	NEVPT2	PQG	PQG+T2
H_2	103.0	99.5	100.9	†
H_2O	104.0	104.2	102.9	102.1
N_2	201.4	204.3	205.1	199.3

[a] ref. from full CI (H_2 and H_2O), and MRCISDTQ (N_2).
† PQG provides exact ensemble N-representability

whereas NEVPT2 deviates by 3.5 kcal/mol. For H_2O, the v2RDM-CASSCF+AC approach deviates from full CI by 1.1 and 1.9 kcal/mol, respectively, in its estimation of the O−H bond strength, when references from v2RDM-CASSCF-PQG or v2RDM-CASSCF (PQG+T2) are used. The NEVPT2 approach, on the other hand, deviates from the full CI estimate by only 0.2 kcal/mol. For N_2, we estimate the strength of the N−N triple bond to be 3.7 kcal/mol above and 2.1 kcal/mol below that predicted with MRCISDTQ, whereas NEVPT2 predicts a value that is 2.9 kcal/mol higher. Table 8.3 summarizes these results.

8.4.2 Relative energies

We apply the AC-v2RDM-CASSCF approach to compute relative energies from a stoichiometric difference in molecular single point energies. We use a test set of molecules for which high-quality CCSD(T)/cc-pVQZ data are available. The electronic structure of this entire set of molecules is dominated by dynamical correlation, and provides a rather extreme test by which we can assess the performance of the v2RDM-CASSCF+AC approach. We also assess the performance of the CASPT2 approach, which would probably be the method most readily available to correct for dynamical correlation effects when using complete active space approaches. We summarize computed relative energies in (Table 8.4). These have been computed from single point energies found in Table C.1 in Appendix C.

In order to assess how the N-representability conditions used in the ground state calculation affect the overall relative energies, we compare the mean and maximum unsigned errors for the v2RDM-CASSCF calculation, using each of the PQG and PQG+T2 constraints. We realize mean unsigned errors of 13.5 and 12.9 kcal/mol, relative to CCSD(T), showing that,

at the v2RDM-CASSCF level of theory, computed relative energies are roughly equivalent between calculations with the PQG and PQG+T2 N-representability conditions. These errors, as we expect, are much larger than those for the methods that account for dynamical correlation effects post-CASSCF.

When we compare relative energies computed with the v2RDM-CASSCF+AC approach, we note mean and maximum unsigned errors of 7.1 and 19.4 kcal/mol, respectively, when the underlying v2RDM-CASSCF calculation involves the PQG N-representability conditions. The mean and maximum unsigned errors are only 2.2 and 6.5 kcal/mol, when the PQG+T2 conditions are used instead. Thus the overall reaction energies are sensitive to the N-representability conditions used in the underlying v2RDM-CASSCF calculation. A similar result is obtained when looking at reaction energies computed at the v2RDM-CASSCF+AC0 level of theory, for which mean unsigned errors are 8.0 and 3.5 kcal/mol, when using RDMs from v2RDM-CASSCF with the PQG and PQG+T2 constraints, respectively.

Lastly, we compare the v2RDM-CASSCF+AC approach to CASPT2, and we see that when using RDMs from v2RDM-CASSCF with the PQG conditions, errors are much larger than those for CASPT2, which gives mean and maximum unsigned errors of 2.4 and 7.6 kcal/mol, respectively. Only when we use RDMs from v2RDM-CASSCF calculations with the PQG+T2 do we get comparable errors. With the v2RDM-CASSCF+AC (PQG+T2) approach , errors in the reaction energies are slightly smaller than those from CASPT2, whereas with the v2RDM-CASSCF+AC0 (PQG+T2), errors are slightly larger.

8.5 Conclusions

We have presented a model for dynamical correlation energy for the v2RDM-CASSCF method. The model is based on the adiabatic connection between the Hamiltonian describing a system at the v2RDM-CASSCF level of theory, and another described by full CI.

We computed potential energy curves for a range of molecules. The potential energy curves we obtain using this method are qualitatively accurate, and predicted equilibrium bond lengths for the singlet ground states are consistent with those from full CI calculations.

Table 8.4: Relative energies (kcal/mol) from CCSD(T), v2RDM-CASSCF+AC(0), and CASPT2 (labeled PT2)

		PQG			PQG+T2			
reaction	CCSD(T)	ref.	AC	AC0	ref.	AC	AC0	PT2
[a]$F_2 + H_2 \rightarrow 2HF$	-134.1	17.7	1.8	-4.4	†	†	†	-2.7
$F_2O + H_2 \rightarrow F_2 + H_2O$	-68.4	6.1	0.2	2.4	4.0	-1.6	0.6	1.9
$O_3 + 3H_2 \rightarrow 3H_2O$	-223.4	45.7	14.3	-22.8	33.8	1.9	2.2	4.7
$H_2O_2 + H_2 \rightarrow 2H_2O$	-86.3	8.3	2.3	4.8	6.3	0.3	2.7	0.3
$CO + H_2 \rightarrow CH_2O$	-4.6	4.7	-12.0	-13.7	15.7	-1.0	-2.1	-2.2
$CO + 3H_2 \rightarrow CH_4 + H_2O$	-63.6	33.3	-5.0	-7.0	37.9	0.8	-0.7	-2.8
$N_2 + 3H_2 \rightarrow 2NH_3$	-38.0	36.7	0.4	2.5	37.5	4.0	9.5	0.9
$^1CH_2 + H_2 \rightarrow CH_4$	-128.8	5.0	-6.7	-6.2	9.3	-1.7	-0.5	-2.7
$N_2O + H_2 \rightarrow N_2 + H_2O$	-80.7	12.5	11.6	13.3	1.9	0.7	2.3	3.8
$C_2H_2 + H_2 \rightarrow C_2H_4$	-49.4	2.2	-11.8	-10.8	12.4	0.6	3.0	1.3
$CH_2{=}C{=}O + 2H_2 \rightarrow CH_2O + CH_4$	-43.1	11.1	6.0	9.6	4.2	-0.3	3.8	1.9
$CO + H_2O \rightarrow CO_2 + H_2$	-6.7	-7.5	-8.6	-0.5	-0.4	-2.4	-5.9	-5.8
$C_2H_2 + HF \rightarrow C_2H_3F$	-27.3	-3.8	-12.8	-9.5	7.6	0.5	–	3.4
$HCN + H_2O \rightarrow CO + NH_3$	-12.6	-5.2	4.7	10.5	-10.4	-5.7	-7.9	3.7
$HCN + NH_3 \rightarrow N_2 + CH_4$	-38.2	-8.6	-0.7	0.9	-10.0	-1.6	-0.8	-0.1
$O_3 + CH_4 \rightarrow 2H_2O + CO$	-159.7	12.5	19.4	21.5	-4.1	1.2	2.9	7.6
$N_2 + F_2 \rightarrow N_2F_2$	17.3	11.9	-10.0	-15.9	25.3	3.6	-1.8	–
$BH_3 + 2F_2 \rightarrow BF + 3HF$	-248.1	0.3	11.6	14.8	-3.9	6.5	9.6	4.6
$2BH_3 \rightarrow B_2H_6$	-43.3	-7.8	-17.2	-17.2	8.7	-1.5	-1.1	-2.0
$CH_2{=}C \rightarrow C_2H_2$	-44.8	3.3	6.7	6.2	-4.5	-2.5	-3.5	-3.4
$HCN \rightarrow CNH(TS)$[b]	47.7	-2.7	-5.3	-5.4	4.5	1.2	1.0	0.6
$HF + H^+ \rightarrow H_2F^+$	-122.9	-22.0	-4.5	4.4	-21.1	-3.6	5.5	2.2
$H_2O + H^+ \rightarrow H_3O^+$	-173.0	-26.5	-5.5	0.1	-24.5	-2.0	5.3	0.0
$NH_3 + H^+ \rightarrow H_4N^+$	-212.9	-27.9	-9.3	-8.4	-22.8	-4.1	-4.0	-2.6
$OH^- + H^+ \rightarrow H_2O$	-412.5	-23.5	-6.7	4.3	-22.4	-5.7	5.3	2.6
$NH_2{}^- + H^+ \rightarrow NH_3$	-426.1	-25.3	-7.1	-1.2	-23.1	-3.6	4.1	-0.3
$2NH_3 \rightarrow (NH_3)_2$	-3.4	-3.9	-3.1	-6.5	1.6	-0.5	–	-0.2
$2H_2O \rightarrow (H_2O)_2$	-5.4	-17.8	-1.5	-3.2	1.3	0.8	1.9	-1.7
$2HF \rightarrow (HF)_2$	-4.9	-3.1	0.2	3.1	1.6	0.5	-0.3	0.7
	MUE	13.5	7.1	8.0	12.9	2.2	3.5	2.4
	MaxUE	45.7	19.4	22.8	37.9	6.5	9.6	7.6

[a] PQG conditions guarantee exact ensemble N-representability.
[b] Transition state geometry.
† PQG provides exact N-representability of the 2RDM.

One of our interests in this study was an assessment of the effects on the correlation energy recovered and on the total energy calculated of the N-representability conditions used in the underlying v2RDM-CASSCF calculation. For the test systems we present (H_2O and N_2), we find that approximately the same amount of correlation energy is recovered when either PQG or PQG+T2 N-representability conditions are used. The total energies computed from v2RDM-CASSCF+AC (PQG) are predictably lower than those from v2RDM-CASSCF+AC (PQG+T2).

We also computed relative energies for a set of 29 reactions. We compare results from the v2RDM-CASSCF+AC and CASPT2 approaches with yardstick values from CCSD(T). We find that, for these reactions, the v2RDM-CASSCF+AC approach slightly outperforms CASPT2, as long as the more stringent PQG+T2 N-representability conditions are used in the underlying v2RDM-CASSCF calculation.

CHAPTER 9

CONCLUDING REMARKS

The goal of quantum chemistry is to develop models that allow us to accurately predict molecular structure and properties, and to explain them using more fundamental principles. Since electrons move at much smaller time scales when compared to nuclei, as far as chemistry is concerned, the molecular structure problem can be recast as an electronic structure problem. In this dissertation, we have described progress made over the last few years developing approaches for electronic structure based on the variational two-electron reduced density matrix (v2RDM) complete active space self-consistent (CASSCF) field method.

The v2RDM-CASSCF method is able to treat a much larger number of orbitals at the CASSCF level than is possible with configuration interaction (CI)- driven CASSCF codes, and it is, in this respect, better posed to address the electron correlation problem in cases where a large number of orbitals may need to be treated at the CASSCF level of theory. We highlight the following

- analytic first-order derivatives of the energy for v2RDM-CASSCF.
- further development of an equation of motion approach for computing excited states.
- the development of a model for dynamical correction for v2RDM-CASSCF.

9.1 Analytic gradients for v2RDM-CASSCF

The development of analytic energy gradients for an electronic structure method involves evaluating the derivatives in terms of quantities that can be computed at the molecular geometry of interest. In this dissertation, we have presented work on the development and implementation of analytic first-order derivatives of the energy for the v2RDM-CASSCF method. The implementation of these derivatives as computer code makes it possible to evaluate gradients accurately. The expression for the first derivative of the energy depends

on the derivatives of the one- and two-electron, as well as the overlap integrals. The rest of the quantities needed to evaluate the gradient are quantities already on hand once the energy has been evaluated at the geometry of interest. Therefore we evaluate gradients more accurately, but also more efficiently, since having an analytic gradient code means one can choose to avoid using finite difference methods, which require that the gradient be computed at every vibrational normal mode. These gradients have been implemented as a freely available plugin to the Psi4[165] electronic structure package.

The work on analytic gradients has been further developed within the DePrince group to take advantage of the computational efficiency afforded by density-fitted (DF)- two-electron integrals.[148] In addition, an implementation of the v2RDM-CASSCF method that makes use of both the central processing unit (CPU) and the graphics processing unit (GPU) has been developed. This has resulted in about a threefold speedup in the calculation of single point energies. This has been a boon for calculations such as geometry optimizations, for which multiple evaluations of single point energies at the v2RDM-CASSCF level of theory are necessary. With the analytic gradient code that makes uses of DF, and the hybrid CPU/GPU implementation of v2RDM-CASSCF, geometry optimizations for systems for which the active space includes several tens of orbitals are routine. The development of higher-order derivatives such as the Hessian is still outstanding. At the moment, second-order derivatives can be computed from a finite difference of the first derivatives.

9.2 Modeling near K-edge excited states using the extended random phase approximation

As explained in chapter 4, the v2RDM-CASSCF method with approximate N-representability constraints on the active space 2RDM yields the lower bound to the CI-CASSCF energy for a given spin symmetry. This has motivated the work that has been done to develop an excited state approach for the method. Since the ground state 2RDM is typically available post-v2RDM-CASSCF, we favored an approach for excited states based Rowe's equation of motion (EOM) and the extended random phase approximation (ERPA). This formulation for computing excited states involves setting up an eigenvalue problem that can be expressed in

terms of elements of the ground state 2RDM. The fact that we use the ERPA partly steered us towards using this method to model excited states associated with NEXAFS, since these excited states are presumably dominated by single excitations. We employ a core-valence separation (CVS) framework to compute excited states, to make sure that the "killer" condition in the EOM is not violated. We find, using RDMs from full valence v2RDM-CASSCF, that excitation energies associated with the prominent $1s \rightarrow \pi^*$ and $1s \rightarrow 3s/p$ excited states are (only) modestly improved ($\approx$ 7 eV, on average, from experimental (reference) values) relative to those where the RDM and orbitals are computed at the Hartree-Fock (HF) level of theory ($\approx$ 12 eV, on average, from experiment). At the same time, time-dependent coupled cluster methods, which involves some doubles excitations, yield much smaller errors relative to experiment ($\approx$ 2 eV, on average).

Evidently, one of the ways of improving the quality of excited states within the EOM framework is to include a higher degree of excitations in our ansatz for the excited state wavefunction. Including double excitations, for instance, yields an EOM in terms of elements of the ground state 4-RDM, which can be computed in our current implementation of v2RDM-CASSCF. Short of developing this more complicated EOM, one may try to account for orbital relaxation effects through an approach such as the static exchange (STEX) approximation. Explicitly time-dependent methods where molecular response is modeled through the changes in its dipole moment can also be used to predict excitation energies, but these can only be applied to cases where the ground to excited state transition is dipole-allowed. In addition, reconstruction of the 3RDM, which closes the EOM of a time-dependent 2RDM, is not trivial.

9.3 A correction for electron correlation energy for v2RDM-CASSCF references

In CASSCF, one typically defines an active space that contains only a small number of orbitals, relative to the total number that defines the molecular system, in order to account for non-dynamical correlation effects. Relative to full CI, CI-CASSCF involves a smaller number of electronic configurations, and so the energy calculated at that level of theory is

always higher than the corresponding full CI energy. The CI-CASSCF wavefunction often needs to be corrected for dynamical correlation that is not accounted for explicitly outside the active space orbitals. This is often done by multireference perturbation theory (MRPT) approaches. We have developed a model for dynamical correlation based on Pernal's adiabatic connection (AC) formula for CASSCF references. We account for dynamical correlation effects by computing a correction to the v2RDM-CASSCF energy. Computing this correction involves knowledge of the 2RDM computed from v2RDM-CASSCF, as well as transition density matrices involving the v2RDM-CASSCF reference and the entire spectrum of excited states. In our case, excited states are computed at the ERPA level of theory, and the computational cost of our approach is dominated by the cost of constructing the matrices that define the generalized eigenvalue problem. A clear advantage of this approach over MRPT is that the treatment of both *non*-dynamical and dynamical correlation energy is more balanced with respect to the size of the active space. With this approach, we can more reliably account for electron correlation effects in systems involving a large number of orbitals in the active space.

9.4 General outlook

Certainly, there has been a lot of progress over the last few decades in developing RDM-based methods for applications in quantum chemistry. The development of constraints for ensemble and pure state N-representability, as well as advances in semidefinite programming (SDP) technqiues made it possible to determine the 2RDM by variational minimization of the energy functional. For this reason, the ground state problem is mostly resolved. In the DePrince Group, work continues to develop post-CASSCF methods for dynamical correlation. The utility of multiconfigurational pair-density functional theory (MC-PDFT) as well as the v2RDM-CASSCF+AC has already been explored. Work is ongoing within the group to develop angular momentum constraints on complex-valued RDMs in order to properly describe states with a non-zero z projection of the orbital angular momentum.

The excited state problem, by contrast, may yet warrant more attention. A means by which excited states and excited state properties can be variationally determined is still

lacking. Of the approaches for excited states that have been discussed in this section, the time-independent EOM approaches hold the most promise. The description of excited states can be systematically improved by increasing the degree of excitations and deexcitations included in the ansatz for the excited state wavefunction. Even though the resulting eigenvalue equations become more complex, and require higher-order RDMs, the challenge really lies in obtaining good approximations to these higher order RDMs.

APPENDIX A

ANALYTIC GRADIENTS

A.1 Errors in equilibrium bond lengths

Table A.1 provides computed equilibrium molecular geometries for a set of twenty small molecules at the full-valence complete active space self-consistent field (CASSCF) level of theory. Both conventional configuration-interaction (CI)-based and variational two-electron reduced-density-matrix (v2RDM)-based CASSCF computations were performed. CASSCF computations employed the cc-pVXZ basis set (X = D, T, Q). The reduced-density matrices in the v2RDM-CASSCF computations satisfied either two-particle[61] (PQG) or two-particle and partial three-particle[48, 249] (PQG+T2) N-representability conditions. The CASSCF equilibrium bond lengths were compared to those determined experimentally. All experimentally-obtained equilibrium bond lengths, with the exception of that for molecular hydrogen, were taken from Ref. 72 and the references therein. For H_2, the equilibrium bond length was taken from Ref. 74.

A.2 Redundant orbital rotations

The v2RDM-CASSCF energy is invariant to rotations among active, inactive, or external orbitals. Here, we provide numerical evidence for the invariance of the v2RDM-CASSCF energy and energy gradient to active-active orbital rotations. Table A.2 provides full-valence v2RDM-CASSCF energies and magnitudes of the energy gradient for the same twenty small molecules considered in the Table A.1 at experimental geometries obtained from the Computational Chemistry Comparison and Benchmark Database[85]. The semidefinite optimization of the active-space two-electron reduced-density matrix was considered converged when the primal ($||\mathbf{Ax} - \mathbf{b}||$) and dual ($||\mathbf{A}^T\mathbf{y} - \mathbf{c} + \mathbf{z}||$) errors fell below 10^{-9} and the primal/dual energy gap ($|E_{\text{primal}} - E_{\text{dual}}|$) fell below 10^{-9} E_h. The orbital optimization procedure was

Table A.1: Errors in computed equilibrium bond lengths (Δr_e, pm) from CI- and v2RDM-CASSCF in the cc-pVXZ (X = D, T, Q) basis sets.[a] Computed bond lengths are compared to those obtained from experiment (r_e, Å). All values of r_e were taken from Ref. 72 and the references therein, with the exception of that for H_2, which was taken from Ref. 74.

		Δr_e									
		cc-pVDZ			cc-pVTZ			cc-pVQZ			
Molecule	Bond	PQG	PQG+T2	CI	PQG	PQG+T2	CI	PQG	PQG+T2	CI	r_e
C_2H_2	C-H	3.0	2.3	2.3	1.9	1.2	1.2	1.9	1.2	1.2	1.062
C_2H_2	C-C	3.3	2.6	2.5	2.0	1.4	1.3	1.9	1.3	1.2	1.203
C_2H_4	C-H	3.3	2.7	2.6	2.3	1.6	1.6	2.3	1.5	1.5	1.081
C_2H_4	C-C	2.4	2.1	2.1	1.6	1.4	1.3	1.6	1.3	1.3	1.334
CH_2	C-H	3.6	3.2	3.2	2.3	1.8	1.8	2.1	1.7	1.7	1.107
CH_2O	C-O	1.5	0.7	0.6	1.0	0.3	0.2	0.8	0.1	0.1	1.203
CH_2O	C-H	3.6	2.9	2.9	2.6	1.7	1.7	2.5	1.6	1.6	1.099
CH_4	C-H	3.3	2.6	2.6	2.3	1.6	1.5	2.3	1.5	1.5	1.086
CO_2	C-O	1.8	1.2	1.1	1.3	0.6	0.6	1.1	0.5	0.4	1.160
CO	C-O	1.8	1.4	1.4	1.2	0.8	0.7	0.9	0.5	0.5	1.128
F_2	F-F	10.5	10.5	10.5	4.9	4.9	4.9	4.8	4.8	4.8	1.412
H_2	H-H	2.9	2.9	2.9	1.4	1.4	1.4	1.3	1.3	1.3	0.741
H_2O_2	O-H	1.0	0.9	0.9	0.2	0.2	0.1	0.1	0.0	0.0	0.967
H_2O_2	O-O	5.5	4.0	4.0	4.0	2.5	2.4	3.7	2.2	2.1	1.456
H_2O	O-H	1.5	1.4	1.4	0.8	0.7	0.7	0.7	0.6	0.5	0.957
HCN	C-H	2.9	2.3	2.3	-0.7	-0.8	-0.8	1.8	-0.8	-0.8	1.065
HCN	C-N	3.1	2.3	2.2	1.2	0.8	0.7	1.8	0.6	0.6	1.153
HF	H-F	0.5	0.5	0.5	0.0	0.0	0.0	-0.2	-0.2	-0.2	0.917
HNC	C-N	2.9	2.1	2.0	1.7	0.9	0.8	1.5	0.7	0.6	1.169
HNC	N-H	2.5	1.7	1.7	1.6	0.9	0.8	1.6	0.9	0.8	0.994
HNO	N-H	2.7	2.6	2.5	1.6	1.5	1.5	1.5	1.4	1.3	1.063
HNO	N-O	1.1	0.3	0.3	0.7	0.0	-0.1	0.5	-0.2	-0.3	1.212
HOF	O-H	1.6	1.4	1.4	0.8	0.6	0.6	0.7	0.5	0.5	0.966
HOF	F-O	6.1	5.6	5.6	3.2	2.8	2.8	3.1	2.6	2.6	1.435
N_2	N-N	2.3	1.9	1.8	1.2	0.9	0.8	1.1	0.7	0.6	1.098
N_2H_2	N-N	1.3	1.4	1.3	0.7	0.8	0.7	0.5	0.6	0.5	1.252
N_2H_2	N-H	3.3	2.6	2.5	2.3	1.6	1.5	2.2	1.4	1.4	1.028
O_3	O-O	4.2	2.6	2.0	3.2	1.7	1.3	2.8	1.4	0.9	1.272
NH_3	N-H	2.5	2.2	2.2	1.5	1.1	1.1	1.4	1.0	1.0	1.012
	MSE[c]	3.0	2.4	2.4	1.7	1.2	1.1	1.7	1.1	1.0	-
	MUE[b]	3.0	2.4	2.4	1.7	1.3	1.2	1.7	1.1	1.1	-
	Max[d]	10.5	10.5	10.5	4.9	4.9	4.9	4.8	4.8	4.8	-

[a] $\Delta r_e = r_e^{\text{CASSCF}} - r_e$. [b] mean signed error. [c] mean unsigned error. [d] maximum unsigned error.

Table A.2: Full-valence v2RDM-CASSCF energies (E_h) and magnitudes of the energy gradients ($E_h a_0^{-1}$) for twenty small molecules at experimental geometries obtained from the Computational Chemistry Comparison and Benchmark Database[85]. The v2RDM-CASSCF orbital optimizations either did or did not include active-active orbital rotations.

	energy		|gradient|	
	active-active rotations?		active-active rotations?	
Molecule	yes	no	yes	no
C_2H_2	-77.0005879659	-77.0005879659	0.0707616781	0.0707616787
C_2H_4	-78.2278654946	-78.2278654946	0.0373411038	0.0373411041
CH_2	-114.036496479	-114.036496481	0.0932386472	0.0932386484
CH_2O	-38.9237035145	-38.9237035145	0.0327917165	0.0327917160
CH_4	-40.2940001093	-40.2940001091	0.0414512353	0.0414512344
CO_2	-187.850687915 7	-187.850687915 2	0.0467292144	0.0467292151
CO	-112.888900317 6	-112.888900318 6	0.0594535374	0.0594535374
F_2	-198.765740654 9	-198.765740655 5	0.0575191239	0.0575191239
H_2	-1.1469295720	-1.1469295720	0.0287647997	0.0287647997
H_2O_2	-150.898780034	-150.898780042	0.0494914313	0.0494914323
H_2O	-76.081487369 4	76.081487370 8	0.0294042832	0.0294042822
HCN	-93.053007051 9	-93.053007052 2	0.0758791629	0.0758791628
HF	-100.043942612 4	-100.043942612 0	0.0080527299	0.0080527297
HNC	-93.0262784072	-93.0262784073	0.0619382277	0.0619382293
HNO	-129.950646313 0	-129.950646313 1	0.0276487230	0.0276487271
HOF	-174.837407777 3	-174.837407777 8	0.0403951421	0.0403951416
N_2	-109.112667018 5	-109.112667018 1	0.0955042450	0.0955042478
N_2H_2	-110.175149905 9	-110.175149906 3	0.0461777019	0.0461777021
O_3	-224.5353702162	-224.5353702162	0.0468856709	0.0468856706
NH_3	-56.275142426 5	-56.275142426 0	0.0408123411	0.0408123423

considered converged when the orbital gradient fell below 10^{-9} E_h and the energy change produced by orbital rotations fell below 10^{-12} E_h. The v2RDM-CASSCF computations were performed within the cc-pVDZ basis set while enforcing the PQG N-representability conditions. Results are presented for computations that either include or ignore active-active orbital rotations. The largest deviation between energies computed with and without such rotations is only 1.4×10^{-9} E_h, which is comparable to the energy convergence criterion employed in this study. The largest deviation between magnitudes of energy gradients computed with and without active-active orbital rotations is only 4.1×10^{-9} $E_h a_0^{-1}$.

APPENDIX B

MODELING CORE-LEVEL EXCITED STATES

B.1 Basis set dependence of computed K-edge features

Principal K-edge features were computed for small molecules using time-dependent equation-of-motion second order approximate coupled cluster (TD-EOM-CC2), time-dependent density functional theory (TDDFT, using the B3LYP functional), the random phase approximation (RPA), and the extended random phase approximation (ERPA). The ground-state one- and two-electron reduced density matrices that enter the ERPA equations were obtained from full-valence variational two-electron reduced-density-matrix-driven complete active space self-consistent field computatiosn. We consider $1s \rightarrow \pi^*$ excitations in molecules containing π bonds (CO, H_2CO, HCN, C_2H_2, N_2, and N_2O). Tables B.1, B.2, B.3, and B.4 provide errors in the excitation energies computed at each level of theory, as compared to experimentally obtained values, when the computations are performed within the cc-pVTZ, cc-pCVTZ, aug-cc-pVTZ, and cc-pVQZ basis sets, respectively.

Table B.1: Core-level excitation energies (eV) from experiment and deviations of the same as computed by linear response TDDFT (B3LYP), TDHF, and the ERPA using the cc-pVTZ basis set and a full valence active-space.

						ERPA	
molecule	transition	exp.	CC2	TDDFT	RPA	PQG	PQG+T2
CO	C $1s \rightarrow \pi^*$	287.4[a]	1.8	-11.2	7.0	5.2	5.0
	O $1s \rightarrow \pi^*$	533.6[b]	1.7	-13.7	16.5	6.9	6.9
H_2CO	C $1s \rightarrow \pi^*$	285.6[c]	2.7	-10.3	8.8	7.0	7.2
	O $1s \rightarrow \pi^*$	530.8[c]	1.6	-14.1	15.2	6.6	6.6
C_2H_2	C $1s \rightarrow \pi^*$	285.8[d]	2.2	-10.5	10.3	6.8	6.9
HCN	C $1s \rightarrow \pi^*$	286.4[e]	2.2	-10.6	9.6	6.5	6.6
	N $1s \rightarrow \pi^*$	399.7[e]	2.0	-12.0	12.3	7.0	7.0
N_2	N $1s \rightarrow \pi^*$	401.0[f]	1.9	-12.4	11.3	6.4	6.4
N_2O	N_t $1s \rightarrow \pi^*$	401.1[g]	2.1	-12.2	12.4	6.6	6.9
	N_c $1s \rightarrow \pi^*$	404.7[g]	2.4	-12.3	11.4	6.6	6.9
	O $1s \rightarrow \pi^*$	534.8[g]	0.9	-14.3	18.5	8.2	8.8
		MUE	2.0	12.1	12.1	6.7	6.8
		MaxUE	2.7	14.3	18.5	8.2	8.8

Experimental results $a-g$ come from references 162, 177, 180, 216, 76, 82 and 217, respectively.

Table B.2: Core-level excitation energies (eV) from experiment and deviations of the same as computed by linear response TDDFT (B3LYP), TDHF, and the ERPA using the cc-pCVTZ basis set and a full valence active-space.

						ERPA	
molecule	transition	exp.	CC2	TDDFT	RPA	PQG	PQG+T2
CO	C $1s \rightarrow \pi^*$	287.4[a]	2.3	-11.3	7.0	5.2	5.0
	O $1s \rightarrow \pi^*$	533.6[b]	1.7	-13.8	16.5	6.9	6.9
H_2CO	C $1s \rightarrow \pi^*$	285.6[c]	2.7	-10.4	8.8	7.0	7.2
	O $1s \rightarrow \pi^*$	530.8[c]	1.6	-14.1	15.1	6.6	6.7
C_2H_2	C $1s \rightarrow \pi^*$	285.8[d]	2.2	-10.5	10.2	6.8	6.9
HCN	C $1s \rightarrow \pi^*$	286.4[e]	2.2	-10.6	9.6	6.5	6.6
	N $1s \rightarrow \pi^*$	399.7[e]	2.0	-12.1	12.3	7.0	7.0
N_2	N $1s \rightarrow \pi^*$	401.0[f]	1.9	-12.5	11.2	6.4	6.4
N_2O	N_t $1s \rightarrow \pi^*$	401.1[g]	2.1	-12.2	12.4	6.6	6.9
	N_c $1s \rightarrow \pi^*$	404.7[g]	2.4	-12.4	11.4	6.6	6.9
	O $1s \rightarrow \pi^*$	534.8[g]	0.9	-14.3	18.5	8.2	8.8
		MUE	2.0	12.2	12.1	6.7	6.9
		MaxUE	2.7	14.3	18.5	8.2	8.8

Experimental results $a-g$ come from references 162, 177, 180, 216, 76, 82 and 217, respectively.

Table B.3: Core-level excitation energies (eV) from experiment and deviations of the same as computed by linear response TDDFT (B3LYP), TDHF, and the ERPA using the aug-cc-pVTZ basis set and a full valence active-space.

						ERPA	
molecule	transition	exp.	CC2	TDDFT	RPA	PQG	PQG+T2
CO	C $1s \rightarrow \pi^*$	287.4[a]	1.7	-11.2	7.0	5.2	5.0
	O $1s \rightarrow \pi^*$	533.6[b]	1.7	-13.7	16.5	6.9	6.9
H_2CO	C $1s \rightarrow \pi^*$	285.6[c]	2.7	-10.4	8.8	7.2	7.2
	O $1s \rightarrow \pi^*$	530.8[c]	1.7	-14.0	15.2	7.3	6.7
C_2H_2	C $1s \rightarrow \pi^*$	285.8[d]	2.2	-10.6	10.2	6.8	6.9
HCN	C $1s \rightarrow \pi^*$	286.4[e]	2.2	-10.7	9.6	6.6	6.6
	N $1s \rightarrow \pi^*$	399.7[e]	2.0	-15.3	12.3	6.6	7.1
N_2	N $1s \rightarrow \pi^*$	401.0[f]	1.9	-12.4	11.3	6.4	6.4
N_2O	N_t $1s \rightarrow \pi^*$	401.1[g]	2.1	-12.2	12.4	6.7	7.0
	N_c $1s \rightarrow \pi^*$	404.7[g]	2.4	-12.4	11.4	6.6	6.9
	O $1s \rightarrow \pi^*$	534.8[g]	1.0	-14.3	18.5	8.3	8.8
		MUE	2.0	12.5	12.1	6.8	6.9
		MaxUE	2.7	15.3	18.5	8.3	8.8

Experimental results $a-g$ come from references 162, 177, 180, 216, 76, 82 and 217, respectively.

Table B.4: Core-level excitation energies (eV) from experiment and deviations of the same as computed by linear response TDDFT (B3LYP), TDHF, and the ERPA using the cc-pVQZ basis set and a full valence active-space.

						ERPA	
molecule	transition	exp.	CC2	TDDFT	RPA	PQG	PQG+T2
CO	C $1s \rightarrow \pi^*$	287.4[a]	1.7	-11.3	7.0	5.2	5.0
	O $1s \rightarrow \pi^*$	533.6[b]	1.7	-13.9	16.5	6.9	6.9
H_2CO	C $1s \rightarrow \pi^*$	285.6[c]	2.7	-10.4	8.7	7.0	7.2
	O $1s \rightarrow \pi^*$	530.8[c]	1.6	-14.2	15.1	6.6	6.7
C_2H_2	C $1s \rightarrow \pi^*$	285.8[d]	2.2	-10.6	10.2	6.8	6.9
HCN	C $1s \rightarrow \pi^*$	286.4[e]	2.2	-10.7	9.6	6.5	6.6
	N $1s \rightarrow \pi^*$	399.7[e]	2.0	-12.2	12.3	6.5	7.0
N_2	N $1s \rightarrow \pi^*$	401.0[f]	1.9	-12.5	11.2	6.4	6.4
N_2O	N_t $1s \rightarrow \pi^*$	401.1[g]	2.1	-12.3	12.4	6.6	6.9
	N_c $1s \rightarrow \pi^*$	404.7[g]	2.4	-12.5	11.3	6.6	6.9
	O $1s \rightarrow \pi^*$	534.8[g]	0.9	-14.4	18.4	8.2	8.8
		MUE	1.9	12.3	12.1	6.7	6.8
		MaxUE	2.7	14.4	18.4	8.2	8.8

Experimental results $a-g$ come from references 162, 177, 180, 216, 76, 82 and 217, respectively.

APPENDIX C

A DYNAMICAL CORRELATION MODEL

Table C.1: Single point energies (Ha) from CCSD(T), v2RDM-CASSCF+AC, and v2RDM-CASSCF+AC0

		PQG			PQG+T2		
molecule	CCSD(T)	ref.	AC	AC0	ref.	AC	AC0
B_2H_6	-53.1591	-53.0048	-53.2428	-53.2323	-52.9603	-53.1939	-53.1809
BF	-124.5386	-124.2738	-124.5620	-124.5518	-124.2713	-124.5583	-124.5471
BH_3	-26.5451	-26.4617	-26.5732	-26.5679	-26.4526	-26.5612	-26.5551
C_2H_2	-77.2091	-77.0296	-77.2705	-77.2675	-77.0031	-77.2450	-77.2415
C_2H_3F	-177.6257	-177.1712	-177.7116	-177.7232	-177.1264	-177.6650	-177.6760
C_2H_4	-78.4616	-78.2568	-78.5398	-78.5352	-78.2140	-78.4946	-78.4872
CH_2=C=O	-152.4036	-152.0387	-152.5024	-152.5050	-151.9892	-152.4504	-152.4498
CH_2=C	-77.1377	-76.9634	-77.2097	-77.2059	-76.9244	-77.1697	-77.1645
CH_2O	-114.3689	-114.0806	-114.4237	-114.4253	-114.0554	-114.3978	-114.3973
$^1CH_2$	-39.0719	-38.9639	-39.0938	-39.0897	-38.9574	-39.0856	-39.0809
CH_4	-40.4509	-40.3130	-40.4814	-40.4766	-40.2997	-40.4654	-40.4588
CNH(TS)[b]	-93.2250	-93.0123	-93.2868	-93.2862	-92.9814	-93.2577	-93.2566
CO_2	-188.3845	-187.9196	-188.4484	-188.4598	-187.8992	-188.4272	-188.4374
F_2	-199.3588	-198.8467	-199.3719	-199.4019	†	†	†
F_2O	-274.4358	-273.7157	-274.4605	-274.5007	-273.7107	-274.4560	-274.4962
H_2F^+	-100.5690	-100.3231	-100.5803	-100.5861	-100.3216	-100.5788	-100.5844
H_2O_2	-151.4082	-150.9641	-151.4324	-151.4500	-150.9577	-151.4261	-151.4433
$(H_2O)_2$	-152.7281	-152.2774	-152.7490	-152.7656	-152.2436	-152.7422	-152.7540
H_2O	-76.3598	-76.1202	-76.3690	-76.3759	-76.1186	-76.3675	-76.3742
H_3O^+	-76.6354	-76.4381	-76.6534	-76.6514	-76.4333	-76.6464	-76.6415
HCN	-93.3011	-93.0840	-93.3544	-93.3537	-93.0646	-93.3357	-93.3342
HCOOH	-189.5616	-189.0627	-189.6346	-189.6467	-189.0341	-189.5988	–
$(HF)_2$	-200.7540	-200.1969	-200.7621	-200.7944	-200.1893	-200.7615	-200.7999
N_2F_2	-308.7354	-307.9494	-308.8059	-308.8448	-307.9190	-308.8134	-308.8134
N_2O	-184.4615	-184.0087	-184.5326	-184.5418	-183.9812	-184.5052	-184.5135
N_2	-109.4042	-109.1492	-109.4456	-109.4452	-109.1403	-109.4371	-109.4362
NH_2^-	-55.8140	-55.5843	-55.8200	-55.8276	-55.5827	-55.8186	-55.8260
$(NH_3)_2$	-112.9916	-112.6191	-113.0321	-113.0326	-112.5999	-113.0137	–
NH_3	-56.4930	-56.3037	-56.5105	-56.5086	-56.2985	-56.5033	-56.4985
H_4N^+	-56.8323	-56.6875	-56.8645	-56.8614	-56.6742	-56.8491	-56.8443
O_3	-225.2020	-224.6216	-225.2584	-225.2793	-224.5975	-225.2341	-225.2546
OH^-	-75.7024	-75.4254	-75.7009	-75.7253	†	†	†
CO	-113.1878	-112.9288	-113.2255	-113.2243	-112.9212	-113.2171	-113.2149

[a] PQG conditions guarantee exact ensemble N-representability.
[b] Transition state geometry.
†: PQG provides exact N-representability.

APPENDIX D

SLATER-CONDON RULES

In quantum chemistry, one usually encounters operators that are a sum of one and two-electron operators. For this reason, we consider here the evaluation of matrix elements $\langle\Phi_K|\mathcal{O}_i|\Phi_L\rangle$, $i \in 1,2$ where $\mathcal{O}_i$ is a sum of i-electron operators, and Φ_K and Φ_L are N-electron Slater determinants. We distinguish three cases for each type of operator.

D.1 Matrix elements between determinants for one-electron operators

- Case 1, when the two determinants are identical, that is $|\Phi_K\rangle = |\Phi_L\rangle = |\cdots nm\cdots\rangle$

$$\langle\Phi_K|\mathcal{O}_1|\Phi_K\rangle = \sum_m^N (m|h|m) \tag{D.1}$$

  where $(m|h|m)$ is a one-center integral defined as in 2.25

- Case 2, when the two determinants differ by one spin orbital, that is, $|\Phi_K\rangle = |\cdots mn\cdots\rangle$ and $|\Phi_L\rangle = |\cdots pn\cdots\rangle$

$$\langle\Phi_K|\mathcal{O}_1|\Phi_L\rangle = (m|h|p) \tag{D.2}$$

- Case 3, when the two determinants differ by two or more orbitals, that is $|\Phi_K\rangle = |\cdots mn\cdots\rangle$ and $|\Phi_L\rangle = |\cdots pq\cdots\rangle$

$$\langle\Phi_K|\mathcal{O}_1|\Phi_L\rangle = 0 \tag{D.3}$$

D.2 Matrix elements between determinants for two-electron operators

- Case 1, when the two determinants are identical, that is $|\Phi_K\rangle = |\Phi_L\rangle = |\cdots nm\cdots\rangle$

$$\langle\Phi_K|\mathcal{O}_2|\Phi_K\rangle = \frac{1}{2}\sum_m^N\sum_n^N[(mm|nn) - (mn|nm)] \tag{D.4}$$

  where $(mm|nn)$ and $(mn|nm)$ are two-center integrals defined as in 2.27

- Case 2, when the two determinants differ by one spin orbital, that is, $|\Phi_K\rangle = |\cdots mn\cdots\rangle$ and $|\Phi_L\rangle = |\cdots pn\cdots\rangle$

$$\langle\Phi_K|\mathcal{O}_2|\Phi_L\rangle = \sum_n^N [(mp|nn) - (mn|np)] \tag{D.5}$$

- Case 3, when the two determinants differ by two or more orbitals, that is $|\Phi_K\rangle = |\cdots mn\cdots\rangle$ and $|\Phi_L\rangle = |\cdots pq\cdots\rangle$

$$\langle\Phi_K|\mathcal{O}_2|\Phi_L\rangle = (mp|nq) - (mq|np) \tag{D.6}$$

Now that we have developed the notation and formalism of second quantization, the reader should hopefully be able to follow closely the rest of this dissertation.

BIBLIOGRAPHY

[1] David A. Mazziotti. *Reduced-Density-Matrix Mechanics: With Application to Many-Electron Atoms and Molecules, Volume 134*, pages 165 – 203. 03 2007.

[2] Hans Ågren, Vincenzo Carravetta, Olav Vahtras, and Lars G. M. Pettersson. Direct SCF direct static-exchange calculations of electronic spectra. *Theor. Chem. Acc.*, 97(1):14–40, Oct 1997.

[3] Hans Ågren, Vincenzo Carravetta, Olav Vahtras, and Lars G.M. Pettersson. Direct, atomic orbital, static exchange calculations of photoabsorption spectra of large molecules and clusters. *Chem. Phys. Lett.*, 222(1):75–81, 1994.

[4] Tomoko Akama and Hiromi Nakai. Short-time Fourier transform analysis of real-time time-dependent Hartree-Fock and time-dependent density functional theory calculations with Gaussian basis functions. *J. Chem. Phys.*, 132(5):054104, 2010.

[5] Farid Alizadeh, Jean-Pierre A Haeberly, and Michael L Overton. Primal-dual interior-point methods for semidefinite programming: convergence rates, stability and numerical results. *SIAM Journal on Optimization*, 8(3):746–768, 1998.

[6] K. Andersson, B.O. Roos, P.-Å. Malmqvist, and P.-O. Widmark. The Cr_2 potential energy curve studied with multiconfigurational second-order perturbation theory. *Chem. Phys. Lett.*, 230(4):391–397, 1994.

[7] Kerstin. Andersson, Per-Åke. Malmqvist, Björn O. Roos, Andrzej J. Sadlej, and Krzysztof. Wolinski. Second-order perturbation theory with a CASSCF reference function. *Journal of Physical Chemistry*, 94(14):5483–5488, 1990.

[8] C. Angeli, R. Cimiraglia, S. Evangelisti, T. Leininger, and J.-P. Malrieu. Introduction of n-electron valence states for multireference perturbation theory. *J. Chem. Phys.*, 114(23):10252–10264, 2001.

[9] C. Angeli, R. Cimiraglia, and J.-P. Malrieu. N-electron valence state perturbation theory: A spinless formulation and an efficient implementation of the strongly contracted and of the partially contracted variants. *J. Chem. Phys.*, 117(20):9138–9153, 2002.

[10] Francesco Aquilante, Jochen Autschbach, Rebecca K. Carlson, Liviu F. Chibotaru, Mickaël G. Delcey, Luca De Vico, Ignacio Fdez. Galván, Nicolas Ferré, Luis Manuel Frutos, Laura Gagliardi, Marco Garavelli, Angelo Giussani, Chad E. Hoyer, Giovanni Li Manni, Hans Lischka, Dongxia Ma, Per Åke Malmqvist, Thomas Müller, Artur Nenov, Massimo Olivucci, Thomas Bondo Pedersen, Daoling Peng, Felix Plasser, Ben Pritchard, Markus Reiher, Ivan Rivalta, Igor Schapiro, Javier Segarra-Martí, Michael Stenrup, Donald G. Truhlar, Liviu Ungur, Alessio Valentini, Steven Vancoillie, Valera Veryazov, Victor P. Vysotskiy, Oliver Weingart, Felipe Zapata, and Roland Lindh. Molcas 8: New capabilities for multiconfigurational quantum chemical calculations across the periodic table. *J. Comp. Chem.*, 37(5):506–541, 2015.

[11] J.O. Arnold, E.E. Whiting, and S.R. Langhoff. MCSCF+CI wavefunctions and properties of the $X^2\Pi$ and $A^2\Pi$ states of ClO. *The Journal of Chemical Physics*, 66(10):4459–4467, 1977.

[12] Ajit Banerjee and F Grein. Multiconfiguration wavefunctions for excited states. selection of optimal configurations: The $b^1\Sigma^+$ and $d^1\Sigma^+$ states of NH. *The Journal of Chemical Physics*, 66(3):1054–1062, 1977.

[13] Jie J Bao, Sijia S Dong, Laura Gagliardi, and Donald G Truhlar. Automatic selection of an active space for calculating electronic excitation spectra by MS-CASPT2 or MC-PDFT. *J. Chem. Theory Comput.*, 14(4):2017–2025, 2018.

[14] G. Barcza, Ö. Legeza, K. H. Marti, and M. Reiher. Quantum-information analysis of electronic states of different molecular structures. *Phys. Rev. A*, 83:012508, Jan 2011.

[15] A Barth and J Schirmer. Theoretical core-level excitation spectra of N_2 and CO by a new polarisation propagator method. *J. Phys. B: At., Mol. Opt. Phys.*, 18(5):867, 1985.

[16] Rodney J Bartlett. Many-body perturbation theory and coupled cluster theory for electron correlation in molecules. *Annual Review of Physical Chemistry*, 32(1):359–401, 1981.

[17] Rodney J Bartlett. *Recent advances in coupled-cluster methods*, volume 3. World Scientific, 1997.

[18] Axel D. Becke. Density-functional thermochemistry. III. the role of exact exchange. *J. Chem. Phys.*, 98(7):5648–5652, 1993.

[19] FW Bobrowicz and WA Goddard III. Methods of electronic structure theory. *Modern Theoretical Chemistry*, 3:79–127, 1977.

[20] Sergey I. Bokarev, Munirah Khan, Mahmoud K. Abdel-Latif, Jie Xiao, Rifaat Hilal, Saadullah G. Aziz, Emad F. Aziz, and Oliver Kühn. Unraveling the Electronic Structure of Photocatalytic Manganese Complexes by L-Edge X-ray Spectroscopy. *J. Phys. Chem. C*, 119(33):19192–19200, 2015.

[21] Max Born and Robert Oppenheimer. Zur quantentheorie der molekeln. *Annalen der physik*, 389(20):457–484, 1927.

[22] M. Bouten, P. Van Leuven, M.V. Mihailović, and M. Rosina. A new particle-hole approach to collective states. *Nucl. Phys. A*, 202(1):127 – 144, 1973.

[23] M. Bouten, P. van Leuven, M.V. Mihailovi, and M. Rosina. Two exactly soluble models as a test of the hermitian operator method. *Nucl. Phys. A*, 221(1):173 – 182, 1974.

[24] Bastiaan J. Braams, Jerome K. Percus, and Zhengji Zhao. *The T1 and T2 Representability Conditions*, pages 93–101. John Wiley & Sons, Inc., 2007.

[25] R.J. Buenker and S.D. Peyerimhoff. Individualized configuration selection in CI calculations with subsequent energy extrapolation. *Theor. Chim. Acta*, 35(1):33–58, 1974.

[26] R.J. Buenker and S.D. Peyerimhoff. Energy extrapolation in ci calculations. *Theor. Chim. Acta*, 39(3):217–228, 1975.

[27] Eric Cancès, Gabriel Stoltz, and Mathieu Lewin. The electronic ground-state energy problem: A new reduced density matrix approach. *J. Chem. Phys.*, 125(6):064101, 2006.

[28] L. S. Cederbaum, W. Domcke, and J. Schirmer. Many-body theory of core holes. *Phys. Rev. A*, 22:206–222, Jul 1980.

[29] P. Celani, H. Stoll, H.-J. Werner, and P.J. Knowles. The CIPT2 method: Coupling of multi-reference configuration interaction and multi-reference perturbation theory. Application to the chromium dimer. *Molecular Physics*, 102(21-22):2369–2379, 2004.

[30] Garnet Kin-Lic Chan and Martin Head-Gordon. Highly correlated calculations with a polynomial cost algorithm: A study of the density matrix renormalization group. *J. Chem. Phys.*, 116(11):4462–4476, 2002.

[31] Agisilaos Chantzis, Joanna K. Kowalska, Dimitrios Maganas, Serena DeBeer, and Frank Neese. Ab Initio Wave Function-Based Determination of Element Specific Shifts for the Efficient Calculation of X-ray Absorption Spectra of Main Group Elements and First Row Transition Metals. *J. Chem. Theory Comput.*, 14(7):3686–3702, 2018.

[32] Koushik Chatterjee and Katarzyna Pernal. Excitation energies from extended random phase approximation employed with approximate one- and two-electron reduced density matrices. *J. Chem. Phys.*, 137(20):204109, 2012.

[33] Sudip Chattopadhyay, Dola Pahari, Debashis Mukherjee, and Uttam Sinha Mahapatra. A state-specific approach to multireference coupled electron-pair approximation like methods: Development and applications. *J. Chem. Phys.*, 120(13):5968–5986, 2004.

[34] L.M. Cheung, K.R. Sundberg, and K. Ruedenberg. Dimerization of carbene to ethylene. *Journal of the American Chemical Society*, 100(25):8024–8025, 1978.

[35] Jerzy Cioslowski. Many-electron densities and reduced density matrices, 2000.

[36] E Clementi and A Veillard. Correlation energy in atomic systems. IV. Degeneracy effects. *J. Chem. Phys.*, 44(8):3050–3053, 1966.

[37] Leon Cohen and C. Frishberg. Hierarchy equations for reduced density matrices. *Phys. Rev. A*, 13:927–930, Mar 1976.

[38] Albert John Coleman and Vyacheslav I. Yukalov. *Reduced density matrices: Coulson's challenge*, volume 72. Springer Science & Business Media, 2000.

[39] F. Colmenero, C. Pérez del Valle, and C. Valdemoro. Approximating q-order reduced density matrices in terms of the lower-order ones. I. General relations. *Phys. Rev. A*, 47:971–978, Feb 1993.

[40] F Colmenero and C Valdemoro. Self-consistent approximate solution of the second-order contracted Schrödinger equation. *Int. J. Quantum Chem.*, 51(6):369–388, 1994.

[41] Sonia Coriani, Ove Christiansen, Thomas Fransson, and Patrick Norman. Coupled-cluster response theory for near-edge X-ray-absorption fine structure of atoms and molecules. *Phys. Rev. A*, 85:022507, Feb 2012.

[42] Sonia Coriani, Thomas Fransson, Ove Christiansen, and Patrick Norman. Asymmetric-Lanczos-chain-driven implementation of electronic resonance convergent coupled-cluster linear response theory. *J. Chem. Theory Comput.*, 8(5):1616–1628, 2012.

[43] Sonia Coriani and Henrik Koch. Communication: X-ray absorption spectra and core-ionization potentials within a core-valence separated coupled cluster framework. *J. Chem. Phys.*, 143(18):181103, 2015.

[44] G Das and Arnold C Wahl. Extended Hartree-Fock Wavefunctions: Optimized Valence Configurations for H_2 and Li_2, Optimized Double Configurations for F_2. *J. Chem. Phys.*, 44(1):87–96, 1966.

[45] Ondřej Demel and Jiří Pittner. Multireference Brillouin-Wigner coupled clusters method with noniterative perturbative connected triples. *J. Chem. Phys.*, 124(14):144112, 2006.

[46] A. Eugene DePrince III. Variational optimization of the two-electron reduced-density matrix under pure-state n-representability conditions. *J. Chem. Phys.*, 145(16):164109, 2016.

[47] Ulf Ekström, Patrick Norman, and Vincenzo Carravetta. Relativistic four-component static-exchange approximation for core-excitation processes in molecules. *Phys. Rev. A*, 73:022501, Feb 2006.

[48] R. M. Erdahl. Representability. *Int. J. Quantum Chem.*, 13(6):697–718, 1978.

[49] R. M. Erdahl, C. Garrod, B. Golli, and M. Rosina. The application of group theory to generate new representability conditions for rotationally invariant density matrices. *J. Math. Phys.*, 20(7):1366–1374, 1979.

[50] R.M. Erdahl. Two algorithms for the lower bound method of reduced density matrix theory. *Rep. Math. Phys.*, 15(2):147–162, 1979.

[51] R.M. Erdahl and B. Jin. The lower bound method for reduced density matrices. *Journal of Molecular Structure: THEOCHEM*, 527(1):207 – 220, 2000.

[52] John D Farnum and David A Mazziotti. Extraction of ionization energies from the ground-state two-particle reduced density matrix. *Chem. Phys. Lett.*, 400(1-3):90–93, 2004.

[53] Timo Fleig, Jeppe Olsen, and Christel M. Marian. The generalized active space concept for the relativistic treatment of electron correlation. I. Kramers-restricted two-component configuration interaction. *J. Chem. Phys.*, 114(11):4775–4790, 2001.

[54] Vladimir Fock. Näherungsmethode zur Lösung des quantenmechanischen Mehrkörperproblems. *Zeitschrift für Physik*, 61(1-2):126–148, 1930.

[55] Vladimir Fock. Konfigurationsraum und zweite quantelung. *Zeitschrift für Physik*, 75(9-10):622–647, 1932.

[56] Jacob Fosso-Tande, Daniel R. Nascimento, and A. Eugene DePrince III. Accuracy of two-particle N-representability conditions for describing different spin states and the singlet-triplet gap in the linear acene series. *Mol. Phys.*, 114(3-4):423–430, 2016.

[57] Jacob Fosso-Tande, Truong-Son Nguyen, Gergely Gidofalvi, and A. Eugene DePrince III. Large-Scale Variational Two-Electron Reduced-Density-Matrix-Driven Complete Active Space Self-Consistent Field Methods. *J. Chem. Theory Comput.*, 12(5):2260–2271, 2016.

[58] Mituhiro Fukuda, Bastiaan J. Braams, Maho Nakata, Michael L. Overton, Jerome K. Percus, Makoto Yamashita, and Zhengji Zhao. Large-scale semidefinite programs in electronic structure calculation. *Math. Prog.*, 109(2-3):553, 2007.

[59] Laura Gagliardi, Donald G Truhlar, Giovanni Li Manni, Rebecca K Carlson, Chad E Hoyer, and Junwei Lucas Bao. Multiconfiguration pair-density functional theory: A new way to treat strongly correlated systems. *Accounts of Chemical Research*, 50(1):66–73, 2016.

[60] C. Garrod, M. V. Mihailović, and M. Rosina. The variational approach to the two-body density matrix. *J. Math. Phys.*, 16(4):868–874, 1975.

[61] Claude Garrod and Jerome K. Percus. Reduction of the n-particle variational problem. *J. Math. Phys.*, 5(12):1756–1776, 1964.

[62] Debashree Ghosh, Johannes Hachmann, Takeshi Yanai, and Garnet Kin-Lic Chan. Orbital optimization in the density matrix renormalization group, with applications to polyenes and β-carotene. *J. Chem. Phys.*, 128(14):144117, 2008.

[63] Gergely Gidofalvi and David A. Mazziotti. Spin and symmetry adaptation of the variational two-electron reduced-density-matrix method. *Phys. Rev. A*, 72:052505, Nov 2005.

[64] Gergely Gidofalvi and David A. Mazziotti. Active-space two-electron reduced-density-matrix method: Complete active-space calculations without diagonalization of the n-electron hamiltonian. *J. Chem. Phys.*, 129(13):134108, 2008.

[65] Loren Greenman and David A. Mazziotti. Electronic excited-state energies from a linear response theory based on the ground-state two-electron reduced density matrix. *J. Chem. Phys.*, 128(11):114109, 2008.

[66] Stefan Grimme. Improved second-order Møller-Plesset perturbation theory by separate scaling of parallel- and antiparallel-spin pair correlation energies. *J. Chem. Phys.*, 118(20):9095–9102, 2003.

[67] Matthias Hanauer and Andreas Köhn. Pilot applications of internally contracted multireference coupled cluster theory, and how to choose the cluster operator properly. *J. Chem. Phys.*, 134(20):204111, 2011.

[68] Kevin P. Hannon, Chenyang Li, and Francesco A. Evangelista. An integral-factorized implementation of the driven similarity renormalization group second-order multireference perturbation theory. *J. Chem. Phys.*, 144(20):204111, 2016.

[69] M Hanrath and B Engels. New algorithms for an individually selecting MR-CI program. *Chem. Phys.*, 225(1-3):197–202, 1997.

[70] Douglas R Hartree. The wave mechanics of an atom with a non-Coulomb central field. Part I. Theory and methods. In *Mathematical Proceedings of the Cambridge Philosophical Society*, volume 24, pages 89–110. Cambridge University Press, 1928.

[71] Douglas Rayner Hartree, W Hartree, and Bertha Swirles. Self-consistent field, including exchange and superposition of configurations, with some results for oxygen. *Philosophical Transactions of the Royal Society of London. Series A, Mathematical and Physical Sciences*, 238(790):229–247, 1939.

[72] Trygve Helgaker, Jürgen Gauss, Poul Jørgensen, and Jeppe Olsen. The prediction of molecular equilibrium structures by the standard electronic wave functions. *J. Chem. Phys.*, 106(15):6430–6440, 1997.

[73] Trygve Helgaker, Poul Jørgensen, and Jeppe Olsen. *Molecular Electronic-Structure Theory*. John Wiley & Sons, Inc., New York, 2000.

[74] G. Herzberg and K.P. Huber. *Molecular Spectra and Molecular Structure: Constants of Diatomic Molecules*. Van Nostrand Reinhold, 1979.

[75] Juergen Hinze. MC-SCF. I. The multi-configuration self-consistent-field method. *J. Chem. Phys.*, 59(12):6424–6432, 1973.

[76] A.P. Hitchcock and C.E. Brion. K-shell excitation of hcn by electron-energy loss spectroscopy. *Journal Of Electron Spectroscopy and Related Phenomena*, 15(Jan):201–206, 1979.

[77] Weijie Hua, Kochise Bennett, Yu Zhang, Yi Luo, and Shaul Mukamel. Study of double core hole excitations in molecules by X-ray double-quantum-coherence signals: a multiconfiguration simulation. *Chem. Sci.*, 7:5922–5933, 2016.

[78] I Hubač and S Wilson. On the generalized multi-reference Brillouin-Wigner coupled cluster theory. *Journal of Physics B: Atomic and Molecular Physics*, 34(21):4259, 2001.

[79] Ivan Hubač, Jozef Mášik, Pavel Mach, Ján Urban, and Peter Babinec. Multireference Brillouin-Wigner Coupled-Cluster Theory. In *Computational Chemistry: Reviews Of Current Trends*, pages 1–48. World Scientific, 1999.

[80] WJ Hunt, PJ Hay, and WA Goddard. Self-Consistent Procedures for Generalized Valence Bond Wavefunctions. Applications H_3, BH, H_2O, C_2H_6, and O_2. *The Journal of Chemical Physics*, 57(2):738–748, 1972.

[81] Andrew Crowther Hurley. *Electron correlation in small molecules*, volume 7. Academic Pr, 1976.

[82] Jun ichi Adachi, Nobuhiro Kosugi, Eiji Shigemasa, and Akira Yagishita. Vibronic coupling and valence mixing in the $1s \rightarrow$ rydberg excited states of C_2H_2 in comparison with N_2 and CO. *Chem. Phys. Lett.*, 309(5):427–433, 1999.

[83] Joseph Ivanic. Direct configuration interaction and multiconfigurational self-consistent-field method for multiple active spaces with variable occupations. I. Method. *J. Chem. Phys.*, 119(18):9364–9376, 2003.

[84] David B. Jeffcoat and A. Eugene DePrince III. N-Representability-Driven Reconstruction of the two-electron Reduced-Density Matrix for a Real-Time Time-Dependent Electronic Structure Method. *J. Chem. Phys.*, 141(21):214104, 2014.

[85] Russell D. Johnson III. NIST Computational Chemistry Comparison and Benchmark Database. Release 16a, August 2013.

[86] Ida Josefsson, Kristjan Kunnus, Simon Schreck, Alexander Föhlisch, Frank de Groot, Philippe Wernet, and Michael Odelius. Ab Initio Calculations of X-ray Spectra: Atomic Multiplet and Molecular Orbital Effects in a Multiconfigurational SCF Approach to the L-Edge Spectra of Transition Metal Complexes. *J. Phys. Chem. Lett.*, 3(23):3565–3570, 2012.

[87] Thom H. Dunning Jr. Gaussian basis sets for use in correlated molecular calculations. I. The atoms boron through neon and hydrogen. *J. Chem. Phys.*, 90(2):1007–1023, 1989.

[88] P.Å. Malmqvist K. Andersson and B.O. Roos. Second-order perturbation theory with a complete active space self-consistent field reference function. *J. Chem. Phys.*, 96(2):1218–1226, 1992.

[89] Joanna Kauczor, Patrick Norman, Ove Christiansen, and Sonia Coriani. Communication: A reduced-space algorithm for the solution of the complex linear response equations used in coupled cluster damped response theory. *J. Chem. Phys.*, 139(21):211102, 2013.

[90] Rick A. Kendall, Thom H. Dunning, and Robert J. Harrison. Electron affinities of the firstrow atoms revisited. systematic basis sets and wave functions. *J. Chem. Phys.*, 96(9):6796–6806, 1992.

[91] Eirik F. Kjønstad and Henrik Koch. Resolving the notorious case of conical intersections for coupled cluster dynamics. *J. Phys. Chem. Lett.*, 8(19):4801–4807, 2017.

[92] Eirik F. Kjønstad, Rolf H. Myhre, Todd J. Martnez, and Henrik Koch. Crossing conditions in coupled cluster theory. *J. Chem. Phys.*, 147(16):164105, 2017.

[93] Stefan Knecht, Erik Donovan Hedegård, Sebastian Keller, Arseny Kovyrshin, Yingjin Ma, Andrea Muolo, Christopher J. Stein, and Markus Reiher. New approaches for ab initio calculations of molecules with strong electron correlation. *Chimia*, 70(4):244–251, 2016.

[94] P.J. Knowles and N.C. Handy. A new determinant-based full configuration interaction method. *Chem. Phys. Lett.*, 111(4):315–321, 1984.

[95] Henrik Koch and Poul Jørgensen. Coupled cluster response functions. *J. Chem. Phys.*, 93(5):3333–3344, 1990.

[96] Henrik Koch, Rika Kobayashi, Alfredo Sanchez de Mers, and Poul Jørgensen. Calculation of sizeintensive transition moments from the coupled cluster singles and doubles linear response function. *J. Chem. Phys.*, 100(6):4393–4400, 1994.

[97] Andreas Köhn, Matthias Hanauer, Leonie Anna Mueck, Thomas-Christian Jagau, and Jürgen Gauss. State-specific multireference coupled-cluster theory. *Wiley Interdiscip. Rev.: Comput. Mol. Sci.*, 3(2):176–197, 2013.

[98] Sven Krönke and Peter Schmelcher. Born-Bogoliubov-Green-Kirkwood-Yvon hierarchy for ultracold bosonic systems. *Phys. Rev. A*, 98:013629, Jul 2018.

[99] K. Kunnus, I. Josefsson, I. Rajkovic, S. Schreck, W. Quevedo, M. Beye, C. Weniger, S. Grübel, M. Scholz, D. Nordlund, W. Zhang, R. W. Hartsock, K. J. Gaffney, W. F. Schlotter, J. J. Turner, B. Kennedy, F. Hennies, F. M. F. de Groot, S. Techert, M. Odelius, Ph. Wernet, and A. Föhlisch. Identification of the dominant photochemical pathways and mechanistic insights to the ultrafast ligand exchange of $Fe(CO)_5$ to $Fe(CO)_4EtOH$. *Struct. Dyn.*, 3(4):043204, 2016.

[100] Kristjan Kunnus, Ida Josefsson, Simon Schreck, Wilson Quevedo, Piter S. Miedema, Simone Techert, Frank M. F. de Groot, Michael Odelius, Philippe Wernet, and Alexander Föhlisch. From Ligand Fields to Molecular Orbitals: Probing the Local Valence Electronic Structure of Ni_2^+ in Aqueous Solution with Resonant Inelastic X-ray Scattering. *J. Phys. Chem. B*, 117(51):16512–16521, 2013.

[101] Yuki Kurashige and Takeshi Yanai. High-performance ab initio density matrix renormalization group method: Applicability to large-scale multireference problems for metal compounds. *J. Chem. Phys.*, 130(23):234114, 2009.

[102] Yuki Kurashige and Takeshi Yanai. Second-order perturbation theory with a density matrix renormalization group self-consistent field reference function: Theory and application to the study of chromium dimer. *J. Chem. Phys.*, 135(9):094104, 2011.

[103] Fabian Lackner, Iva Březinová, Takeshi Sato, Kenichi L. Ishikawa, and Joachim Burgdörfer. Propagating two-particle reduced density matrices without wave functions. *Phys. Rev. A*, 91:023412, Feb 2015.

[104] Fabian Lackner, Iva Březinová, Takeshi Sato, Kenichi L. Ishikawa, and Joachim Burgdörfer. High-harmonic spectra from time-dependent two-particle reduced-density-matrix theory. *Phys. Rev. A*, 95:033414, Mar 2017.

[105] A. J. Lee, F. D. Vila, and J. J. Rehr. Local time-correlation approach for calculations of X-ray spectra. *Phys. Rev. B*, 86:115107, Sep 2012.

[106] B. H. Lengsfield. General secondorder MCSCF theory for large CI expansions. *J. Chem. Phys.*, 77(8):4073–4083, 1982.

[107] Bernard Levy and Gaston Berthier. Generalized Brillouin theorem for multiconfigurational SCF theories. *International Journal of Quantum Chemistry*, 2(2):307–319, 1968.

[108] Chenyang Li and Francesco A. Evangelista. Multireference driven similarity renormalization group: A second-order perturbative analysis. *J. Chem. Theory Comput.*, 11(5):2097–2108, 2015. PMID: 26574413.

[109] Xiangzhu Li and Josef Paldus. The general-model-space state-universal coupled-cluster method exemplified by the LiH molecule. *J. Chem. Phys.*, 119(11):5346–5357, 2003.

[110] Xiangzhu Li and Josef Paldus. General-model-space state-universal coupled-cluster theory: Connectivity conditions and explicit equations. *J. Chem. Phys.*, 119(11):5320–5333, 2003.

[111] Xiangzhu Li and Josef Paldus. Performance of the general-model-space state-universal coupled-cluster method. *J. Chem. Phys.*, 120(13):5890–5902, 2004.

[112] Giovanni Li Manni, Rebecca K. Carlson, Sijie Luo, Dongxia Ma, Jeppe Olsen, Donald G. Truhlar, and Laura Gagliardi. Multiconfiguration pair-density functional theory. *J. Chem. Theory Comput.*, 10(9):3669–3680, 2014.

[113] Giovanni Li Manni, Dongxia Ma, Francesco Aquilante, Jeppe Olsen, and Laura Gagliardi. SplitGAS Method for Strong Correlation and the Challenging Case of Cr_2. *J. Chem. Theory Comput.*, 9(8):3375–3384, 2013. PMID: 26584093.

[114] Giovanni Li Manni, Simon D. Smart, and Ali Alavi. Combining the complete active space self-consistent field method and the full configuration interaction Quantum Monte Carlo within a Super-CI framework, with application to challenging metal-porphyrins. *J. Chem. Theory Comput.*, 12(3):1245–1258, 2016. PMID: 26808894.

[115] Matthias W. Löble, Jason M. Keith, Alison B. Altman, S. Chantal E. Stieber, Enrique R. Batista, Kevin S. Boland, Steven D. Conradson, David L. Clark, Juan Lezama Pacheco, Stosh A. Kozimor, Richard L. Martin, Stefan G. Minasian, Angela C. Olson, Brian L. Scott, David K. Shuh, Tolek Tyliszczak, Marianne P. Wilkerson, and Ralph A. Zehnder. Covalency in Lanthanides. an X-ray Absorption Spectroscopy and Density Functional Theory Study of $LnCl_6^{x-}$ ($x = 3, 2$). *Journal of the American Chemical Society*, 137(7):2506–2523, 2015.

[116] K. Lopata, B. E. Van Kuiken, M. Khalil, and N. Govind. Linear-Response and Real-Time Time-Dependent Density Functional Theory Studies of Core-Level Near-Edge X-ray Absorption. *J. Chem. Theory Comput.*, 8(9):3284–3292, 2012. PMID: 26605735.

[117] Robert R Lucchese and David R Yarkony. Symmetry restricted multiconfiguration annihilation of single excitations. II. applications: Electronic states of methylnitrene. *J. Chem. Phys.*, 68(6):2696–2701, 1978.

[118] D.I. Lyakh, M. Musiał, V.F. Lotrich, and R.J. Bartlett. Multireference nature of chemistry: The coupled-cluster view. *Chemical Reviews*, 112(1):182–243, 2011.

[119] Dongxia Ma, Giovanni Li Manni, and Laura Gagliardi. The generalized active space concept in multiconfigurational self-consistent field methods. *J. Chem. Phys.*, 135(4):044128, 2011.

[120] Yingjin Ma, Stefan Knecht, Sebastian Keller, and Markus Reiher. Second-order self-consistent-field density-matrix renormalization group. *J. Chem. Theory Comput.*, 13(6):2533–2549, 2017.

[121] U Sinha Mahapatra, B Datta, and D Mukherjee. A state-specific multi-reference coupled cluster formalism with molecular applications. *Mol. Phys.*, 94(1):157–171, 1998.

[122] Uttam Sinha Mahapatra, Barnali Datta, and Debashis Mukherjee. A size-consistent state-specific multireference coupled cluster theory: Formal developments and molecular applications. *J. Chem. Phys.*, 110(13):6171–6188, 1999.

[123] J. Malick, J. Povh, F. Rendl, and A. Wiegele. Regularization methods for semidefinite programming. *SIAM Journal on Optimization*, 20(1):336–356, 2009.

[124] Per-Åke. Malmqvist, Alistair. Rendell, and Björn O. Roos. The restricted active space self-consistent-field method, implemented with a split graph unitary group approach. *Journal of Physical Chemistry*, 94(14):5477–5482, 1990.

[125] Elvis Maradzike and A Eugene DePrince III. Modeling core-level excitations with variationally optimized reduced-density matrices and the extended random phase approximation. *J. Chem. Phys.*, 149(23):234101, 2018.

[126] Elvis Maradzike, Gergely Gidofalvi, Justin M. Turney, Henry F. Schaefer, and A. Eugene DePrince. Analytic energy gradients for variational two-electron reduced-density-matrix-driven complete active space self-consistent field theory. *J. Chem. Theory Comput.*, 13(9):4113–4122, 2017. PMID: 28731720.

[127] Konrad H. Marti, Irina Malkin Ondík, Gerrit Moritz, and Markus Reiher. Density matrix renormalization group calculations on relative energies of transition metal complexes and clusters. *J. Chem. Phys.*, 128(1):014104, 2008.

[128] David A. Mazziotti. 3,5-contracted Schrödinger equation: Determining quantum energies and reduced density matrices without wave functions. *Int. J. Quantum Chem.*, 70(4-5):557–570, 1998.

[129] David A Mazziotti. Approximate solution for electron correlation through the use of Schwinger probes. *Chem. Phys. Lett.*, 289(5-6):419 – 427, 1998.

[130] David A. Mazziotti. Contracted Schrödinger equation: Determining quantum energies and two-particle density matrices without wave functions. *Phys. Rev. A*, 57:4219–4234, Jun 1998.

[131] David A. Mazziotti. Pursuit of N-representability for the contracted Schrödinger equation through density-matrix reconstruction. *Phys. Rev. A*, 60:3618–3626, Nov 1999.

[132] David A Mazziotti. Complete reconstruction of reduced density matrices. *Chemical Physics Letters*, 326(3-4):212–218, 2000.

[133] David A. Mazziotti. Variational minimization of atomic and molecular ground-state energies via the two-particle reduced density matrix. *Phys. Rev. A*, 65:062511, Jun 2002.

[134] David A. Mazziotti. Extraction of electronic excited states from the ground-state two-particle reduced density matrix. *Phys. Rev. A*, 68:052501, Nov 2003.

[135] David A. Mazziotti. Anti-Hermitian Contracted Schrödinger Equation: Direct Determination of the two-electron Reduced Density Matrices of Many-Electron Molecules. *Phys. Rev. Lett.*, 97:143002, Oct 2006.

[136] David A. Mazziotti. Variational reduced-density-matrix method using three-particle N-representability conditions with application to many-electron molecules. *Phys. Rev. A*, 74:032501, Sep 2006.

[137] David A. Mazziotti. Multireference many-electron correlation energies from two-electron reduced density matrices computed by solving the anti-Hermitian contracted Schrödinger equation. *Phys. Rev. A*, 76:052502, Nov 2007.

[138] David A. Mazziotti. Large-scale semidefinite programming for many-electron quantum mechanics. *Phys. Rev. Lett.*, 106:083001, Feb 2011.

[139] David A. Mazziotti and Robert M. Erdahl. Uncertainty relations and reduced density matrices: Mapping many-body quantum mechanics onto four particles. *Phys. Rev. A*, 63:042113, Mar 2001.

[140] A. D. McLachlan and M. A. Ball. Time-Dependent Hartree-Fock Theory for Molecules. *Rev. Mod. Phys.*, 36:844–855, Jul 1964.

[141] M.V. Mihailović and M. Rosina. The variational approach to the density matrix for light nuclei. *Nucl. Phys. A*, 237(2):221–228, 1975.

[142] Stefan G. Minasian, Jason M. Keith, Enrique R. Batista, Kevin S. Boland, David L. Clark, Stosh A. Kozimor, Richard L. Martin, David K. Shuh, and Tolek Tyliszczak. New evidence for $5f$ covalency in actinocenes determined from carbon K-edge XAS and electronic structure theory. *Chemical Science*, 5:351–359, 2014.

[143] A. O. Mitrushenkov, Roberto Linguerri, Paolo Palmieri, and Guido Fano. Quantum chemistry using the density matrix renormalization group II. *J. Chem. Phys.*, 119(8):4148–4158, 2003.

[144] Alexander O. Mitrushenkov, Guido Fano, Fabio Ortolani, Roberto Linguerri, and Paolo Palmieri. Quantum chemistry using the density matrix renormalization group. *J. Chem. Phys.*, 115(15):6815–6821, 2001.

[145] Yukio Mizuno and Takeo Izuyama. Remarks on Mayer's Reduced Density Matrix Method. *Progress of Theoretical Physics*, 18(1):33–38, 1957.

[146] Mohammad Mostafanejad and A. Eugene DePrince. Combining pair-density functional theory and variational two-electron reduced-density matrix methods. *J. Chem. Theory Comput.*, 15(1):290–302, 2019.

[147] Debashis Mukherjee and Werner Kutzelnigg. Irreducible brillouin conditions and contracted schrödinger equations for n-electron systems. i. the equations satisfied by the density cumulants. *J. Chem. Phys.*, 114(5):2047–2061, 2001.

[148] J. Wayne Mullinax, Evgeny Epifanovsky, Gergely Gidofalvi, and A. Eugene DePrince. Analytic energy gradients for variational two-electron reduced-density matrix methods within the density fitting approximation. *J. Chem. Theory Comput.*, 15(1):276–289, 2019.

[149] M. Musiał and Rodney J Bartlett. Fock space multireference coupled cluster method with full inclusion of connected triples for excitation energies. *J. Chem. Phys.*, 121:1670–1675, 2004.

[150] Rolf H. Myhre, Sonia Coriani, and Henrik Koch. Near-Edge X-ray Absorption Fine Structure within Multilevel Coupled Cluster Theory. *J. Chem. Theory Comput.*, 12(6):2633–2643, 2016.

[151] Maho Nakata, Hiroshi Nakatsuji, Masahiro Ehara, Mitsuhiro Fukuda, Kazuhide Nakata, and Katsuki Fujisawa. Variational calculations of fermion second-order reduced density matrices by semidefinite programming algorithm. *J. Chem. Phys.*, 114(19):8282–8292, 2001.

[152] Hiroshi Nakatsuji. Equation for the direct determination of the density matrix. *Phys. Rev. A*, 14:41–50, Jul 1976.

[153] Hiroshi Nakatsuji and Koji Yasuda. Direct determination of the quantum-mechanical density matrix using the density equation. *Phys. Rev. Lett.*, 76:1039–1042, Feb 1996.

[154] Daniel R. Nascimento and A. Eugene DePrince. Linear Absorption Spectra from Explicitly Time-Dependent Equation-of-Motion Coupled-Cluster Theory. *J. Chem. Theory Comput.*, 12(12):5834–5840, 2016. PMID: 27779862.

[155] Daniel R. Nascimento and A. Eugene DePrince. Simulation of Near-Edge X-ray Absorption Fine Structure with Time-Dependent Equation-of-Motion Coupled-Cluster Theory. *J. Phys. Chem. Lett.*, 8(13):2951–2957, 2017. PMID: 28609098.

[156] Frank Neese. The ORCA program system. *Wiley Interdisciplinary Reviews: Computational Molecular Science*, 2(1):73–78, 2012.

[157] Simon P. Neville and Michael S. Schuurman. A general approach for the calculation and characterization of X-ray absorption spectra. *J. Chem. Phys.*, 149(15):154111, 2018.

[158] Marcel Nooijen and Rodney J Bartlett. Description of core-excitation spectra by the open-shell electron-attachment equation-of-motion coupled cluster method. *J. Chem. Phys.*, 102(17):6735–6756, 1995.

[159] Miguel Ochmann, Inga von Ahnen, Amy A. Cordones, Abid Hussain, Jae Hyuk Lee, Kiryong Hong, Katrin Adamczyk, Oriol Vendrell, Tae Kyu Kim, Robert W. Schoenlein, and Nils Huse. Light-Induced Radical Formation and Isomerization of an Aromatic Thiol in Solution Followed by Time-Resolved X-ray Absorption Spectroscopy at the Sulfur K-edge. *Journal of the American Chemical Society*, 139(13):4797–4804, 2017.

[160] Roberto Olivares-Amaya, Weifeng Hu, Naoki Nakatani, Sandeep Sharma, Jun Yang, and Garnet Kin-Lic Chan. The ab-initio density matrix renormalization group in practice. *J. Chem. Phys.*, 142(3):034102, 2015.

[161] Jeppe Olsen, Björn O. Roos, Poul Jørgensen, and Hans Jørgen Jensen. Determinant based configuration interaction algorithms for complete and restricted configuration interaction spaces. *J. Chem. Phys.*, 89(4):2185–2192, 1988.

[162] S. J. Osborne, A. Ausmees, S. Svensson, A. Kivimäki, O.P. Sairanen, A. Naves de Brito, H. Aksela, and S. Aksela. The vibrationally resolved participator Auger spectra of selectively excited C $1s(2\sigma)^{-1}2\pi^1$ vibrational states in carbon monoxide. *J. Chem. Phys.*, 102(19):7317–7324, 1995.

[163] Josef Paldus and Xiangzhu Li. Analysis of the multireference state-universal coupled-cluster ansatz. *J. Chem. Phys.*, 118(15):6769–6783, 2003.

[164] Josef Paldus, Xiangzhu Li, and Nicholas DK Petraco. General-model-space state–universal coupled-cluster method: Diagrammatic approach. *Journal of Mathematical Chemistry*, 35(3):215–251, 2004.

[165] Robert M. Parrish, Lori A. Burns, Daniel G. A. Smith, Andrew C. Simmonett, A. Eugene DePrince, Edward G. Hohenstein, Uur Bozkaya, Alexander Yu. Sokolov, Roberto Di Remigio, Ryan M. Richard, Jrme F. Gonthier, Andrew M. James, Harley R. McAlexander, Ashutosh Kumar, Masaaki Saitow, Xiao Wang, Benjamin P. Pritchard, Prakash Verma, Henry F. Schaefer, Konrad Patkowski, Rollin A. King, Edward F. Valeev, Francesco A. Evangelista, Justin M. Turney, T. Daniel Crawford, and C. David Sherrill. Psi4 1.1: An open-source electronic structure program emphasizing automation, advanced libraries, and interoperability. *J. Chem. Theory Comput.*, 2017. DOI:10.1021/acs.jctc.7b00174.

[166] E. Pastorczak and K. Pernal. Correlation energy from the adiabatic connection formalism for complete active space wave functions. *J. Chem. Theory Comput.*, 14(7):3493–3503, 2018.

[167] Kenley Pelzer, Loren Greenman, Gergely Gidofalvi, and David A. Mazziotti. Strong correlation in acene sheets from the active-space variational two-electron reduced density matrix method: Effects of symmetry and size. *J. Phys. Chem. A*, 115(22):5632–5640, 2011.

[168] Bo Peng, Patrick J. Lestrange, Joshua J. Goings, Marco Caricato, and Xiaosong Li. Energy-specific equation-of-motion coupled-cluster methods for high-energy excited states: Application to K-edge X-ray absorption spectroscopy. *J. Chem. Theory Comput.*, 11(9):4146–4153, 2015. PMID: 26575909.

[169] E. Pérez-Romero, L. M. Tel, and C. Valdemoro. Traces of spin-adapted reduced density matrices. *International Journal of Quantum Chemistry*, 61(1):55–61, 1997.

[170] Katarzyna Pernal. Electron correlation from the adiabatic connection for multireference wave functions. *Phys. Rev. Lett.*, 120:013001, Jan 2018.

[171] Piotr Piecuch and Karol Kowalski. The state-universal multi-reference coupled-cluster theory: An overview of some recent advances. *Int. J. Mol. Sci.*, 3(6):676–709, 2002.

[172] Jiří Pittner and Ondřej Demel. Towards the multireference Brillouin-Wigner coupled-clusters method with iterative connected triples: MR BWCCSDT-α approximation. *J. Chem. Phys.*, 122(18):181101, 2005.

[173] Jiří Pittner, Xiangzhu Li, and Josef Paldus. Multi-reference Brillouin–Wigner coupled-cluster method with a general model space. *Mol. Phys.*, 103(15-16):2239–2245, 2005.

[174] Jiří Pittner. Continuous transition between Brillouin-Wigner and Rayleigh-Schrödinger perturbation theory, generalized Bloch equation, and Hilbert space multireference coupled cluster. *J. Chem. Phys.*, 118(24):10876–10889, 2003.

[175] O. Plekan, V. Feyer, R. Richter, M. Coreno, M. de Simone, K.C. Prince, A.B. Trofimov, E.V. Gromov, I.L. Zaytseva, and J. Schirmer. A theoretical and experimental study of the near edge X-ray absorption fine structure (NEXAFS) and X-ray photoelectron spectra (XPS) of nucleobases: Thymine and adenine. *Chem. Phys.*, 347(1-3):360 – 375, 2008.

[176] J. Povh, F. Rendl, and A. Wiegele. A boundary point method to solve semidefinite programs. *Computing*, 78(3):277–286, 2006.

[177] R. Püttner, I. Dominguez, T. J. Morgan, C. Cisneros, R. F. Fink, E. Rotenberg, T. Warwick, M. Domke, G. Kaindl, and A. S. Schlachter. Vibrationally resolved O 1s core-excitation spectra of CO and NO. *Phys. Rev. A*, 59:3415–3423, May 1999.

[178] Krishnan Raghavachari. Electron correlation techniques in quantum chemistry: Recent advances. *Annual Review of Physical Chemistry*, 42(1):615–642, 1991.

[179] Krishnan Raghavachari and James B. Anderson. Electron correlation effects in molecules. *The Journal of Physical Chemistry*, 100(31):12960–12973, 1996.

[180] G. Remmers, M. Domke, A. Puschmann, T. Mandel, C. Xue, G. Kaindl, E. Hudson, and D. A. Shirley. High-resolution K-shell photoabsorption in formaldehyde. *Phys. Rev. A*, 46:3935–3944, Oct 1992.

[181] Julia E. Rice, Roger D. Amos, Nicholas C. Handy, Timothy J. Lee, and Henry F. Schaefer. The analytic configuration interaction gradient method: Application to the cyclic and open isomers of the S_3 molecule. *J. Chem. Phys.*, 85(2):963–968, 1986.

[182] Alexandre B. Rocha. Spin-orbit splitting for inner-shell 2p states. *Journal of Molecular Modeling*, 20(8):2355, Jul 2014.

[183] Björn O. Roos. *The Complete Active Space Self-Consistent Field Method and its Applications in Electronic Structure Calculations*, volume 68, pages 399–445. John Wiley & Sons, Inc., 1987.

[184] Björn O. Roos, Peter R. Taylor, and Per E.M. Siegbahn. A complete active space SCF method (CASSCF) using a density matrix formulated super-CI approach. *Chem. Phys.*, 48(2):157–173, 1980.

[185] M. Rosina. Application of the two-body density matrix of the ground state for calculations of some excited states. *Int. J. Quantum Chem.*, 13(6):737–742, 1978.

[186] M. Rosina and C. Garrod. The variational calculation of reduced density matrices. *J. Comput. Phys.*, 18(3):300–310, 1975.

[187] D. J. Rowe. Equations-of-motion method and the extended shell model. *Rev. Mod. Phys.*, 40:153–166, Jan 1968.

[188] D. J. Rowe. Methods for calculating ground-state correlations of vibrational nuclei. *Phys. Rev.*, 175:1283–1292, Nov 1968.

[189] Nora Sabelli and Jürgen Hinze. Atomic multiconfiguration self-consistent-field wavefunctions. *J. Chem. Phys.*, 50(2):684–700, 1969.

[190] Elvira R Sayfutyarova, Qiming Sun, Garnet Kin-Lic Chan, and Gerald Knizia. Automated construction of molecular active spaces from atomic valence orbitals. *J. Chem. Theory Comput.*, 13(9):4063–4078, 2017.

[191] Henry F Schaefer. *Methods of electronic structure theory*, volume 3. Springer Science & Business Media, 2013.

[192] Stefan Schiefer, Martin Huth, Alexander Dobrinevski, and Bert Nickel. Determination of the crystal structure of substrate-induced pentacene polymorphs in fiber structured thin films. *Journal of the American Chemical Society*, 129(34):10316–10317, 2007. PMID: 17672461.

[193] Michael W. Schmidt, Kim K. Baldridge, Jerry A. Boatz, Steven T. Elbert, Mark S. Gordon, Jan H. Jensen, Shiro Koseki, Nikita Matsunaga, Kiet A. Nguyen, Shujun Su, Theresa L. Windus, Michel Dupuis, and John A. Montgomery. General atomic and molecular electronic structure system. *J. Comp. Chem.*, 14(11):1347–1363, 1993.

[194] U. Schollwöck. The density-matrix renormalization group. *Rev. Mod. Phys.*, 77:259–315, Apr 2005.

[195] Ulrich Schollwöck. The density-matrix renormalization group in the age of matrix product states. *Ann. Phys.*, 326(1):96 – 192, 2011. January 2011 Special Issue.

[196] Isaiah Shavitt. Matrix element evaluation in the unitary group approach to the electron correlation problem. *Int. J. Quantum Chem.*, 14(S12):5–32, 1978.

[197] Ron Shepard, Gary S. Kedziora, Hans Lischka, Isaiah Shavitt, Thomas Mller, Pter G. Szalay, Mihly Kllay, and Michael Seth. The accuracy of molecular bond lengths computed by multireference electronic structure methods. *Chem. Phys.*, 349(13):37 – 57, 2008.

[198] C David Sherrill and Henry F Schaefer III. The configuration interaction method: Advances in highly correlated approaches. In *Advances in quantum chemistry*, volume 34, pages 143–269. Elsevier, 1999.

[199] Yinan Shu, Edward G. Hohenstein, and Benjamin G. Levine. Configuration interaction singles natural orbitals: An orbital basis for an efficient and size intensive multireference description of electronic excited states. *J. Chem. Phys.*, 142(2):024102, 2015.

[200] Per Siegbahn, Anders Heiberg, Björn Roos, and Bernard Levy. A comparison of the super-CI and the Newton-Raphson scheme in the complete active space SCF method. *Phys. Scripta*, 21:323–327, 1980.

[201] Per E. M. Siegbahn, Jan Almlöf, Anders Heiberg, and Björn O. Roos. The complete active space SCF (CASSCF) method in a Newton-Raphson formulation with application to the HNO molecule. *J. Chem. Phys.*, 74(4):2384–2396, 1981.

[202] Uttam Sinha Mahapatra, Barnali Datta, and Debashis Mukherjee. Molecular applications of a size-consistent state-specific multireference perturbation theory with relaxed model-space coefficients. *J. Phys. Chem. A*, 103(12):1822–1830, 1999.

[203] John C Slater. Note on Hartree's method. *Physical Review*, 35(2):210, 1930.

[204] Christopher J Stein and Markus Reiher. Automated selection of active orbital spaces. *J. Chem. Theory Comput.*, 12(4):1760–1771, 2016.

[205] Christopher J Stein and Markus Reiher. Automated identification of relevant frontier orbitals for chemical compounds and processes. *CHIMIA International Journal for Chemistry*, 71(4):170–176, 2017.

[206] M Stener, G Fronzoni, and M de Simone. Time dependent density functional theory of core electrons excitations. *Chem. Phys. Lett.*, 373(1):115 – 123, 2003.

[207] J. Stöhr. *NEXAFS Spectroscopy.* Springer, 1992.

[208] Qiming Sun, Jun Yang, and Garnet Kin-Lic Chan. A general second order complete active space self-consistent-field solver for large-scale systems. *Chem. Phys. Lett.*, 683:291–299, 2017.

[209] Attila Szabo and Neil S Ostlund. *Modern quantum chemistry: Introduction to advanced electronic structure theory.* Courier Corporation, 2012.

[210] Szilrd Szalay, Max Pfeffer, Valentin Murg, Gergely Barcza, Frank Verstraete, Reinhold Schneider, and Örs Legeza. Tensor product methods and entanglement optimization for ab initio quantum chemistry. *Int. J. Quantum Chem.*, 115(19):1342–1391, 2015.

[211] Tait Takatani, Edward G. Hohenstein, and C. David Sherrill. Improvement of the coupled-cluster singles and doubles method via scaling same- and opposite-spin components of the double excitation correlation energy. *J. Chem. Phys.*, 128(12):124111, 2008.

[212] Robert E. Thomas, Qiming Sun, Ali Alavi, and George H. Booth. Stochastic multiconfigurational self-consistent field theory. *J. Chem. Theory Comput.*, 11(11):5316–5325, 2015.

[213] Akama Tomoko, Imamura Yutaka, and Nakai Hiromi. Application of real-time time-dependent density functional theory with the CVB3LYP functional to core excitations. *Chemistry Letters*, 39(4):407–409, 2010.

[214] R. H. Tredgold. Density matrix and the many-body problem. *Phys. Rev.*, 105:1421–1423, Mar 1957.

[215] A. B. Trofimov, T. É. Moskovskaya, E. V. Gromov, N. M. Vitkovskaya, and J. Schirmer. Core-level electronic spectra in ADC(2) approximation for polarization propagator: Carbon monoxide and nitrogen molecules. *J. Struct. Chem.*, 41(3):483–494, May 2000.

[216] M Tronc, G C King, and F H Read. Carbon K-shell excitation in small molecules by high-resolution electron impact. *Journal of Physics B: Atomic and Molecular Physics*, 12(1):137, 1979.

[217] M Tronc, G C King, and F H Read. Nitrogen K-shell excitation in N_2 , NO and N_2O by high-resolution electron energy-loss spectroscopy. *Journal of Physics B: Atomic and Molecular Physics*, 13(5):999, 1980.

[218] Carmela Valdemoro, Diego R. Alcoba, Ofelia B. Oña, Luis M. Tel, and Encarnación Pérez-Romero. Combining the g-particle-hole hypervirial equation and the hermitian operator method to study electronic excitations and de-excitations. *Journal of Mathematical Chemistry*, 50(3):492–509, 2012.

[219] Helen van Aggelen, Brecht Verstichel, Guillaume Acke, Matthias Degroote, Patrick Bultinck, Paul W. Ayers, and Dimitri Van Neck. Extended random phase approximation method for atomic excitation energies from correlated and variationally optimized second-order density matrices. *Comp. and Theor. Chem.*, 1003(0):50 – 54, 2013.

[220] Helen van Aggelen, Brecht Verstichel, Patrick Bultinck, Dimitri Van Neck, and Paul W. Ayers. Considerations on describing non-singlet spin states in variational second order density matrix methods. *J. Chem. Phys.*, 136(5):014110, 2012.

[221] Lieven Vandenberghe and Stephen Boyd. Semidefinite programming. *SIAM Rev.*, 38(1):49–95, March 1996.

[222] Brecht Verstichel, Helen van Aggelen, Dimitri Van Neck, Patrick Bultinck, and Stijn De Baerdemacker. A primal-dual semidefinite programming algorithm tailored to the variational determination of the two-body density matrix. *Comput. Phys. Commun.*, 182(6):1235 – 1244, 2011.

[223] Brecht Verstichel, Helen van Aggelen, Dimitri Van Neck, Paul W. Ayers, and Patrick Bultinck. Variational determination of the second-order density matrix for the isoelectronic series of beryllium, neon, and silicon. *Phys. Rev. A*, 80:032508, Sep 2009.

[224] Konstantinos D. Vogiatzis, Dongxia Ma, Jeppe Olsen, Laura Gagliardi, and Wibe A. de Jong. Pushing configuration-interaction to the limit: Towards massively parallel mcscf calculations. *J. Chem. Phys.*, 147(18):184111, 2017.

[225] Arnold C Wahl and G Das. The method of optimized valence configurations: A reasonable application of the multiconfiguration self-consistent-field technique to the quantitative description of chemical bonding. In *Advances in quantum chemistry*, volume 5, pages 261–296. Elsevier, 1970.

[226] Florian Weigend. A fully direct RI-HF algorithm: Implementation, optimised auxiliary basis sets, demonstration of accuracy and efficiency. *Physical Chemistry Chemical Physics*, 4(18):4285–4291, 2002.

[227] Florian Weigend. Hartree-Fock exchange fitting basis sets for H to Rn. *J. Comp. Chem.*, 29(2):167–175, 2008.

[228] Jan Wenzel, Michael Wormit, and Andreas Dreuw. Calculating core-level excitations and X-ray absorption spectra of medium-sized closed-shell molecules with the Algebraic Diagrammatic Construction scheme for the polarization propagator. *J. Comp. Chem.*, 35(26):1900–1915, 2014.

[229] Jan Wenzel, Michael Wormit, and Andreas Dreuw. Calculating X-ray absorption spectra of open-shell molecules with the unrestricted Algebraic-Diagrammatic Construction scheme for the polarization propagator. *J. Chem. Theory Comput.*, 10(10):4583–4598, 2014.

[230] Hans-Joachim Werner and Peter J Knowles. An efficient internally contracted multiconfiguration–reference configuration interaction method. *J. Chem. Phys.*, 89(9):5803–5814, 1988.

[231] Philippe Wernet, Kristjan Kunnus, Simon Schreck, Wilson Quevedo, Reshmi Kurian, Simone Techert, Frank M. F. de Groot, Michael Odelius, and Alexander Föhlisch. Dissecting local atomic and intermolecular interactions of transition-metal ions in solution with selective X-ray spectroscopy. *J. Phys. Chem. Lett.*, 3(23):3448–3453, 2012.

[232] Phillippe Wernet, Kristjan Kunnus, Ida Josefsson, Ivan Rajkovic, Wilson Quevedo, Martin Beye, Simon Schreck, Sebastian Grübel, Mirko Scholz, Dennis Nordlund, et al. Orbital-specific mapping of the ligand exchange dynamics of $Fe(CO)_5$ in solution. *Nature*, 520(7545):78–81, 2015.

[233] Steven R. White. Density matrix formulation for quantum renormalization groups. *Phys. Rev. Lett.*, 69:2863–2866, Nov 1992.

[234] Steven R. White. Density-matrix algorithms for quantum renormalization groups. *Phys. Rev. B*, 48:10345–10356, Oct 1993.

[235] Stephen Wilson. *Electron correlation in molecules*. Courier Corporation, 2014.

[236] David E. Woon and Thom H. Dunning. Gaussian basis sets for use in correlated molecular calculations. V. Core-valence basis sets for boron through neon. *J. Chem. Phys.*, 103(11):4572–4585, 1995.

[237] Sebastian Wouters, Ward Poelmans, Paul W. Ayers, and Dimitri Van Neck. CheMPS2: A free open-source spin-adapted implementation of the density matrix renormalization group for ab initio quantum chemistry. *Comput. Phys. Commun.*, 185(6):1501–1514, 2014.

[238] Sebastian Wouters and Dimitri Van Neck. The density matrix renormalization group for ab initio quantum chemistry. *Eur. Phys. J. D*, 68(9):272, 2014.

[239] Stephen J. Wright. *Primal-dual Interior-point Methods*. Society for Industrial and Applied Mathematics, Philadelphia, PA, USA, 1997.

[240] Takeshi Yanai, Yuki Kurashige, Debashree Ghosh, and Garnet Kin-Lic Chan. Accelerating convergence in iterative solution for large-scale complete active space self-consistent-field calculations. *Int. J. Quantum Chem.*, 109(10):2178–2190, 2009.

[241] Takeshi Yanai, Yuki Kurashige, Eric Neuscamman, and Garnet Kin-Lic Chan. Multireference quantum chemistry through a joint density matrix renormalization group and canonical transformation theory. *J. Chem. Phys.*, 132(2):024105, 2010.

[242] Li Yang, Hans Ågren, Vincenzo Carravetta, and Lars G M Pettersson. Static exchange and quantum defect analysis of X-ray absorption spectra of carbonyl compounds. *Physica Scripta*, 54(6):614, 1996.

[243] David Yarkony. *Modern electronic structure theory*, volume 2. World Scientific, 1995.

[244] Koji Yasuda. Direct determination of the quantum-mechanical density matrix: Parquet theory. *Phys. Rev. A*, 59:4133–4149, Jun 1999.

[245] Koji Yasuda and Hiroshi Nakatsuji. Direct determination of the quantum-mechanical density matrix using the density equation. II. *Phys. Rev. A*, 56:2648–2657, Oct 1997.

[246] Danny L Yeager and Poul Jørgensen. Convergency studies of second and approximate second order multiconfigurational Hartree-Fock procedures. *J. Chem. Phys.*, 71(2):755–760, 1979.

[247] Dominika Zgid and Marcel Nooijen. On the spin and symmetry adaptation of the Density Matrix Renormalization Group method. *J. Chem. Phys.*, 128(1):014107, 2008.

[248] Yu Zhang, Jason D. Biggs, Daniel Healion, Niranjan Govind, and Shaul Mukamel. Core and valence excitations in resonant X-ray spectroscopy using restricted excitation window time-dependent density functional theory. *J. Chem. Phys.*, 137(19):194306, 2012.

[249] Zhengji Zhao, Bastiaan J. Braams, Mituhiro Fukuda, Michael L. Overton, and Jerome K. Percus. The reduced density matrix method for electronic structure calculations and the role of three-index representability conditions. *J. Chem. Phys.*, 120(5):2095–2104, 2004.

BIOGRAPHICAL SKETCH

Elvis Maradzike

Education

- Florida State University − Ph.D. in Physical Chemistry
  Prof. A. Eugene DePrince, III, advisor
- Florida State University − M.S. in Chemistry, 2017
  Prof. A. Eugene DePrince, III, advisor
- Amherst College − B.A. majors: Physics, French

Honors & Awards

- Jyotsna Dalal Graduate Student Award in Physical Chemistry − 2019
- Philip Schlenoff Graduate Student Travel Award − 2018
- 2nd Best Poster Award, South East Theoretical Chemistry Conference meeting − 2016

Research Experience

- Florida State University: Doctoral Research, 2014−2019
  Electronic Structure Theory: Methods for ground and excited electronic states
  Prof. A. Eugene DePrince, III, advisor
- University of Cape Town: Postgraduate Research, 2011-2011
  Molecular mechanics: Parameterizing a force field for carbohydrates
  Prof. K. Naidoo, advisor
- Amherst College: Undergraduate Research, 2009−2010
  Experimental condensed matter physics: Investigating resonant tunneling in the magnetization of Mn_{12}-t-Bu-Ac, a single molecule magnet
  Prof. J. R. Friedman, advisor

Publications

- **E. Maradzike** and A. E. DePrince, III, "A dynamical correlation model for v2RDM-CASSCF", *in preparation*, 2019.
- J. Wayne Mullinax, Lauren Koulias, **Elvis Maradzike**, Evgeny Epifanovsky, Gergely Gidofalvi, and A. Eugene DePrince III, "A heterogeneous CPU + GPU algorithm for variational two-electron reduced-density matrix driven complete active space self-consistent field theory", *submitted*, 2019.
- **E. Maradzike** and A. E. DePrince, III, "Modeling core-level excitations with variationally optimized reduced-density matrices and the extended random phase approximation", *Journal of Chemical Physics,* **149 (23)**, 2018.
- **E. Maradzike**, G. Gidofalvi, J.M. Turney, H.F. Schaefer, and A.E. DePrince III, "Analytic Energy Gradients for Variational Two-Electron Reduced-Density-Matrix-Driven Complete Active Space Self-Consistent Field Theory", *Journal of Chemical Theory and Computation*, **13 (9)**, 2017.

Teaching Experience

- Florida State University:
  Teaching Assistant, CHM 1046L: General Chemistry II Laboratory − Spring 2019
  Teaching Assistant, CHM 1045R: General Chemistry I − Fall 2018
  Teaching Assistant, CHM 4410L: Physical Chemistry Laboratory − Summer 2018
  Teaching Assistant, CHM 1045L: General Chemistry I Laboratory − Fall 2014, Spring 2015

Conference Presentations

Oral

- **Elvis Maradzike** and A. E. DePrince, III, "A dynamical correlation model for v2RDM-CASSCF", *Florida ACS Meeting (FAME)*, 2019, Palm Harbor, FL
- **Elvis Maradzike** and A. E. DePrince, III, "A dynamical correlation model for v2RDM-CASSCF", *ACS Spring National meeting and Expo*, 2019, Orlando, FL

- **Elvis Maradzike** and A. E. DePrince, III, "Modeling core-level excitations with variationally optimized reduced-density matrices and the extended random phase approximation", *Southeastern Theoretical Chemistry Association Meeting*, 2018, Baton-Rouge, LA

- **Elvis Maradzike** and A. E. DePrince, III, "Analytic Gradients for v2RDM-CASSCF methods", *Florida ACS Meeting (FAME)*, 2017, Palm Harbor, FL

Poster

- **Elvis Maradzike** and A. E. DePrince, III, "A dynamical correlation model for v2RDM-CASSCF", *Southeastern Theoretical Chemistry Association Meeting*, 2019, Knoxville, TN

- **Elvis Maradzike** and A. E. DePrince, III, "A dynamical correlation model for v2RDM-CASSCF", *59th Sanibel Symposium*, 2019, St. Simon's island, GA

- **Elvis Maradzike** and A. E. DePrince, III, "Modeling core-level excitations with variationally optimized reduced-density matrices and the extended random phase approximation", *Gordon Research Conference in Computational Chemistry*, 2018, West Dover, VT

- **Elvis Maradzike** and A. E. DePrince, III, "Analytic Gradients for v2RDM-CASSCF methods", *Southeastern Theoretical Chemistry Association Meeting*, 2018, Oxford, MS

- **Elvis Maradzike** and A. E. DePrince, III, "Analytic Gradients for v2RDM-CASSCF methods", *57th Sanibel Symposium*, 2017, St. Simon's island, GA

- **Elvis Maradzike** and A. E. DePrince, III, "Analytic Gradients for v2RDM-CASSCF methods", *68th Southeastern Regional Meeting of the American Chemical Society*, 2016, St. Columbia, SC

- **Elvis Maradzike** and A. E. DePrince, III, "Modeling electron dynamics in polyacenes using time-dependent configuration interaction", *Southeastern Theoretical Chemistry Association Meeting*, 2016, Tallahassee, FL

- **Elvis Maradzike** and A. E. DePrince, III, "Modeling electron dynamics in polyacenes using time-dependent configuration interaction", *Florida ACS Meeting (FAME)*, 2016, Palm Harbor, FL